6-1-2003

Steady-state and transient analysis of electro-thermal microactuators using finite element methods

Amarendra Atre

STEADY- STATE AND TRANSIENT ANALYSIS OF ELECTRO-THERMAL MICROACTUATORS USING FINITE ELEMENT METHODS

by

AMARENDRA ATRE

A Thesis Submitted in Partial Fulfillment of the Requirement for the degree of

MASTER OF SCIENCE

IN

MECHANICAL ENGINEERING

Approved by:

Dr. Stephen Boedo _____

Department of Mechanical Engineering (Thesis Advisor)

Dr. Hany Ghoneim _____

Department of Mechanical Engineering

Dr. Satish Kandlikar _____

Department of Mechanical Engineering

Dr. Edward Hensel _____

Department Head of Mechanical Engineering

DEPARTMENT OF MECHANICAL ENGINEERING

ROCHESTER INSTITUTE OF TECHNOLOGY

JUNE 2003

STEADY- STATE AND TRANSIENT ANALYSIS OF ELECTRO-THERMAL MICROACTUATORS USING FINITE ELEMENT METHODS

I, Amarendra Atre, hereby grant permission to the Wallace Library of Rochester Institute of Technology to reproduce my thesis in whole or part. Any reproduction will not be for commercial use or profit.

Amarendra Atre

June 2003

Acknowledgements

I would like to thank my faculty advisor Dr. Stephen Boedo for taking an interest and supporting my initial research in the analysis of the thermal microactuator. I express my thanks to my committee members Dr. Hany Ghoneim and Dr. Satish Kandlikar for taking the time to review my thesis. I especially thank Dr. Ghoneim for giving me an opportunity to improve my skills in ANSYS through the Advanced Computational Techniques teaching practicum and the EA-6B Flaperon Hydraulic Actuator failure analysis research project.

My sincere thanks go to Nilesh Mankame at the University of Pennsylvania. He spared a lot of time from his doctoral work to answer my e-mails. He had a knack for pointing me in the right direction when I was stuck and is responsible for clearing up a lot of nasty "gremlins" in my thesis. I also thank Robert Johnstone at the Simon Fraser University, Canada for reviewing my very first model and his numerous suggestions towards improving the model accuracy. I would like to express my appreciation to Dr. Larry Howell, Dr. Timothy McLain and Christian Lott at the Brigham Young University, Utah for expressing an interest in my research and taking the time to respond to my queries. I would like to thank Rob Messenger, also at the Brigham Young University, Utah for sharing his research with me and pointing out the possible errors in my model during my comparisons with Christian Lott's models. I also thank Dr. Victor Bright at the University of Colorado, Boulder for directing my questions to the concerned faculty so that I could get relevant information.

My sincere appreciation also goes to Ellen Sheppard at the Sandia National Laboratories, New Mexico for patiently working with me towards getting information about design and analysis from the Intelligent Micromachine Department at Sandia. I thank Busbee Hardy at Cronos for answering my queries on the MUMPs process. I also thank ANSYS Inc., Pittsburgh and the members of XANSYS for pointing out the possible solutions when my model gave me convergence problems.

I would like to express my deepest appreciation to my parents, my brother Suhrud, my sister in law Gayatri and my cousin sister Malavika. They were always there to listen to me when my research was not going in the correct direction. I also thank my ASME mentor Michael

King. His e-mail support always boosted my morale in my research work and doctoral applications. I thank the Department of Mechanical Engineering staff at RIT for all of their help in my graduate studies. I thank my roommates Amit and Rajiv for "feeding" me so I could work on my thesis. I also thank my friends from the "Khujal" group for making life more enjoyable. I especially thank Sany, JK and Gurjinder. Their presence in the lab made the thesis more fun to work on. I think we spent a lot of time on trying to figure out the answer to the question "What is the thesis?" but I don't think we actually managed to work it out completely.

Finally, I would like to dedicate my thesis to all the people mentioned above; without their help this thesis would never have been as complete as it is today.

Abstract

Recent techniques in radar and communication systems favor the development of phased arrays. The major problems to such systems are size and cost due to the large number of individual transmit/receive modules required. Photonic systems implemented in MEMS technology have reduced bulk optical systems to microscale proportions. This reduction in scale is particularly important to phased arrays since it allows flexibility in deployment.

This thesis aims to understand the steady state and transient characteristics of an electrically heated, thermally driven, surface micromachined MEMS polysilicon beam flexure actuator to be employed for the rotation of an r-f phase shifter utilized in phased array systems. The characteristics of the thermal actuator are examined through finite element analysis by investigating the relative importance of the temperature dependencies of the material properties of MUMPs polysilicon. The comprehensive finite element model of the thermal actuator developed using ANSYS 5.6, a commercial finite element package, has the ability to include full temperature dependencies of all parameters and also has the capacity to impose all heat transfer modes, which are beyond the capabilities of current analytical models.

Steady-state thermal profiles of the thermal actuator are presented for the thermal actuator in an environment of air and vacuum. The model is validated indirectly by comparing the steady-state deflections with measured data of six thermal actuators of different geometries. The finite element simulations are also validated with a previous analytical model to compare model accuracy. The dynamic behavior of the thermal actuator is examined in both air and vacuum, which gives an insight into power and energy consumption of the thermal actuator. Initial results show a limited power and energy savings for the thermal actuator operated in vacuum over that operated in air.

Design optimization of the thermal actuator is investigated using the ANSYS Parametric Design Language (APDL) with the Subproblem Approximation Method for maintaining low power consumption. An indirect method is employed by maximizing the steady-state deflection for unloaded actuators and minimizing the steady-state deflection for loaded actuators for the same applied voltage. A significant reduction in power consumption with an increase in the maximum steady-state deflection has been observed for unloaded

actuators. For loaded actuators the available force output is increased slightly, the steady-state deflection decreased slightly and the power consumption increased slightly.

Contents

List of Figures

List of Tables

Nomenclature

Symbol	Definition
L	Length, μm
T	Reference temperature, °C
ΔT	Change in temperature, °C
ΔL	Change in length, μm
α	Coefficient of thermal expansion, $^{\circ}C^{-1}$
ΔV	Volumetric deformation, $(\mu m)^3$
v	Volume, $(\mu m)^3$
β	Coefficient of volume expansion, $^{\circ}C^{-1}$
A	Area, $(\mu m)^2$
V	Applied Voltage
I	Current, pA
$\vec{J}$	Current density, pA/ $(\mu m)^2$
$\vec{E}$	Electric field, V/μm
ϱ	Electrical resistivity, T Ωμm
R	Resistance, Ω
ϱ_0	Resistivity at reference temperature, T Ωμm
T_0	Reference temperature, °C
α_r	Resistivity temperature coefficient, $^{\circ}C^{-1}$
P	Joule heating, pW
R_a	Thermal resistance of air, $(\mu m)^2$/pW °C
R_n	Thermal resistance nitride, $(\mu m)^2$/pW °C
R_{Si}	Thermal resistance of silicon, $(\mu m)^2$/pW °C
t_a	Thickness of air layer, μm
t_n	Thickness of nitride layer, μm

t_{Si}	Thickness of silicon substrate, μm
k_a	Thermal conductivity of air, pW/μm°C
k_n	Thermal conductivity of nitride, pW/μm°C
k_{Si}	Thermal conductivity of silicon, pW/μm°C
h	Conductive heat transfer coefficient, pW/(μm)^2°C
t	Thickness of polysilicon layer, μm
w	Width of polysilicon segment, μm
S	Shape factor
h_i	Convective heat transfer coefficient, pW/(μm)^2°C
Nu	Nusselt's number
Ra	Rayleigh number
L_i	Length of polysilicon segment, μm
ν	Kinematic viscosity air, (μm)^2/s
T_a	Ambient temperature, °C
T_i	Temperature of polysilicon segment, °C
k_p	Thermal conductivity of polysilicon, pW/μm°C
c	Specific heat, pJ/(kg)(°C)
F	Force, μN
k	Stiffness, μN/ μm
$d_0(V)$	Deflection due to applied voltage, μm
d	Deflection, μm
{I}	Nodal value of net current
{V}	Nodal voltages
{T}	Nodal temperatures
$\{\dot{T}\}$	Variation of nodal temperatures with time
{q}	Nodal value of net heat flow.
$\{q_v\}$	Heat flow into node caused by Joule heating

$\{d\} \equiv \begin{Bmatrix} d_x \\ d_y \\ d_z \end{Bmatrix}$	Nodal displacements
$\{F\} \equiv \begin{Bmatrix} F_x \\ F_y \\ F_z \end{Bmatrix}$	Net nodal forces
$\{\alpha(T)\}$	Thermal expansion vector
$[\rho(T)]$	Electrical conductivity matrix
$[K(T)]$	Thermal conductivity matrix
$[C(T)]$	Specific heat matrix
$[Y(T)]$	Young's Modulus matrix
l_t	Length of thin arm, μm
l_w	Length of wide arm, μm
l_f	Length of flexure arm, μm
w_t	Width of thin arm, μm
w_w	Width of wide arm, μm
w_f	Width of flexure arm, μm
g	Gap, μm
e	End connection, μm

CHAPTER 1

INTRODUCTION

Actuators are used to perform work on the surroundings. Depending on the type of actuation many different methods exist for actuation of components at the microscale, such as, magnetic, piezoelectric, electrostatic and thermal expansion. Actuation by employing thermal expansion has many advantages and has been widely applied in microsystems. This chapter gives an introduction to the application of thermal actuators for optical MEMS applications. A brief description of the theory behind the thermal actuator is presented in section 1.2. A literature survey pertaining to the design, analysis and fabrication of the thermal actuator is given in section 1.3. The objectives and contributions of the thesis are described in sections 1.4 and sections 1.5, respectively.

1.1 MICROELECTROMECHANICAL SYSTEMS (MEMS)

MicroElectroMechanical Systems (MEMS) typically refer to devices having a length of less than 1 mm but greater than 1 μm, which combine electrical and mechanical components and are fabricated using Integrated Circuit (IC) technology. MEMS have tremendous application in today's mechanical, industrial and medical fields. Accelerometers for automobile airbags, micropumps for inkjet printing, and pumps controlling delivery of medication are just a few of the numerous examples. On the optical side, MEMS have been successfully employed for rotating and positioning optical components, micromirrors and stepper motors.

Any MEMS device, which is to be utilized in such commercial applications, must have a certain means of actuation to control its motion precisely. Microactuators, a critical component of most microsystems, precisely control the orientation and position of other MEMS components. The range of deflection and force provided by microactuators increase their functionality in microsystems.

A complete MEMS device thus consists of an actuating mechanism and the actuated component, which performs the desired function. An example of this is a microsystem

designed by Comtois and Bright [1]. This device rotates an optical grating with a stepper motor, which serves as the component performing the necessary function. The movement of the motor is achieved by an array of thermal actuators, which provide the required force for positioning the grating.

Micromechanical devices have been created with a large variety of manufacturing processes, nearly all of them employing photolithography. Any MEMS device is composed of two sets of materials irrespective of the manufacturing process-a structural material that performs the necessary function and a sacrificial material that is removed to release the structural material. The method of deposition of these materials, number of layers of deposition, and patterning is highly dependent upon whether the manufacturing process is surface micromachining or bulk micromachining.

Efficient MEMS development not only requires reliable fabrication processes, but it also requires flexible design and analysis tools. Several commercial entities have developed analysis tools, which can be applied to such MEMS devices. In the field of MEMS, learning design mistakes by failure of systems is extremely inefficient and expensive. The time between design and fabrication is usually months, and the price per fabrication run can run into thousands of dollars. Fabricating a microsystem with rudimentary design as done by Sandia National Laboratories for majority of their devices [2] can prove to be expensive for university laboratories, which do not have effective batch fabrication capabilities, either in time or money. Senturia [3] has presented a comprehensive introduction to the design of microsystems with emphasis on modeling and simulation.

This thesis aims to understand the steady state and transient characteristics of a surface micromachined MEMS polysilicon thermal actuator to be employed for the rotation of an r-f phase shifter utilized in phased array systems. Though the device has a specific task, the analysis method is generic and can be utilized for the design of any microsystem that requires r-f phase shift or any device employing similar components.

1.2 MICROSYSTEM COMPONENTS

Many techniques for actuation have been established at the microscale. Out of these, electro-thermal actuation provides an easily controlled micro-actuation method compatible with standard microelectronics. A voltage source consistent with IC technology is sufficient to control the actuation. Electro-thermal actuators can provide large forces in comparison with other methods, such as electrostatic actuation. Varying the electrical resistivity of the material of these actuators by doping is common in the semiconductor industry. This ability to change the electrical resistivity gives additional control over the design of the actuators. Employing a number of actuators in an array increases the force output of these mechanisms. Since the majority of these actuators are made from a single material, they can be easily fabricated in any process that has a single releasable current carrying layer. The only drawback of these actuators is their large power requirements and inability to perform at higher frequencies.

Guckel et al. [4] proposed a topology for an electro-thermally actuated microactuator which has been developed extensively by Comtois and Bright [1,5,6,7,8,9], Moulton and Ananthasuresh [10] and Kolesar et al. [1,11,12]. This thermal actuator is also known as the pseudo bimorph or heatuator. Figure 1 shows the basic geometry of the thermal microactuator.

The thermal microactuator produces deflection due to the asymmetric thermal expansion of the two arms. Upon application of a potential difference, the thin arm expands more than the wide arm, leading to motion of the actuator tip towards the wide arm. An array of such thermal actuators is employed as the actuation device for rotating the r-f phase shifter mainly because it has been implemented in various configurations [5,8,9], it allows a wide variety of force-deflection characteristics, it can be fabricated easily and its characteristics can be varied qualitatively and quantitatively by altering the geometry.

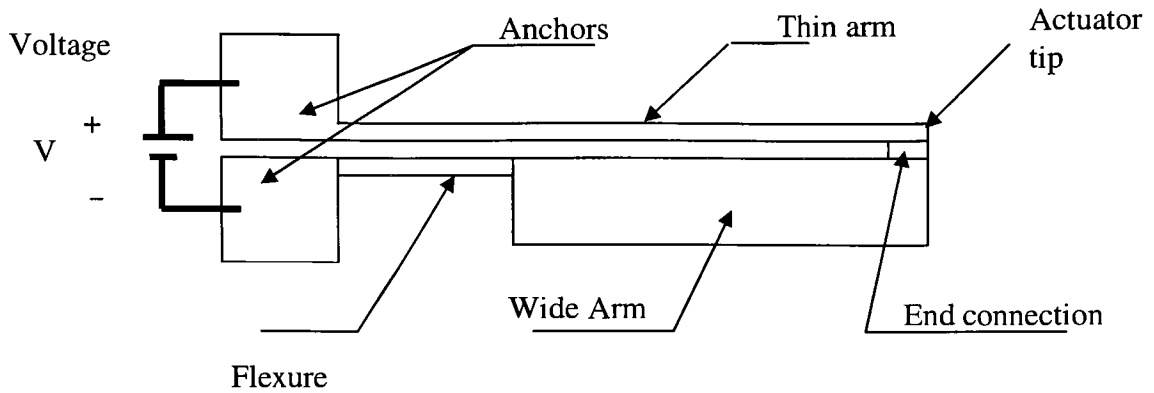

Figure 1: Geometry of the thermal actuator

A majority of optical microsystems implement a micro-motor driven by a toothed rack as the components for positioning the device. Such systems require two arrays of actuators. The first array actuates the motor while the second array brings the rack in alignment with the motor (for example see Comtois and Bright [5,8,9]). An alternative approach proposed here and shown in Figure 2 uses similar components but replaces the traditional motor by a toothed rack and pinion arrangement.

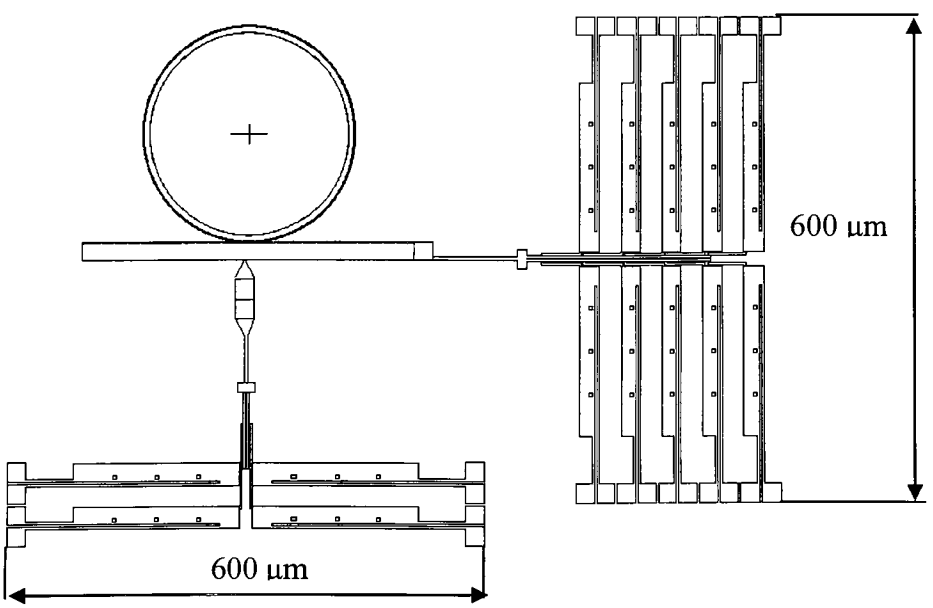

Figure 2: Complete microsystem using two arrays of actuators, employed to rotate an optical phase shifter.

The device employs two sets of arrays; one actuates the rack to rotate the gear and position the r-f phase shifter while the other brings it in contact with the gear.

1.3 LITERATURE REVIEW

Some of the earliest work on thermal actuators was started by Guckel et al. [4] who investigated thermo-magnetic compliant metal flexure actuators. They conducted finite element analysis to understand the magnetic and thermal effects on the design of the actuator. Following the initial work of Guckel et al. [4], a large amount of experimental and theoretical work followed on the design of actuators using Joule heating of a single material such as polysilicon. The majority of the work that followed on these actuators was done by Comtois and Bright (for example see [1,5,8,9]). They refined the shape considerably to simplify the fabrication of the device by surface micromachining [6], and they implemented the actuator in a variety of optical switching applications using actuator arrays coupled to micro optical components [5,8,9]. Lerch et al. [13] designed polysilicon micro-actuators based on asymmetrical heating, which were then implemented as micro-grippers.

Comtois et al. [14] experimentally investigated the performance characteristics of these actuators in terms of force, deflection, power and current. They conducted experimental studies of force-deflection characteristics, observed the device operation for loaded actuators, and examined dynamic response of these actuators for capturing the operating frequencies. They also offered design guidelines for coupling these actuators together in arrays and tested different actuator array configurations. Kolesar et al. [11,12] also performed similar experimental characterization of these actuators. The force-deflection-power-current characteristics were also evaluated experimentally by Comtois and Bright [15].

From the modeling and analysis perspective, Bright et al. [16,17] conducted finite element analysis of these devices using SPICE, an electric circuit simulator that allows simultaneous analysis of integrated MEMS and Microsystems [17]. They observed the voltage-current characteristics of these actuators. They, however, did not characterize the actuator for its force-deflection characteristics. Reid and Silversmith [18] characterized the actuator for deflection and temperature fields using finite element analysis. Allen et al. [19] conducted a

similar analysis to observe the deflection, thermal and the frequency characteristics of these actuators. Moulton and Ananthasuresh [10] conducted coupled electro-thermal analysis to design a building block of these actuators. Huang and Lee [20,21] developed an extensive analytical model for the electro-thermal micro actuator to characterize its temperature, displacement and force characteristics. Their model ignored the temperature dependency of material properties and the effect of radiation assuming safe modes of operation.

Lin and Chiao [22] performed electro-thermal analysis of polysilicon line shape microstructures. Their model also ignored temperature dependency and radiation effects under the same assumption. They analyzed the heat transfer characteristics of a microbeam heated to high temperatures and suspended at a very low (2 μm) distance above a silicon substrate. They concluded conduction as the main mode of heat transfer in micro devices suspended 2 μm above the substrate. They also established conduction shape factors to account for the heat losses from the vertical faces of a micro device. Mastrangelo et al. [23] conducted modeling of a silicon filament vacuum-sealed incandescent light source. They assumed a constant thermal conductivity and small radiative heat loss. Pan and Hsu [24] analyzed a laterally driven polysilicon microactuator for its transient characteristics. They also assumed constant material properties along with small radiative and convective losses.

Mankame and Ananthasuresh [25,26,27] conducted a more comprehensive analysis of a bulk micromachined silicon electro-thermo-mechanical actuator, which included variation of thermophysical properties, convective and radiative heat losses. They showed the inaccuracies arising out of ignoring these boundary conditions on a thermal expansion device. However, they considered convection as the dominant mode of heat transfer in their micro devices. They confirmed this experimentally and this can be attributed to the fact that their devices were suspended 20 μm above a silicon substrate. They, however, have not characterized the device transient behavior, and they have not studied the force-deflection characteristics.

Lott [28,29] conducted a comprehensive analysis on a Thermo Mechanical In-Plane surface micromachined polysilicon microactuator. He characterized the force, deflection and current characteristics for this actuator in air and vacuum. He investigated the relative importance of

temperature dependent parameters, particularly, the thermal conductivity of polysilicon and thermal conductivity of air, that affect the analysis by employing three models for the simulations. The first model assumes constant thermal conductivity of air and polysilicon, the second model assumes a constant thermal conductivity of polysilicon with thermal conductivity of air varying with temperature and the third takes into account temperature dependencies of both. He validated the deflections of the TIM actuator with the third model.

Hickey [30] conducted a similar comprehensive analysis of a surface micromachined thermal actuator in varying ambient conditions and laid down design optimization guidelines. He conducted a separate CFD analysis to determine the basic mode of heat transfer in the thermal microactuator. The geometry of his setup is similar to that of Lin and Chiao [22]. His analysis agrees with Lin and Chiao [22] establishing conduction as the main mode of heat transfer in these thermal microactuators suspended 2 μm above the substrate. He computed a convective heat transfer coefficient to account for the heat loss by conduction. He also conducted dynamic testing and simulation of the actuator to characterize its response frequency. He has obtained the temperature profile for the actuator by a steady state numerical solution to the governing equation for the heat transfer from the thermal actuator. The model assumes constant material properties with average values for the thermal conductivity of polysilicon and air to take into account their temperature dependency. He has computed the deflection of the actuator analytically using structural mechanics. The model assumes the hot arm to be heated uniformly and he has used an effective hot arm temperature for estimating the deflection. He has laid down guidelines for design optimization with a trial and error approach using his thermal and structural models.

Significant experimental work has been conducted on the thermophysical and heat transfer properties of polysilicon at the microscale. Manginell [31] established a fit for the temperature dependency of Sandia's large grained laminated polysilicon, and McConnell et al. [32] showed the dependency of the thermal conductivity of polysilicon on the nature and amount of doping. Okada and Tokumaru [33] obtained an expression for the thermal coefficient of expansion of polysilicon, which has been employed by others to model polysilicon growth. Lide and Kehiaian [34] established the temperature dependency of

thermal conductivity of polysilicon. Manginell [31] showed the acceptance of the temperature dependency of silicon's specific heat for modeling polysilicon with a maximum uncertainty of 5%. Sharpe et al. [35] conducted tensile tests on MUMPs polysilicon specimen and reported the variation of Elastic Modulus of polysilicon with temperature. Kato and Ono [36] showed the changes in electrical resistivity that take place at high temperatures due to secondary breakdown of polysilicon. Mankame [25] computed experimentally the net electrical resistance of the device at different voltages.

Any uncertainity in the material properties leads to inconsistent models. Any problem in fabrication leads to inconsistent device behavior. Hence, the inaccuracies in the finite element models and the fabricated systems may arise from problems in either one of them. This directs the question whether analyzing these devices is practical and does it provide feasible results, which can be implemented in optimizing the design. Senturia [3] gives a comprehensive introduction to the design of microsystems with emphasis on modeling and simulation. If implemented comprehensively, finite element analysis will provide an effective tool for the analysis of microsystems leading to a cost and time reduction in the long run.

1.4 THESIS OBJECTIVES

This thesis aims to design a surface micromachined polysilicon thermally actuated microsystem for application in phased array systems using finite element analysis. Previous research on the design and analysis of these actuators has been based on analytical or semi-analytical models. A comprehensive finite element analysis of this surface micromachined polysilicon actuator which investigates the relative importance of thermophysical properties has not been performed. The finite element method has the ability to include full temperature dependencies of all parameters and the method also has the capacity to impose all heat transfer modes, which are beyond the capabilities of current analytical models.

Previous models have focused on characterizing the actuators for deflection, current and temperature profile by employing constant or average material properties. Based on previous research, this thesis aims to analyze the actuator characteristics by investigating the importance of temperature dependent parameters that affect the analysis. The actuator

performance is analyzed for each material property parameter separately, by assuming a constant value as well as its temperature dependency, if applicable. This will give insight as to the material properties that influence the behavior of the actuator. For example, analytical models employing constant material properties might agree with experiment but finite element models may or may not give more accurate results by employing temperature variations of properties. This will also provide knowledge as to whether more research is warranted on the temperature dependency of the material properties of polysilicon, or if the current equations are valid for use in finite element simulations.

The steady state model that best fits experimental work is then employed to investigate the dynamic characteristics of the actuator. Dynamic performance of thermal micro-actuators has been previously studied only through analytical models. The analytical and experimental model results are compared to finite element simulations, which may or may not provide a better alternative for investigating the transient behavior of the actuator.

Application of the actuators in vacuum environment has not been recommended. This thesis investigates the actuator behavior in vacuum environment under both steady state and transient conditions.

Design optimization of the thermal actuator has been attempted by a trial and error approach. This thesis investigates the optimization of the thermal actuator by employing a multi-variable non-linear sub-problem approximation finite element method. A generalized command or batch file is created by using the ANSYS Parametric Design Language, which will enable a designer to optimize the thermal actuator with specified design variables for the required application.

CHAPTER 2

PROBLEM FORMULATION

This chapter gives a brief overview of the principles of thermal actuation and Joule heating. An explanation of the geometry of the thermal actuator and parameters associated with it follows. The boundary conditions that dictate the response of the thermal actuator are discussed in detail. The temperature dependencies of thermophysical and material properties associated with the actuator are also discussed. The chapter ends with a discussion of the two dimensional approximation of the thermal actuator.

2.1 PHYSICAL PRINCIPLES OF THERMAL ACTUATION

2.1.1 Thermal Expansion

Consider a material of length L at a constant reference initial temperature T. If the temperature of the material is changed by an amount ΔT from the reference value, the change in length of the material ΔL is predicted by the equation

$$\Delta L = L \alpha \Delta T \tag{2.1}$$

where coefficient of thermal expansion α depends upon the material and temperature. Similarly, the volumetric deformation ΔV for expansion of a solid is given by

$$\Delta V = v\beta\Delta T \tag{2.2}$$

where v is the volume at reference temperature T, and β is the coefficient of volume expansion for the material. Most materials expand isotropically which makes $\beta \sim 3\alpha$ [37].

The majority of MEMS thermal actuators use polycrystalline silicon (polysilicon) as the structural layer. The thermal expansion of polysilicon is similar to those for crystalline solids which are held together in a three dimensional periodic lattice by interatomic forces. The

individual atoms vibrate about lattice sites with the amplitude of vibration varying as a function of temperature. An increase in temperature increases the average distance between neighboring atoms, which makes the solid expand. The thermal coefficient of expansion is a measure of how the average atomic distance changes for different materials over given temperature ranges.

2.1.2 Resistivity and Resistance

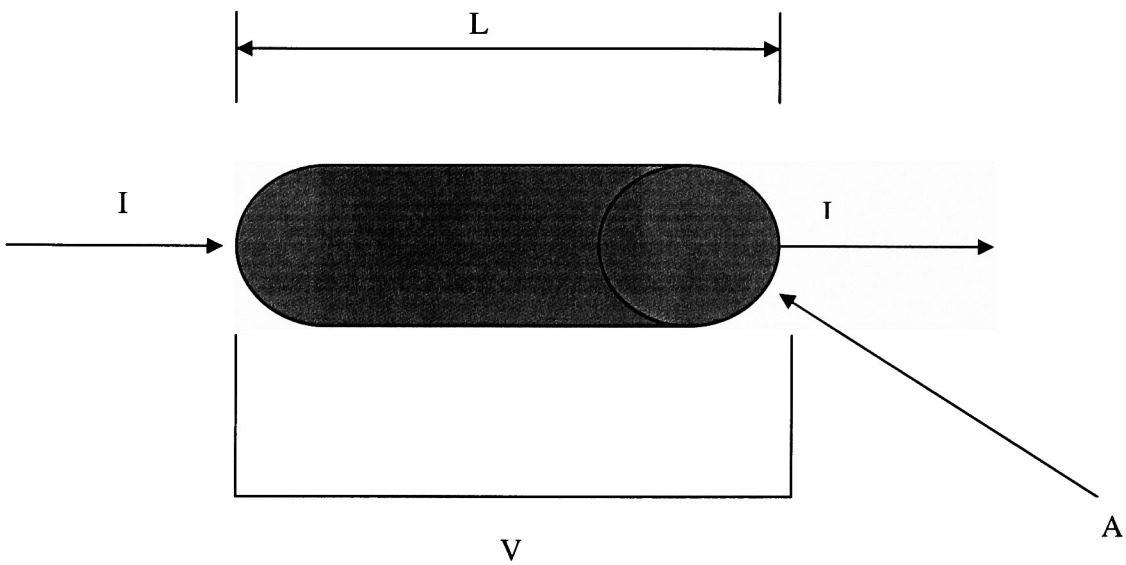

Figure 3: Cylinder carrying current I due to applied potential V

Consider a cylinder with cross-sectional area A and length L with a potential difference (voltage) V applied to its ends. The voltage creates an essentially uniform electric field $\vec{E}$ and essentially uniform current density $\vec{J}$ (current per unit area) within the cylinder parallel to the axis of symmetry of the cylinder [38]. For isotropic materials the resistivity of a material ϱ is given by the local form of Ohm's law; i.e.

$$\varrho = E/J \tag{2.3}$$

where $E \equiv |\vec{E}|$, $J \equiv |\vec{J}|$

The magnitude of the electric field is

$$E=V/L \tag{2.4}$$

and the global form of Ohm's Law is given by

$$R=V/I \tag{2.5}$$

From the above equations and the magnitude of current density

$$J = I/A \tag{2.6}$$

we get the following equation for resistance:

$$R = \varrho\, L/A \tag{2.7}$$

The above equation gives the relationship between resistance and resistivity. The resistance is the property of an object while the resistivity is the property of a material [38]. For most materials, resistivity is linear with temperature and is described by the following empirical relationship

$$\varrho = \varrho_0 [1+\alpha_r (T-T_0)] \tag{2.8}$$

where ϱ_0 is the resistivity at a reference temperature T_0 and α_r is the resistivity temperature coefficient. For silicon α_r = -70 X 10^{-3} K^{-1} and ϱ_0= 2.5x 10^3 Ω-m at 293 K [37]. For most metals such as aluminum, the coefficient of resistivity is positive, indicating an increase in resistivity with temperature. Silicon, however, shows the opposite trend, indicating as silicon heats up, electrical resistance decreases. This is undesirable for thermal microactuators as a substantial increase in current is needed for an additional rise in temperature [37].

2.1.3 Ohmic Heating

If we consider the above conductor with a potential difference V applied across its ends causing a current I to flow through it, then its resistance and potential V are related as V=IR. The power loss (rate of energy loss per unit time) in a resistor appears in the form of thermal energy and is given by

$$P = V I = I^2 R \tag{2.9}$$

This power loss is also known as ohmic heating, Joule heating, or I^2 R loss. Per equation (2.7), for the same resistivity and a given length, members with smaller cross-sectional area will have higher resistance. This difference in cross sectional area allows for different expansion rates for different parts of MEMS devices made of a single material. For a given current input, the smaller cross sectional area member will have a higher resistance, greater increase in temperature and elongate more than other members with the same length due to greater ohmic heating.

2.2 GEOMETRY OF THE THERMAL MICROACTUATOR

The basic MEMS polysilicon electro thermal actuator as shown in Figure 4 uses Joule heating for thermal expansion and movement. The thin, wide and flexure arms are connected together and constrained elastically at the anchors. The anchors in turn are rigidly attached to the substrate. An electric potential difference applied at the anchors generates a non-uniform electric field in it. The electrical resistivity of the material and the current density gives rise to Joule heating. The larger current density in the thin arm causes a greater thermal expansion than that in the wide arm. The thin arm expands and pushes on the wide arm through the end connection. This causes the actuator to rotate clockwise, that is, towards the wide arm side. If the material does not yield, the device returns to its equilibrium position after the potential difference is removed. An advantage of this device is that it requires only one material, so a wide number of geometries are possible through current bulk and surface micromachining processes.

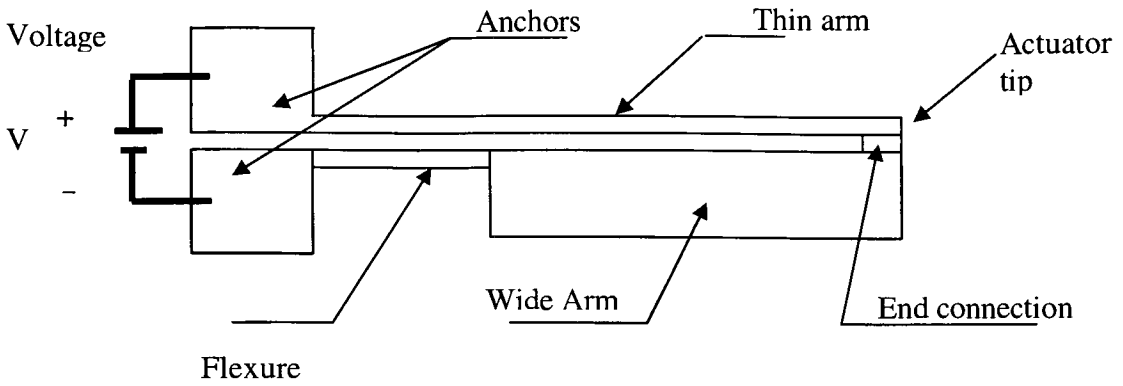

Figure 4: Geometry of the thermal actuator

Design features include a flexure arm between the wide arm and anchors to produce a large deflection of the device. The flexure allows motion of the wide arm. In absence of a flexure, the cold arm would be too stiff to bend. Dimples on the underside of the device prevent stiction to the substrate and bossing helps to keep motion in the plane of the substrate [1]. The amount of deflection produced by the actuator depends upon the temperature difference between the thin and wide arm. Hence, increasing the temperature difference between the two arms increases the thermal efficiency of the actuator. Some methods suggested by Comtois and Bright [5] are to make the cold arm wider or taller or etch a trench under the thin arm to decrease heat loss to the substrate. Hickey [30] has laid down similar guidelines for enhanced performance of the actuator.

The incorporation of the flexure arm in the actuator design is an important design parameter. Ideally, the thinner the flexure arm, the better the deflection performance, as the flexure converts more of the force generated by the hot arm into motion of the actuator tip. However, if the flexure arm is too thin, it may heat up more than the thin arm and get destroyed by the excessive heat. The flexure arm has to be sufficiently long so that the thin arm can bend it elastically. If the flexure arm is too long, then it may expand more than the thin arm and oppose the desired actuator movement [39].

The use of 'backbending' effect for increased force output is often employed in thermal microactuators [5]. When the actuator is driven past the point when it stops deflecting in the

forward direction, plastic deformation of the hot arm results. When the driving force is removed, the actuator is permanently backbent. Then the actuator will start from a 'negative' deflection position [5]. A longer actuator can be used to produce larger force. But with a longer actuator the chances of the device failing with stiction increase. The electrical resistance also increases. In the end, the actuator may actually deliver less force due to bowing. The alternative approach used to increase force output is to employ an array of actuators as shown in Figure 5 rather than change the geometry of the individual actuator. A flexible yoke connecting an array of actuators provides a good method of increasing the force output. Connecting two actuators opposite to each other with a yoke provides pure linear motion of the actuators and combines the force, while retaining desirable force-deflection features of the single actuator.

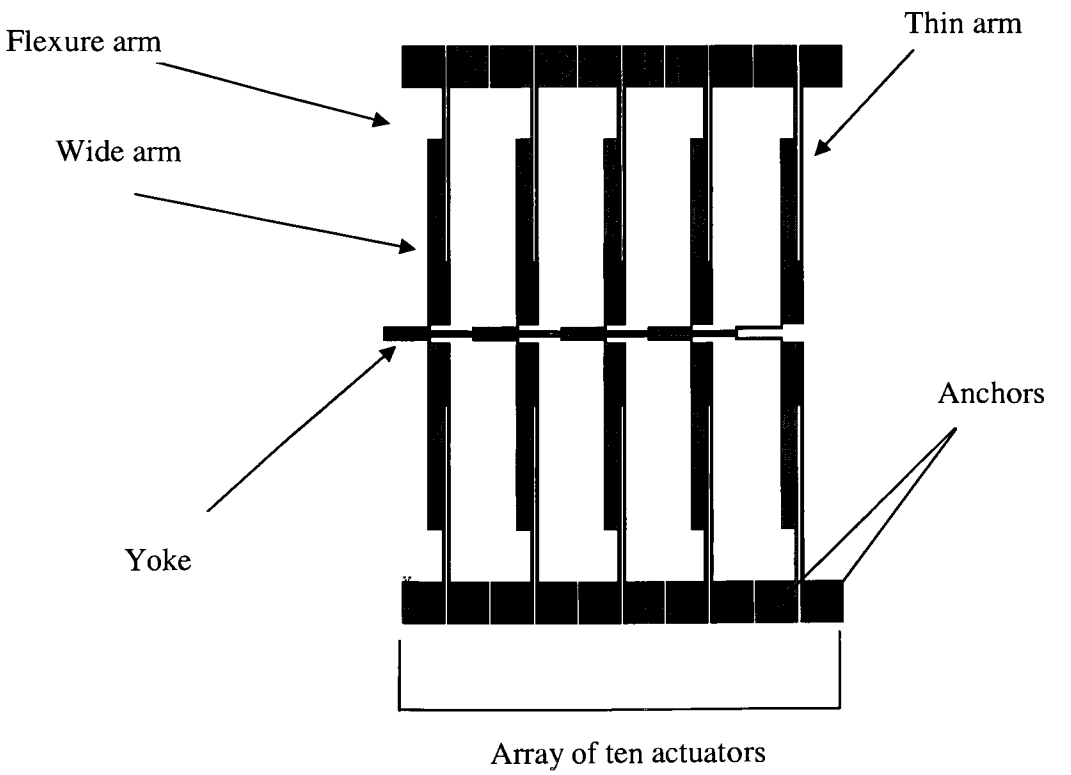

Figure 5: Array of actuators tethered with a flexible yoke

Such microactuator arrays have been successfully employed for rotating micromirrors and stepper motors [5]. The device in this thesis uses a similar arrangement, where the actuators are wired in parallel. One array pushes the rack to bring it in contact with the gear while the other actuates the gear, which in turn rotates the optical phase shifter.

The main advantage for application of these thermal actuators over other MEMS actuators is their simplicity in operation. They are easy to design and fabricate. Another benefit of using these devices is their response time. The thermal response time for such actuators can be as low as 0.3 ms, which encourages their use in sensing applications. They can also be employed in periodic application for millions of cycles without fatigue failure.

The main disadvantage of these actuators is power consumption. The amount of power required for steady state operation can be very high, as a large amount of the heat generated is lost to the surroundings. The force availability from these actuators is also limited. At high voltages the thin arm of the actuator can reach melting temperatures. Buckling of the thin arm is also observed at high voltages [30], and stiction to the substrate can also cause the actuator to buckle.

2.3 ANALYSIS STRATEGY

The implementation of the thermal actuator in the microsystem requires knowledge of basic design parameters, based on the particular application. The thermal actuators in this thesis are designed for specific implementation in optical MEMS. The objective from the analysis of the surface micromachined polysilicon thermal actuator is to get an insight on the deflection, force, current, thermal, power consumption and response characteristics. Based on these characteristics, the actuator can be effectively implemented per the specific need of the microsystem (for example, large deflection, large force, low power consumption, fast response).

Electro-thermal mechanisms involve the coupling of electrical, thermal and elastic energy domains. The analysis of the actuator thus requires the solution of a coupled non-linear thermal boundary value problem. In the electrical energy domain, an electric potential is applied which generates current and serves as the heat source in the thermal domain. Joule

heating in the thermal domain produces a temperature field. The electrical resistivity of the material is highly dependent on temperature. The current distribution depends on the resistivity, which in turn affects the temperature field.

The strain field in the quasi-static thermo-elastic problem is dependent on the thermal expansion. The coefficient of thermal expansion and Young's modulus depend on the temperature. The elastic deformation thus depends on the temperature field obtained from the thermal analysis. However, a reasonable assumption is that geometry changes caused by deformation will not have a significant effect on the heat transfer characteristics. Electrical-thermal effects and thermal-elastic effects are thus separately coupled. The following sections examine this analysis in detail

2.4 BOUNDARY CONDITIONS

The thermal microactuator is generally fabricated by a surface micromachining process such as MUMPs (See Appendix A). Figure 6 shows a 3-D view of the actuator suspended above the substrate after release. The actuator arms are separated from the substrate by a 2 μm air gap while the anchors remain attached to the substrate. The substrate and the surrounding air are not modeled directly but their effects are included indirectly through various boundary conditions. An electrical potential difference V is applied across the anchors, which causes non-uniform Joule heating. The deflection of the actuator due to this heating is parallel to the substrate.

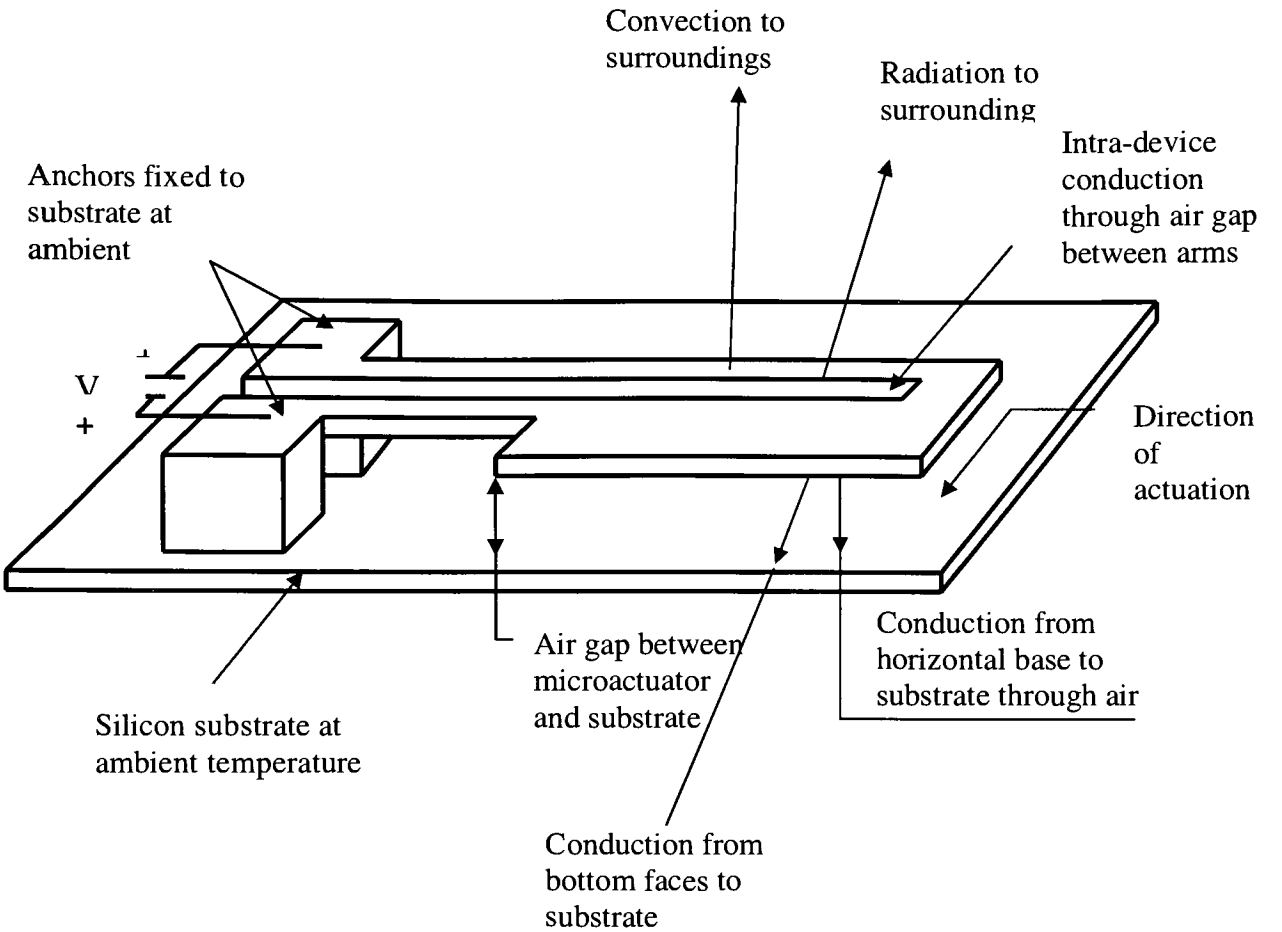

Figure 6: 3-D view of the actuator showing boundary conditions

2.4.1 Heat Transfer Boundary Conditions

The silicon substrate is assumed to be at fixed ambient temperature as it is much larger than the actuator. Hence, a constant room temperature boundary condition is specified at the anchors, which are attached to the substrate [20,40]. The anchors thus act as heat sources and heat sinks to the rest of the actuator. Under normal modes of operation, the actuator will transfer heat to the surroundings and substrate by all three basic modes of heat transfer: conduction, convection and radiation, though some modes will dominate over the others. This section examines these modes of heat transfer in detail.

2.4.1.1 Conduction

The arms of the thermal actuator are separated from the substrate by an air gap and a thin layer of silicon nitride. A portion of the heat generated is lost through the air. The mode of this heat transfer depends on the geometry and setup of the particular device. Hickey [30] has commented that as devices are scaled down to the micro level, conduction dominates the heat transfer. This statement is not entirely true as the heat loss will also depend upon the thickness of the air gap between the substrate and the actuator arms [25,41].

For the devices fabricated by the MUMPs process which are released 2 μm above the substrate, it has been shown that conduction is the major mode of heat transfer through the air [20,22,28,30,40]. The heat loss to the substrate through the air gap is modeled as an effective conductive heat transfer coefficient as shown in Figure 7. This is more computationally efficient than modeling the actuator with the substrate and surrounding air.

In Figure 7, R_a, R_n, R_{Si} represent the thermal resistance of air, silicon nitride, and silicon substrate, respectively. T_c and T_{sub} represent the actuator surface and substrate temperatures, respectively. The thickness of the air, nitride and silicon layers are represented by t_a, t_n and t_{Si} respectively. The thermal conductivities of air, nitride and silicon are denoted by k_a, k_n, k_{Si} respectively, which are the inverses of the respective thermal resistances.

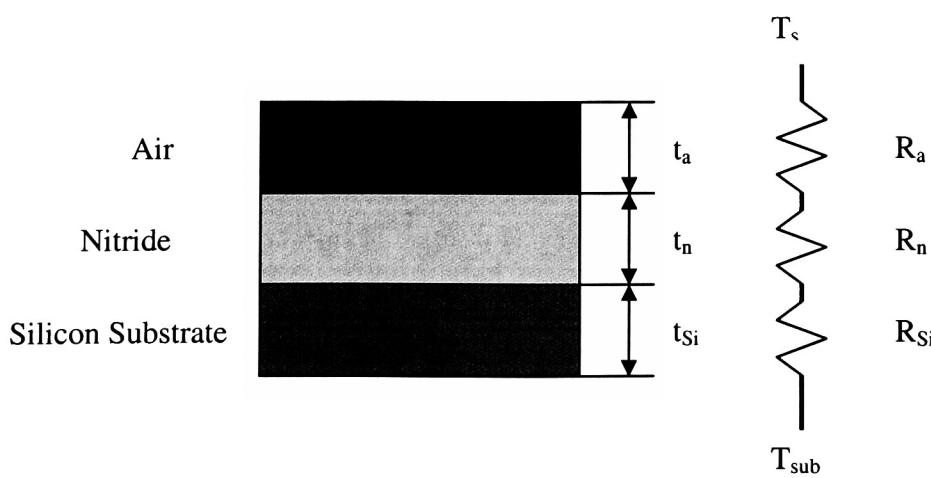

Figure 7: Circuit for computation of conductive heat transfer coefficient

From basic heat transfer analysis, an equivalent heat transfer coefficient h is given by

$$h = \frac{1}{\left(t_a/k_a + t_n/k_n + t_{Si}/k_{Si}\right)} \tag{2.10}$$

As an example, thermal conductivity values at room temperature are k_a = 0.026 W-m^{-1} -°C^{1}, k_n = 2.25 W-m^{-1} °C^{-1}, k_{Si} = 150 W-m^{-1}-°C^{-1}, [20,22,25,28,29]. Typical thickness values are given by t_a =2 μm, t_n = 0.6 μm, t_{Si} = 600 μm (see Appendix A). Equation (2.10) gives h =13,200 W-m^{-2} -°C^{-1}for the horizontal faces which is in basic agreement with the conduction heat transfer coefficient computed by Hickey [30] through a more comprehensive CFD analysis (14,990 W-m^{-2} - °C^{-1}).

However, the thermal conductivity of air is an important parameter in modeling as it is a strong function of temperature. As mentioned above a constant value of 0.026 W-m^{-1}- °C^{-1}at room temperature (20°C) is generally employed for analysis [20,22]. Lott [28] has fitted a third-order polynomial expression based on measured properties given by:

$$k_a(T) = 3.9539 \times 10^{-4} + (9.886 \times 10^{-5})\,T - (4.367 \times 10^{-8})\,T^2 + (1.301 \times 10^{-11})\,T^3 \tag{2.11}$$

where k_a is in W-m^{-1}-°K^{-1} and T is the absolute temperature in degrees Kelvin.

This expression can be employed for temperatures up to and greater than the melting point of silicon (1411°C). The thermal actuators however are rarely taken beyond 800°C due to irreversible changes in the polysilicon that might occur [28]. Figure 8 shows a fit to equation (2.11).

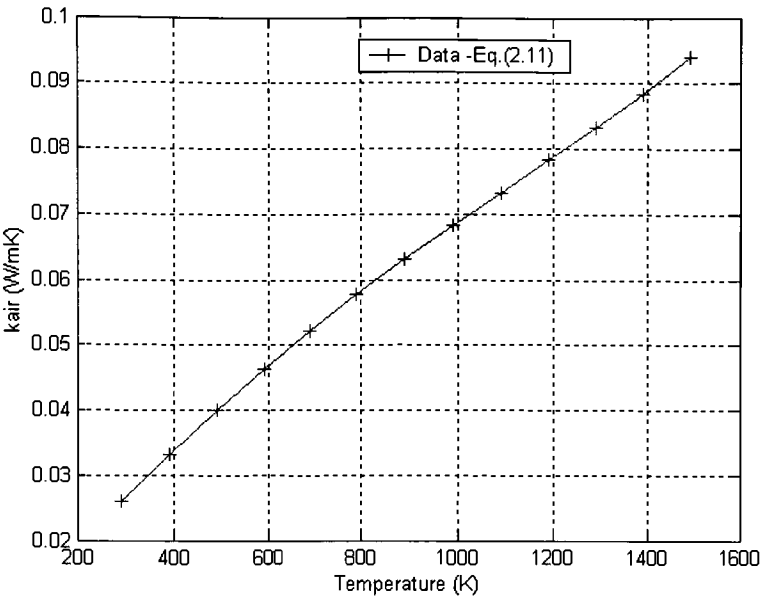

Figure 8: Variation of thermal conductivity of air with temperature

Since the thermal conductivity of air varies with temperature, the conductive heat transfer coefficient given by equation (2.10) also varies. The thermal actuator is analyzed by using a constant value of thermal conductivity of air. The importance of the temperature dependency of the thermal conductivity of air is also investigated using this equation. This will give insight as to whether it is necessary to consider the temperature dependency of thermal conductivity of air or whether a constant value can cover a broad range of temperatures.

For the models, which assume a constant thermal conductivity of air a value of 0.026 $W\text{-}m^{-1}$ $°C^{-1}$ [20,22, 28,29] (20°C) is used for computing the conductive heat transfer coefficient. A constant value of thermal conductivity 2.25 $W\text{-}m^{-1}$ $°C^{-1}$ (20 °C) [20,22] is used for silicon nitride and a constant value of 150 $W\text{-}m^{-1}\text{-}C^{-1}$ (20 °C) is used for silicon for both the models [25].

The conductive heat loss from the vertical faces of the actuator is modeled by multiplying the effective conductive heat transfer coefficient from the horizontal faces by a conduction shape factor [20,22,28,29,40].

The shape factor is given by:

$$S = (t/w)[2t_a/t + 1] + 1 \tag{2.12}$$

where t, w, t_a represent the thickness of polysilicon, thickness of the air gap and the width of the individual polysilicon segment, respectively. This factor is the ratio of the total heat loss from the vertical faces and the bottom of the beam to the heat loss from the bottom of the beam only [22]. This factor is applied to all the models in this thesis.

2.4.1.2 Convection

The actuator will also convect heat from the top horizontal faces to the surrounding air. This heat loss though may be extremely small in comparison with the conductive heat loss. For computation of the heat transfer coefficients, the actuator is divided into four segments: thin arm, wide arm, flexure arm and end connection. There is a limited amount of data available on convective heat transfer at the microscale. Hence, the heat transfer coefficients for the individual segments are computed from the correlations developed for a heated horizontal plate facing upwards. This serves as a good starting approximation in absence of actual data. The expression for the heat transfer coefficients for this case is given as [25,42]

$$hi = \overline{N}uk/L_i \tag{2.13}$$

where $\overline{N}u =$

$$0.54(Ra_L)^{1/4} \; for 10^5 < Ra_L < 2\times10^7$$
$$0.14(Ra_L)^{1/3} \; for 2\times10^7 < Ra_L < 3\times10^{10} \tag{2.14}$$

with

$$Ra_L = \frac{\beta \Delta T g L^3}{\upsilon \alpha} \tag{2.15}$$

Here, L is the shorter dimension of any i^{th} segment. $\overline{N}u$ is the average Nusselt number. Ra_L is the Rayleigh number. β, α, ν, k, ΔT, g denote respectively the volumetric coefficient of

thermal expansion, thermal diffusivity of air, kinematic viscosity of air, thermal conductivity of air, the temperature difference between the segment (Ti) and ambient (T_a) and the acceleration due to gravity. These properties are computed at the mean temperature $T_m = (T_i + T_a)/2$. Since the size of the devices exceeds the range of the heat transfer coefficient expressions the expressions have to be extrapolated to cover the entire range [25]. The variation of the heat transfer coefficients for the thin arm, wide arm, flexure and end connection are shown in Figures 9 and 10. The curves are based on equation (2.13) and are plotted at discrete temperature points of the segment (T_i). Each of the parameters is computed at the mean temperature.

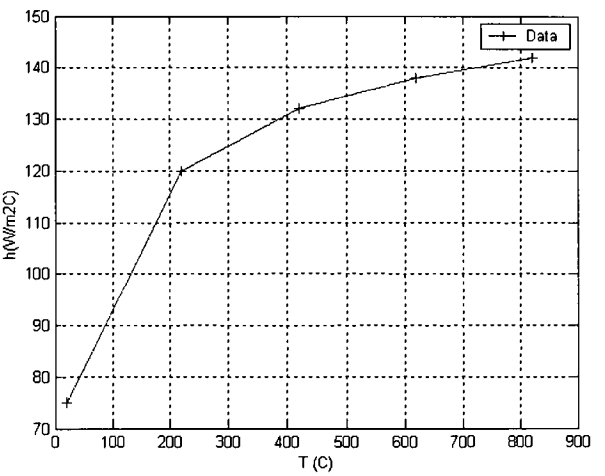

Figure 9: Variation of heat transfer coefficient with temperature for the thin arm, flexure arm and end connection.

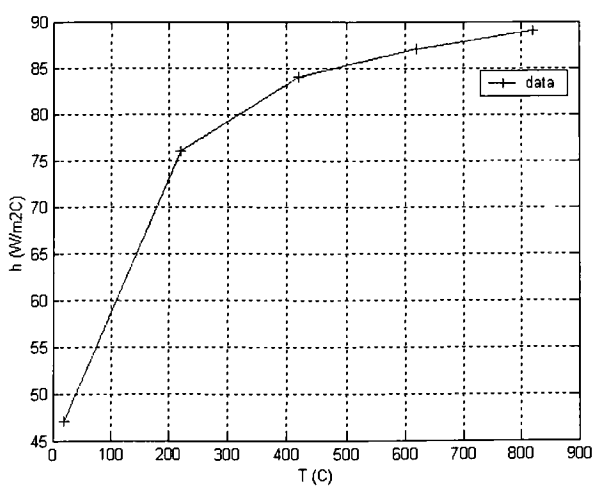

Figure 10: Variation of heat transfer coefficient with temperature for the wide arm

2.4.1.3 Radiation

At high voltages the hot arm reaches extreme temperatures where radiation effects can become important. The radiation heat transfer acts in parallel to the convection heat transfer. Intra-device radiation from the hot arm to the cold arm will also occur through the air gap separating the two arms [20]. This is dependent on the width of the air gap. For such micromachined actuators for small air gaps between the two arms (2 μm) the intra-device radiation that will occur is claimed to be negligible [20]. The effects of radiation are included for all models in this thesis. The application of radiation is discussed in detail in Chapter 3.

2.4.2 Structural Boundary Conditions

The thermal results from the electro-thermal analysis are applied as loads to obtain a quasi-static thermal-elastic solution. Quasi-static deformation implies that inertia effects are negligible, even in the presence of transient temperature variations [25]. The complete thermoelastic problem considers the temperature and strain to be interdependent [25]. The temperature field causes thermal expansion, which contributes to the strain field. The elastic modulus and the coefficient of thermal expansion are also dependent on temperature. Heat generated due to the work of deformation is negligible to that generated by Joule heating [25]. The elastic problem thus depends on temperature but not vice versa [25]. The boundary conditions for the structural problem are constraining the bottom faces of the anchors and applying the temperature field from the thermo-elastic analysis.

2.5 MATERIAL PROPERTIES

The typical surface micromachined MUMPs thermal actuator consists of three polysilicon layers poly0, poly1 and poly2, with poly1 as the released structural layer (Appendix A). Thermal as well as structural material properties of polysilicon layers are highly dependent on temperature. This temperature dependency must be included for accurate implementation of the boundary conditions described above. This section describes the temperature

dependencies of polysilicon thermal and structural material properties applicable to the analysis.

2.5.1 Thermal Conductivity of Polysilicon

A solid is comprised of free electrons and atoms bound in a periodic arrangement called lattice. Crystalline materials show higher thermal conductivities than amorphous materials and are also more sensitive to temperature. Thermal conductivity of crystalline silicon has been reported to drop from 150 to 22 $W\text{-}m^{-1}\cdot{}^{o}C^{-1}$ between room temperature (20°C) and melting point (1411°C) [28,43]. Such variations in polysilicon have not been reported which may be attributed to variations in impurity concentrations and grain size from different fabrication processes [28,44].

Okada et al. [33] measured the thermal conductivity of polysilicon in the temperature range from 80 to 400 K. They reported a thermal conductivity of 29 $W\text{-}m^{-1}\text{-}{}^{o}C^{-1}$ with little variation above room temperature. Tai et al. [28,45] reported the average thermal conductivity for heavily doped (10^{20} atoms/cm^3) LPCVD polysilicon film as 32 $W\text{-}m^{-1}\cdot{}^{o}C^{-1}$.

Manginell [31] fit to experimental data the thermal conductivity of large-grained laminated polysilicon measured from 25°C to 527 °C. This silicon was also heavily doped with phosphorus (10^{20} atoms/cm^3). The fitted equation from this study is

$$k_p(T) = [(-2.2*10^{-11})T^3 + (9.0*10^{-8})T^2 + (-1.0*10^{-5})T + 0.014]^{-1} \qquad (2.16)$$

where k_p is in $W\text{-}m^{-1}\text{-}{}^{o}C^{-1}$ and T is in °C. Figure 11 shows a curve fit to Manginell's data based on equation (2.16).

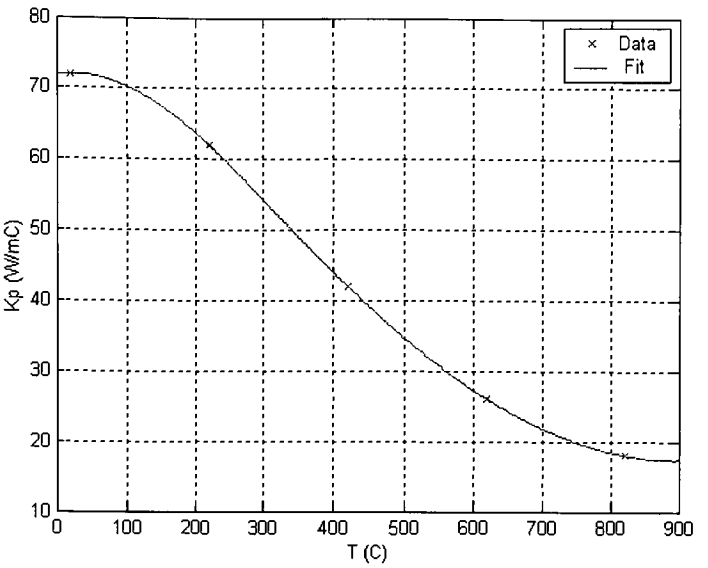

Figure 11: Variation of thermal conductivity of polysilicon with temperature

McConnell et al. [32] investigated the influence of impurity type and concentration for 1 μm thick LPCVD polysilicon layers doped in the range of 2 X 10^{18} to 4.1 X 10^{19} atoms/cm^3 between 20 and 320 K. They reported that the thermal conductivity of doped polysilicon strongly depends on grain size, concentration and type of doping and deposition temperature. The data from their study shows strong reduction in the thermal conductivity values of doped polysilicon at all temperatures in comparison with that of similarly doped single-crystal silicon. The room temperature (293 K) thermal conductivity of the doped polysilicon layers was reported to be in the range of 45.6 W-m^{-1}-$°C^{-1}$ to 57.6 W-m^{-1}-$°C^{-1}$ [32]. The measurement of thermal conductivity for the MUMPs process is most consistent with the work of Tai et al. [45]. Other electro-thermal studies employ a value between 29 to 34 W-m^{-1}-$°C^{-1}$ [16,20,22]. A constant value can be employed to account for temperature dependency with small grain sizes and high dopant concentrations such as 10^{20} atoms/cm^3. However, Manginell's [28] data must be examined because of the contribution of polysilicon's grain size and doping concentration in the temperature dependency of thermal conductivity.

The thermal actuator in this thesis is analyzed with a constant value of thermal conductivity of 32 W-m^{-1} -$°C^{-1}$ from the studies of Tai et al. [45]. The model is also investigated employing

Manginell's equation to account for the variation in the thermal conductivity. This gives insight as to whether a constant value can be employed or whether the full temperature dependency must be included for the analysis. The model with the best prediction at steady state is then used for further analysis.

2.5.2 Electrical Resistivity of Polysilicon

Electrical resistivity of polysilicon is one of the most important parameters in the electro-thermal modeling of microactuators. Polysilicon shows a higher value of resistivity in comparison with similarly doped single crystal silicon [28]. At low dopant concentrations resistivity changes slowly, at intermediate levels it falls rapidly and at high concentrations (10^{20} atoms/cm^3), it approaches the resistivity of single crystal silicon for similar dopant concentrations [28]. Beyond approximately 800-1000 °C resistivity is difficult to estimate due to irreversible structural changes in polysilicon [28]. High currents and self-heating cause this phenomenon, which results in local melting of polysilicon crystal grain boundary layers [28]. Above these temperatures, Kato and Ono [36] report that the resistance drop can be restored by passing a current that is lower than previously applied but higher than that needed to cause boundary layer melting. The second current will cause heating of boundary layer because of resistance drop that will cause a thermal diffusion of the concentrated impurity.

Equation (2.8) has been employed to model the temperature dependency of resistivity in microactuator applications in polysilicon [16,20,28]. The equation however is not accurate above extreme temperatures such as 800-1000 °C. The resistivity temperature coefficient α_r for polysilicon has been reported in the range 1.1 X 10^{-3} °C^{-1} to 1.3 X 10^{-3} °C^{-1} [16,20]. For models in this thesis a value of 1.25 X 10^{-3} °C^{-1} was used [28]. A resistivity value of 2 X 10^{-3} Ω-cm at room temperature (20°C) was obtained from the MUMPs run data [46,47]. The temperature dependency of electrical resistivity is shown in Figure 12. The curve is plotted using equation (2.8) at discrete temperature points. As noted above, the equation can be employed approximately up to 800 °C. This limits the application of the above equation in the actuator analysis approximately upto 800 °C. Above 800 °C no accuracy in equation (2.8) is claimed.

An alternative to this equation has been implemented by Mankame [25]. Since the temperature depends on the applied voltage, he computed experimentally the variation of net electrical resistance of the device with respect to the applied voltage. The geometry of the actuator is then used to compute a mean value of resistivity for each voltage, which is then implemented in the analysis as a constant value for the specified voltage [25]. In absence of facilities for experimentation this method was not employed in this thesis.

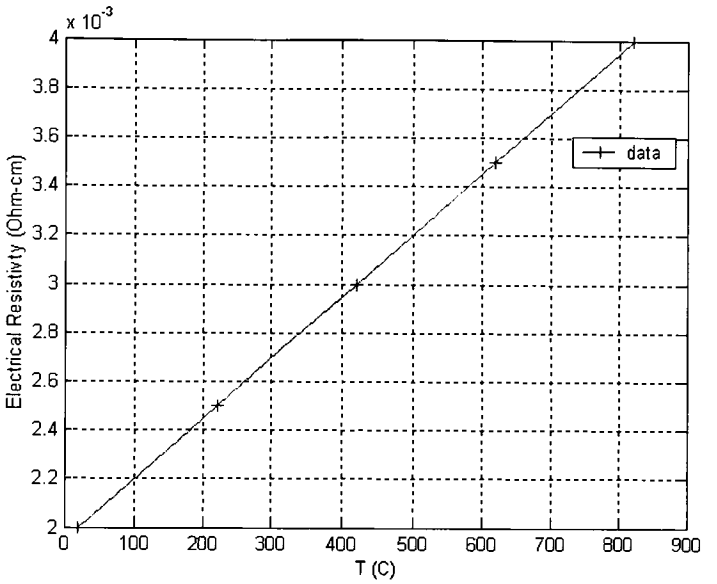

Figure 12: Variation of electrical resistivity of polysilicon with temperature

2.5.3 Thermal expansion coefficient

The temperature dependency of the thermal expansion coefficient from empirically fit data is given by [28,33]:

$$\alpha(T) = (3.725\{1-\exp(-5.88*10^{-3}(T-125))\} + 5.548*10^{-4}T) * 10^{-6} \qquad (2.17)$$

valid for 120 K $\leq$ T $\leq$ 1500 K. A curve fit to the above equation is shown in Figure 13. This equation has been typically employed by others to model the expansion of polysilicon [16,28]. A constant value of 2.7 X 10^{-6} K^{-1} (near 293 K) is used when the temperature dependency is not included in analysis [20,28].

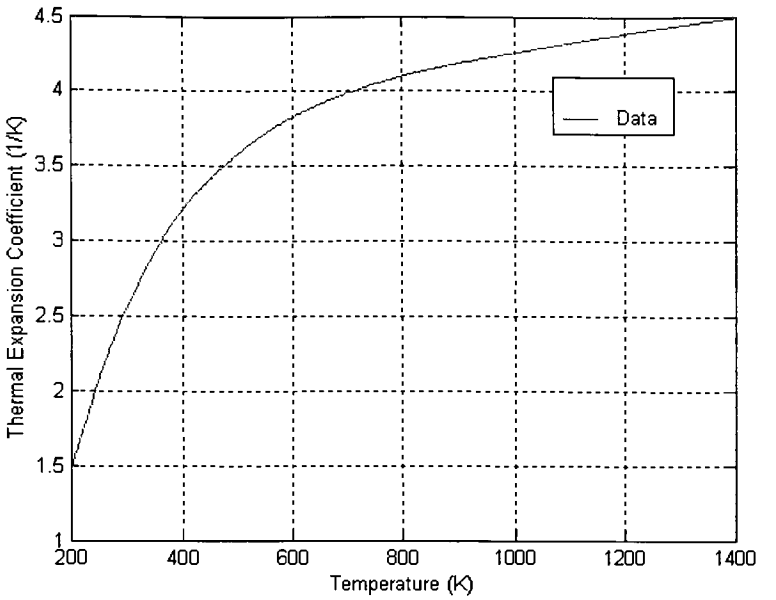

Figure 13: Variation of the coefficient of thermal expansion of polysilicon with temperature

2.5.4 Specific Heat

Manginell [31] has carried out experiments on polysilicon and single crystal silicon. He has concluded that within a 5 percent error bound the specific heat of silicon can be used for polysilicon. Equations curve fit to data for specific heat c of silicon are [28]:

For 292 K ≤ T ≤700 K

$$c= (1.976362*10^{-6}) T^3- (3.766786*10^{-3}) T^2+ (2.622954)T+2.149586*10^2$$

For 701 K≤ T ≤ 1685 K

$$c= -(3.377784*10^{-5})T^2+(2.388945*10^{-1})T+7.324063*10^2 \quad (2.18)$$

A constant value of 705 J-kg^{-1}-K^{-1} (at 293 K) is typically used when the temperature dependent expression is not employed. Figure 14 shows the temperature dependency of the

specific heat fitted using equation (2.18). Unless otherwise specified analysis in this thesis employs this temperature dependency for all the models.

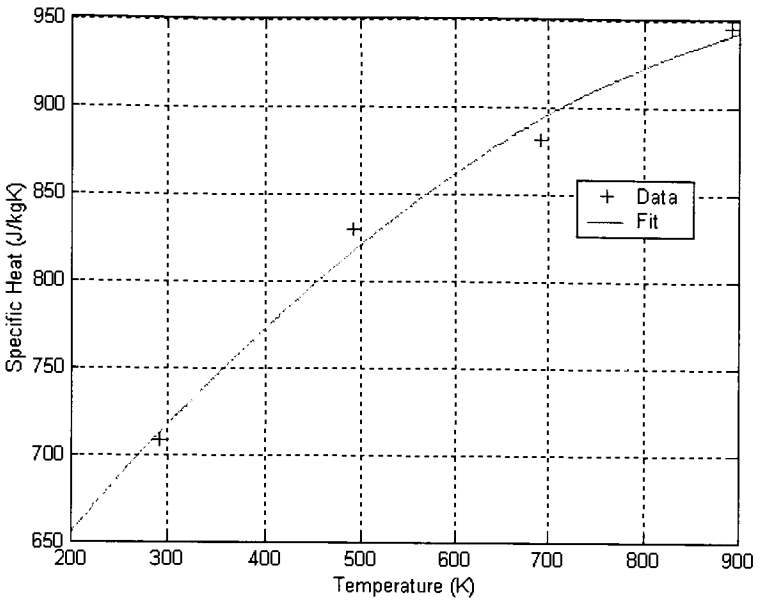

Figure 14: Variation of specific heat of polysilicon with temperature

2.5.5 Other Properties

Sharpe et al. [34] have reported the elastic modulus of polysilicon for MUMPs polysilicon specimens to be 158 ± 10 GPa with no effects of specimen size. They have also reported a maximum decrease of 10% or 15 GPa in the Elastic Modulus of polysilicon from 0 to 250 °C. A constant value of 169 GPa has been used for the models in this thesis [34,48] and the modulus of elasticity decrease is employed for temperature dependency. A Possion's ratio value of 0.22 is used [34,48,28]. The yield strength of polysilicon is reported to be 1.2 GPa [48], and the melting point is approximately 1411 °C [28]. A value of 0.6 is employed for the emissivity; a value of 2330 kg/m^3 is used for the density and a value of 5.67 X 10^{-8} W-m^{-2}-°C^{-4} is used for the Stefan-Boltzmann constant [28,29]. A constant value of 2.25 W-m^{-1}-°C^{-1} is used for the thermal conductivity of silicon nitride [22] and a constant value of 150 W-m^{-1}-°C is used for the thermal conductivity of silicon [25].

2.6 FORCE MEASUREMENTS

Thermal actuators are typically utilized to do work. In addition to deflection, they are required to produce force. Consider an actuator as shown in Figure 15. For simplicity, the actuator is shown as a cantilever beam. With external force equal to zero, the actuator will deflect an amount d_0 resulting from an applied input potential difference V at the anchors.

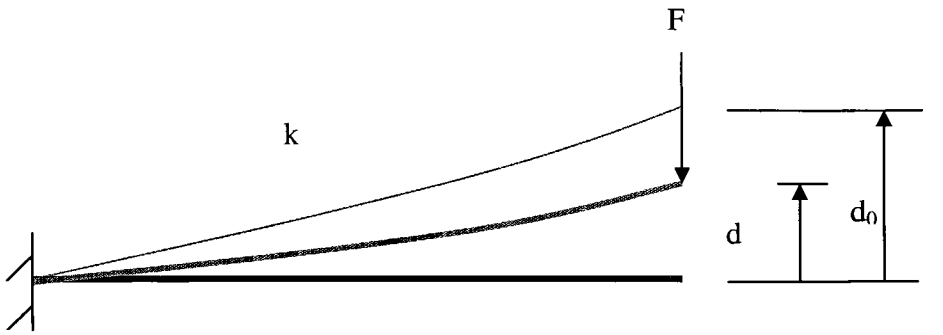

Figure 15: Loaded actuator for force measurements. Actuator is represented as a cantilever beam for simplicity.

The application of an external load F will result in a deflection d given by

$$F = k(d_0(V) - d)$$

Or

$$d = \frac{F - kd_0(V)}{k} \tag{2.22}$$

where k is the stiffness of the actuator. If the elastic strain of the actuator is small, then stiffness k is proportional to Young's modulus. Thus, if the temperature field in the actuator is constant, then k is constant whenever small strains are present. In terms of design, it is easiest to fix the required actuation distance. Then the force available from the actuators can

be determined. Alternatively one can fix force as the design criteria and determine the maximum actuation distance the actuator can provide while still meeting the force design.

Further if there are N numbers of similar actuators coupled together in an array (figure 2) then equation (2.22) modifies to [49]:

$$F = Nk(d_0(V) - d) \tag{2.23}$$

2.7 TRANSIENT RESPONSE

Typically, standard thermal actuators can respond in 0.3 to 0.4 ms, but each segment of the actuator will have a different response time. The response time is dependent on the thermal boundary conditions and material properties such as density and specific heat. Since thermal actuators have a small mass and high heat transfer coefficient, they have a small time constant, where the time constant is defined as the time required to reach 63% of a steady state temperature imposed by a constant voltage. The response time of the thermal actuator is the time required to achieve 99% of the theoretically steady state temperature profile.

In this thesis, the actuator is driven by a periodic pulse input voltage signal to investigate the response time. The remaining boundary conditions remain essentially the same in each pulse. Figure 16 shows the first pulse input signal.

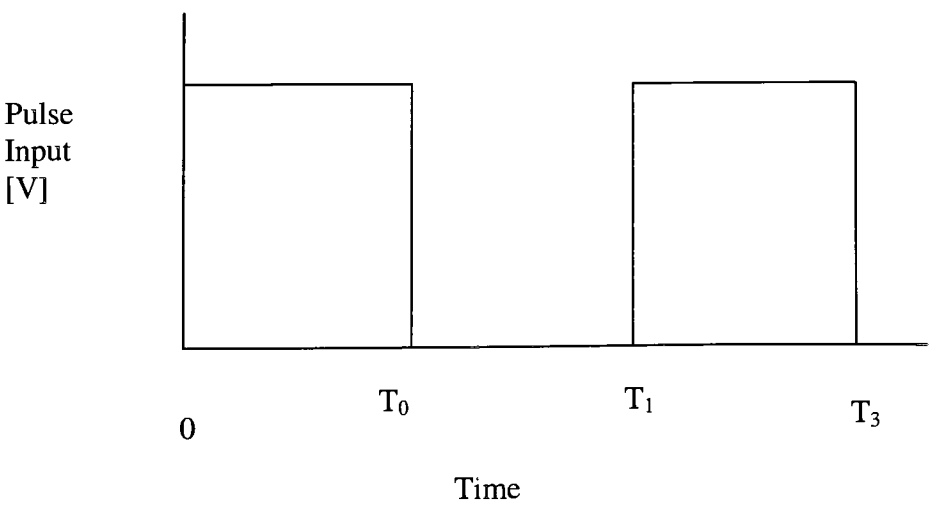

Figure 16: Periodic voltage pulse input signal

The pulse can be varied in width and/or amplitude. Then, depending on the time response of the actuator it may not have time to reach steady state or cool down completely. This will control the deflection response of the actuator

2.5 2D APPROXIMATION

Experimental results show that the motion of the actuator tip is essentially parallel to the substrate. Hence, it would be desirable to conduct a 2D analysis of the actuator. Figure 17 shows the 2D view of the actuator. Material properties will be the same as those applied for the 3D analysis. The 2D approximation arises mainly from the heat transfer boundary conditions. In the 2D case, it is not possible to model the conductive heat transfer from the bottom and the sidewalls of the actuator to the substrate, which are potentially a major source of heat loss in the device, as seen previously. It will be possible to model convection and radiation through the sides of the actuator.

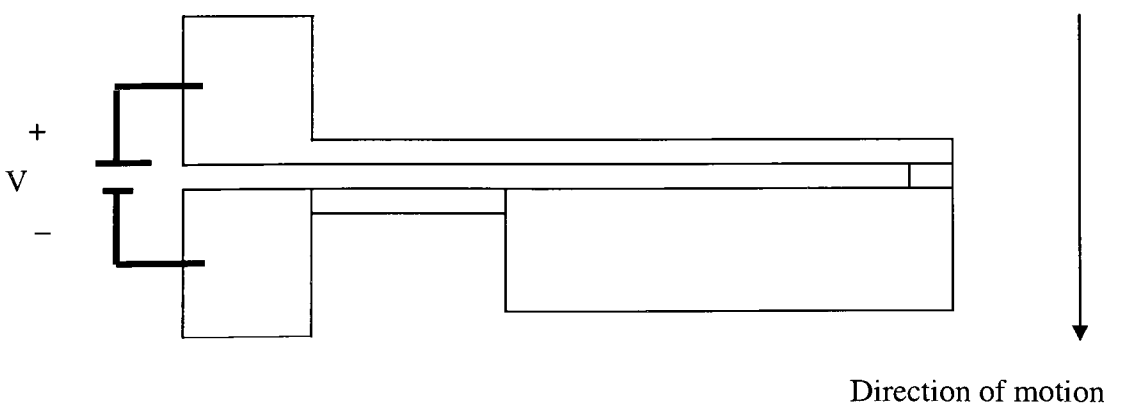

Figure 17: 2D (top view) model of the thermal actuator

CHAPTER 3

FINITE ELEMENT ANALYSIS

This chapter describes the methodology of solving the problem explained in Chapter 2. Finite element analysis is implemented to solve the electro-thermal-elastic problem. The chapter explains the physics of the finite element solution. The finite element package ANSYS 5.6/7.0 [50] is implemented for obtaining the solution. It offers strong non-linear capabilities for solving such a problem [51]. The chapter ends with an overview of the elements selected for the analysis.

3.1 FINITE ELEMENT METHOD

Figure 18 shows a 3D view of the thermal actuator, which is discretized into a contiguous set of finite elements connected at nodes.

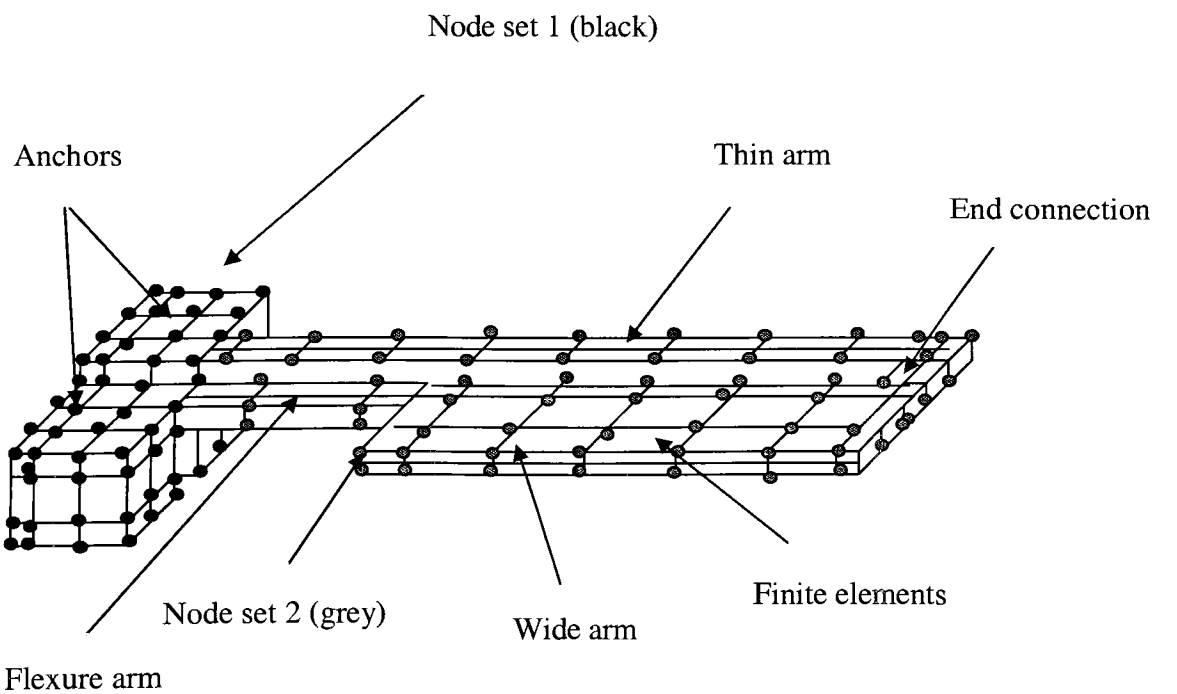

Figure 18: Finite element model of the thermal actuator.

The actuator is divided into five separate segments namely: anchors, hot arm, end connection, cold arm, and flexure arm for application of the boundary conditions. The boundary conditions are applied as explained in the previous chapter. An overview of the boundary conditions is given below for convenience:

1. Application of potential difference (voltage) at anchors.
2. Application of ambient temperature at anchors.
3. Anchors are structurally constrained for all degrees of freedom.
4. Application of conductive heat transfer coefficient including shape factor at base of thin arm, flexure arm, wide arm and end connection.
5. Application of convection on top faces of thin arm, wide arm, end connection and flexure arm.
6. Application of radiation from thin arm, wide arm, end connection and flexure arm faces.

The thermal actuator is separated into two parts: the anchors and the arms. Figure 18 shows the representation of the elements and nodes for the two parts. The solution is computed at each node of the actuator. The terminology for the physics of the problem is explained below.

3.1.1 Terminology

{I} = Nodal value of net current

{V} = Nodal voltages

{T}= Nodal temperatures

$\{\dot{T}\}$= Variation of nodal temperatures with time

{q}= Nodal value of net heat flow.

$\{q_v\}$= Heat flow into node caused by Joule heating

$$\{d\} \equiv \begin{Bmatrix} d_x \\ d_y \\ d_z \end{Bmatrix} = \text{Nodal displacements}$$

$$\{F\} \equiv \begin{Bmatrix} F_x \\ F_y \\ F_z \end{Bmatrix} = \text{Net nodal forces}$$

$\{\alpha(T)\}$= Thermal expansion vector

$[\rho(T)]$= Electrical conductivity matrix

$[K(T)]$= Thermal conductivity matrix

$[C(T)]$= Specific heat matrix

$[Y(T)]$= Young's Modulus matrix

3.1.2 Steady state analysis

This effort borrows work from the work of Kohnke and Swanson [52] and is included here for completeness.

Step 1: Initially a nodal temperature field {T} is assumed. The material properties $\rho(T)$, K (T), C (T) are generated from the assumed thermal profile. There are two inter-relationships between the electrical and thermal part of the solution. The Joule heating (q_v) used by thermal solution is generated from electrical part of solution while the electrical resistivity $\rho(T)$ is computed from the thermal part of the solution. The subscripts denote node set 1 at the anchors and node set 2 at the rest of the actuator (Figure 18). Ohm's law applied to the system requires:

$$\begin{Bmatrix} I_1 \\ I_2 \end{Bmatrix} = \begin{bmatrix} \rho_{11}(T) & \rho_{12}(T) \\ \rho_{21}(T) & \rho_{22}(T) \end{bmatrix} \begin{Bmatrix} V_1 \\ V_2 \end{Bmatrix} \tag{3.1}$$

Voltage and current partitions form a complementary set of unknowns:

Variable	Node set 1	Node set 2
V	Known	Unknown
I	Unknown	Known = 0

From the initially assumed temperature profile, an initial electrical resistivity matrix is computed. The nodal voltage at the anchors is specified and the net nodal current at the arms is zero. Solution of equation (3.1) computes the nodal voltage distribution in the arms of the actuator and the net nodal current at the anchors.

Step 2: Step 1 is now applied to equation (3.2) to compute the heat flow in the actuator. The thermal conductivity matrix is computed from the thermal profile. The net nodal heat flux in the arms is zero. Joule heating is computed from the nodal current and electrical resistivity obtained from equation (3.1). Joule heating is applied to compute an updated thermal profile of the actuator with appropriate thermal boundary conditions. This establishes an updated set of nodal temperatures.

$$\begin{Bmatrix} q_1 \\ q_2 \end{Bmatrix} = \begin{bmatrix} K_{11}(T) & K_{12}(T) \\ K_{21}(T) & K_{22}(T) \end{bmatrix} \begin{Bmatrix} T_1 \\ T_2 \end{Bmatrix} + \begin{Bmatrix} q_{v_1} \\ q_{v_2} \end{Bmatrix} \tag{3.2}$$

Variable	Node set 1	Node set 2
T	Known	Unknown
q	Unknown	Known = 0

Step 3: The thermal profile computed in Step 2 modifies the temperature dependent electrical and thermal resistivity matrices. Using the new electrical resistivity matrix; Steps 1 and 2 are repeated until a converged temperature profile is obtained. This establishes the steady state temperature profile of the actuator.

Step 4: The previous steps computed a steady-state converged thermal profile. The nodal temperatures are now applied as loads for the thermal-structural solution. The anchors are structurally fixed while initially the net nodal forces at the arms of the actuator are zero. The thermal profile is applied to compute the thermal expansion. Equation (3.3) gives the nodal displacements.

$$\begin{Bmatrix} F_1 \\ F_2 \end{Bmatrix} = \begin{bmatrix} Y_{11}(T) & Y_{12}(T) \\ Y_{21}(T) & Y_{22}(T) \end{bmatrix} \begin{Bmatrix} d_1 \\ d_2 \end{Bmatrix} + \begin{Bmatrix} \alpha_1(T) \\ \alpha_2(T) \end{Bmatrix} \tag{3.3}$$

Load	Node set 1	Node set 2
d	Known = 0	Unknown
F	Unknown	Known=0

3.1.3 Transient dynamic analysis

A transient dynamic analysis is conducted to compute the thermal response and time constant of the actuator. This is computed by inclusion of the mass and specific heat in the analysis. Equation (3.2) is modified as

$$\begin{Bmatrix} q_1 \\ q_2 \end{Bmatrix} = \begin{bmatrix} K_{11}(T) & K_{12}(T) \\ K_{21}(T) & K_{22}(T) \end{bmatrix} \begin{Bmatrix} T_1 \\ T_2 \end{Bmatrix} + \begin{Bmatrix} q_{v_1} \\ q_{v_2} \end{Bmatrix} + \begin{bmatrix} C_{11}(T) & C_{12}(T) \\ C_{21}(T) & C_{22}(T) \end{bmatrix} \begin{Bmatrix} \dot{T}_1 \\ \dot{T}_2 \end{Bmatrix} \tag{3.4}$$

Load	Node Set 1	Node Set 2
T	Known	Known
q	Unknown	Known = 0
$\dot{T}$	Known = 0	Unknown

The temperature field is then updated by numerical integration in time, and Joule heating is updated using equation (3.1).

3.1.4 Force applications

As explained previously actuators are generally employed to do some form of work. Equation (2.23) can be employed to compute the force of the actuator through its range of motion. The deflection at this node (node 3 in Figure 19) can be found by a modification of equation (3.3):

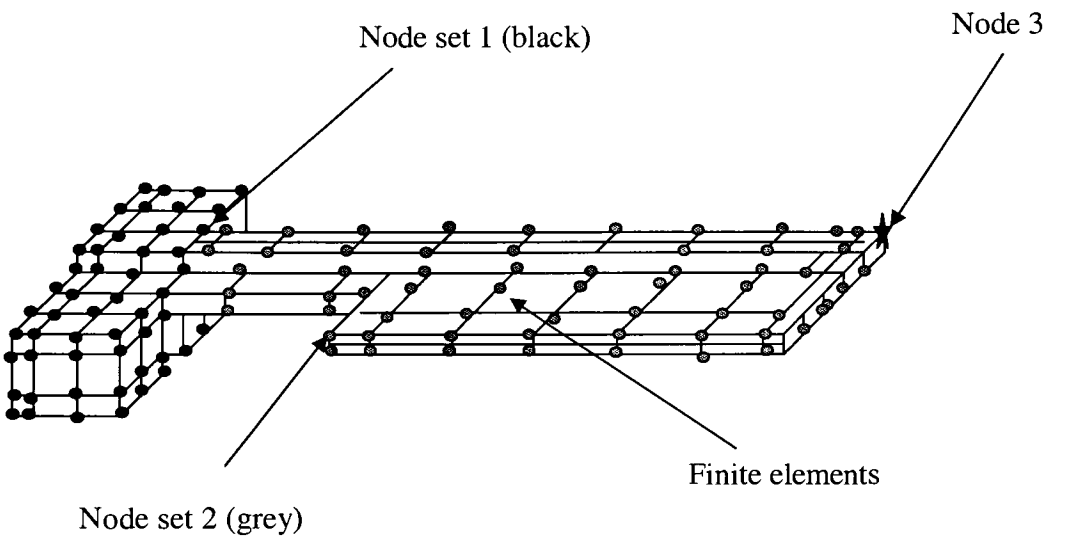

Figure 19: Finite element model of actuator for force computation

$$\begin{Bmatrix} F_1 \\ F_2 \\ F_3 \end{Bmatrix} = [Y(T)] \begin{Bmatrix} d_1 \\ d_2 \\ d_3 \end{Bmatrix} + \begin{Bmatrix} \alpha_1(T) \\ \alpha_2(T) \\ \alpha_3(T) \end{Bmatrix} \tag{3.5}$$

Variable	Node set 1	Node set 2	Node set 3
d	Known = 0	Unknown	Unknown
F	Unknown	Known = 0	Known

The deflection at node 3 is the desired deflection arising from specified external load at node 3.

3.2 ELEMENT SELECTION

The electro-thermal-elastic analysis can be solved by two methods in ANSYS. The first method called the sequential solution, applies the thermal solution from the thermo-electric domain as body force loads on the thermal-elastic domain. In ANSYS, PLANE67 and PLANE42 can be used for this purpose [53]. These elements however, can only represent a 2-D model. Hence, they are not capable of supporting surface boundary conditions such as conduction to the substrate. Alternative 3-D elements offered by ANSYS to remedy this situation are SOLID69 and SOLID45. These elements can be used to solve the electro-thermal and thermo-elastic problems separately with all the necessary boundary conditions.

Another approach to solving the problem is using a 3D element with all the appropriate degrees of freedom applicable to the electro-thermal-elastic analysis (VOLT, TEMP, UX, UY, UZ). This is called the direct method. ANSYS offers SOLID5 and SOLID98 elements for this purpose. SOLID5 is a 8 noded brick element while SOLID98 is a 10 noded, tetrahedral element. Out of these, SOLID98 is capable of supporting irregular geometry [53].

The steady state simulations in this thesis are done using the direct method employing SOLID98 elements. These elements show good convergence rate and allow the application of all the necessary boundary conditions. Inclusion of radiation, however, is computationally

more expensive. The direct method displays convergence problems in the transient solution, when small time steps are used, which may be attributed to the small inertia of the device.

3.2.1 Radiation Implementation in ANSYS

Thermal radiation depends on the fourth power of the body's absolute temperature, which makes the analysis highly non-linear. Radiation is modeled by an enclosure, which is a set of surfaces radiating to the ambient air or to another surface. If the surfaces radiate to ambient air a space node must be created for representing the ambient temperature. Only the emissivity of the body and Stefan-Boltzmann constant needs to be specified in the analysis.
ANSYS offers three methods for the inclusion of radiation [53]. The first method involves superimposing a mesh of SURF152 elements on the original SOLID98 mesh. These elements capture radiation between surface and a point. The second method called, the AUX12 method, imposes a mesh of SHELL57 on the original mesh and creates a matrix of form factors. The last method called the Radiosity Solver method, allows the creation of an enclosure for radiating to a space node, which captures the ambient temperature. The method computes the outgoing radiative heat flux for each surface when the temperatures of all surfaces are known. The radiosity solver is a relatively easy method in comparison with the other methods. It does not require superimposition of surface elements on the original mesh and the form factors are computed automatically. The method shows a fairly good convergence rate. The radiating surfaces are defined by an enclosure and typically a space node is required to be created which captures the radiation from the surface of the enclosure to ambient. The radiosity solver method is employed for analysis of all the models in this thesis.

CHAPTER 4

PARAMETRIC STUDIES

This chapter describes the results of parametric studies conducted on the thermal actuator employing the finite element analysis model developed in Chapter 3. The models provide information on the relative importance of thermophysical properties of polysilicon that influence actuator parameters, performance of the actuator in vacuum, transient response, power and energy requirements and force characteristics. Section 4.1 describes important modeling assumptions. Section 4.2 gives the layout of the analysis procedure. Section 4.3 describes the actuator nomenclature. Section 4.4 describes the analytical model. Section 4.5 discusses the results of a mesh refinement study. Section 4.6 evaluates the inclusion of shape factors by analyzing the conductive heat loss thermal profile. Sections 4.7 and 4.8 describe the influence of polysilicon material properties on actuator deflection and thermal profile in air in comparison with experimental and analytical data. Section 4.9 compares results from 2D approximation of the actuator with the best 3D model that matches experimental data. Section 4.10 provides insight into application of these actuators in vacuum over an air environment. Section 4.11 compares the experimental current characteristics of the actuator in air and vacuum to those predicted by the finite element model. In Section 4.12 dynamic performance of the actuator in air and vacuum is examined. Section 4.13 compares the power and energy performance of the thermal actuator in air and vacuum. Section 4.14 extends the transient model to observe the effects of pulse width modulation for specific actuator applications. Finally, Section 4.15 describes force characteristics of the actuator.

4.1 MODELING ASSUMPTIONS

1. The modeling is based on the MUMPs process. All the relevant data for the thermophysical properties is obtained from the MUMPs runs used for the fabrication of these actuators [46].

2. The simulations are conducted to the best available data in regards to the thermophysical properties of polysilicon.
3. The MUMPs process produces devices, which do not exactly conform the specified geometry of the device. The simulations are conducted for the specified geometry.
4. With respect to stress-strain (constitutive) relations, polysilicon is assumed as a homogenous and isotropic material.
5. The doping profile is not uniform in the MUMPs process. The polysilicon is doped by diffusion. As a result, the sidewall is more heavily doped than the center. This leads to electrical resistivity variations across the structure. The models in this thesis assume a uniform doping profile.
6. A direct heat path to the substrate is assumed. The spreading resistance in the substrate, which occurs when heat flows from a smaller cross sectional area to a larger cross sectional area, is neglected [54,55].
7. The conductive heat loss from the vertical walls of the thermal actuator is accounted by taking into account the conduction shape factor (equation 2.12).
8. The essential boundary conditions are applied for the analysis. This assumes the substrate to act as a large thermal mass at ambient temperature.
9. The intra-device conduction from the air gap between the arms is neglected.
10. The finite element models are compared to the best approximation of analytical and experimental data available.

4.2 ANALYSIS STRATEGY

1. The material properties of polysilicon are highly dependent on temperature. Using finite element analysis the importance of the temperature dependencies of the properties is examined sequentially by comparison with experimental and analytical results. The maximum deflection achieved by the actuator is used as criteria for comparison of the models.
2. A mesh refinement study is conducted on a finite element model assuming constant material properties. The study is used to define the mesh density, which is employed for analysis of the rest of the finite element models.

3. The inclusion of shape factors to account for the heat loss from the sidewalls of the actuator affects the analysis results considerably. A comparison is made between the direct heat path finite element model and the comprehensive model, which includes the air around the actuator to observe the effect of inclusion of shape factors. This will provide insight whether the shape factor are appropriate for use in further finite element analysis.
4. Initially the thermal actuator is analyzed with constant material properties. Then, the variation in electrical resistivity, coefficient of thermal expansion and modulus of elasticity is introduced sequentially.
5. The thermal conductivity of polysilicon is an important parameter in the analysis. Polysilicon grain size and dopant concentration affect the temperature dependency of the thermal conductivity. This variation in thermal conductivity is examined in the finite element model.
6. The thermal conductivity of air increases with temperature. The model is examined by including a temperature dependent conductive heat transfer coefficient of air.
7. The model which agrees closely with experimental data is compared to a similar 2D analysis to verify if the 2D model approximates the actuator characteristics.
8. The best model is then compared for current characteristics obtained from the finite element analysis to that predicted by experiment.
9. Transient analysis of the actuator is then performed, which provides insight into the response time predicted by finite element analysis to that predicted by experiment and analytical models.
10. The thermal actuator is analyzed for deflection and transient characteristics in vacuum and compared to the model in air. This might provide an option for application of these actuators with low power and energy consumption.
11. Finally, the range of forces available from the thermal actuator model is examined.

4.3 THERMAL ACTUATOR NOMENCLATURE

Figure 20 shows the geometric design parameters of the actuator. Unless otherwise indicated, all the parameters represented are in microns. The nomenclature of the different finite element models is also explained below in Table 1:

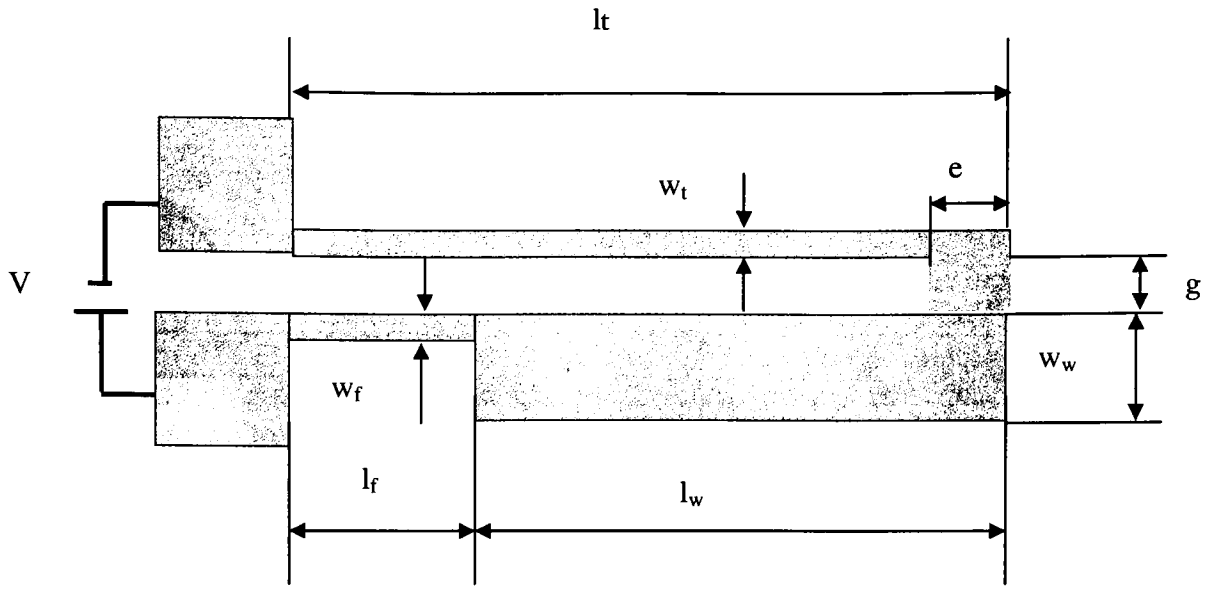

Figure 20: Geometric design parameters of the thermal microactuator

l_t = Length of thin arm

l_w = Length of wide arm

l_f = Length of flexure arm

w_t = width of thin arm

w_w = width of wide arm

w_f = width of flexure arm

g = gap

t = thickness

e = end connection length

V = Applied voltage

Parameter / Analysis Model	Electrical Resistivity of poly.(R_{var})	Coeff. Of Thermal Expansion of poly. (CTE_{var})	Modulus of Elasticity of poly. (E_{var})	Thermal Conductivity of poly. (K_{pvar})	Thermal Conductivity of air (K_{airvar})
Constant	Constant (Room Temp.)	Constant (Room Temp.)	Constant (Room Temp.)	Constant (Room Temp.)	Constant (Room Temp.)
Constant (Average)	Constant (Temp. Avg.)	Constant (Temp. Avg.)	Constant (Temp. Avg.)	Constant (Temp. Avg.)	Constant (Temp. Avg.)
R_{var}	Variable	Constant (Room Temp.)	Constant (Room Temp.)	Constant (Room Temp.)	Constant (Room Temp.)
R_{var},CTE_{var}	Variable	Variable	Constant (Room Temp.)	Constant (Room Temp.)	Constant (Room Temp.)
R_{var},CTE_{var},E_{var} or Constant k_p	Variable	Variable	Variable	Constant (Room Temp.)	Constant (Room Temp.)
K_{pvar}	Variable	Variable	Variable	Variable	Constant (Room Temp.)
K_{airvar}	Variable	Variable	Variable	Constant (Room Temp.)	Variable
K_{pvar},K_{airvar}	Variable	Variable	Variable	Variable	Variable

Table 1: Finite element model nomenclature

Constant model = Model that assumes constant room temperature material properties.

Constant (Average) model = Model that assumes constant but temperature averaged material properties to take into account thermophysical property variation.

R_{var} model = Model that assumes temperature variation in electrical resistivity only, other parameters assumed from constant model.

R_{var},CTE_{var} = Model that assumes temperature variation in electrical resistivity and coefficient of thermal expansion only, other parameters assumed from constant model.

R_{var},CTE_{var},E_{var} or Constant k_p= Model that assumes temperature variation in electrical resistivity, coefficient of thermal expansion and modulus of elasticity only, other parameters assumed from constant model.

K_{pvar} = Model that assumes temperature variation in electrical resistivity, coefficient of thermal expansion, modulus of elasticity and thermal conductivity of polysilicon only, other parameters assumed from constant model.

K_{airvar}= Model that assumes temperature variation in electrical resistivity, coefficient of thermal expansion, modulus of elasticity and thermal conductivity of air only, other parameters assumed from constant model.

K_{pvar},K_{airvar}= Model that assumes variation in electrical resistivity, coefficient of thermal expansion, modulus of elasticity, thermal conductivity of polysilicon and thermal conductivity of air.

4.4 ANALYTICAL MODEL

The analytical model developed by Hickey [30] predicts the deflection of the actuator based on the effective thin arm temperature, which is obtained by equation (4.1) described below. This equation gives the thermal profile at steady state for a prismatic bar of polysilicon where the temperatures are known at each end (20°C). Since, the thermal conductivity of air varies from 0.026 W/m°C to 0.06 W/m°C [28] and the thermal conductivity of polysilicon varies from 72 W/m°C to 18 W/m°C [31] from 20°C to 800°C the analytical model assumes constant average material properties to account for the variations due to temperature [30]. The analytical model assumes a one-dimensional treatment for modeling the thermal actuator since the length dimension is much larger than any dimension of the cross-section (Figure 21). The one-dimensional analysis assumes uniform temperature along the actuator

cross-section [30]. Hence, the thermal profile of the unfolded thermal actuator is used as a basis for a comparison of the different finite element models and the analytical model.

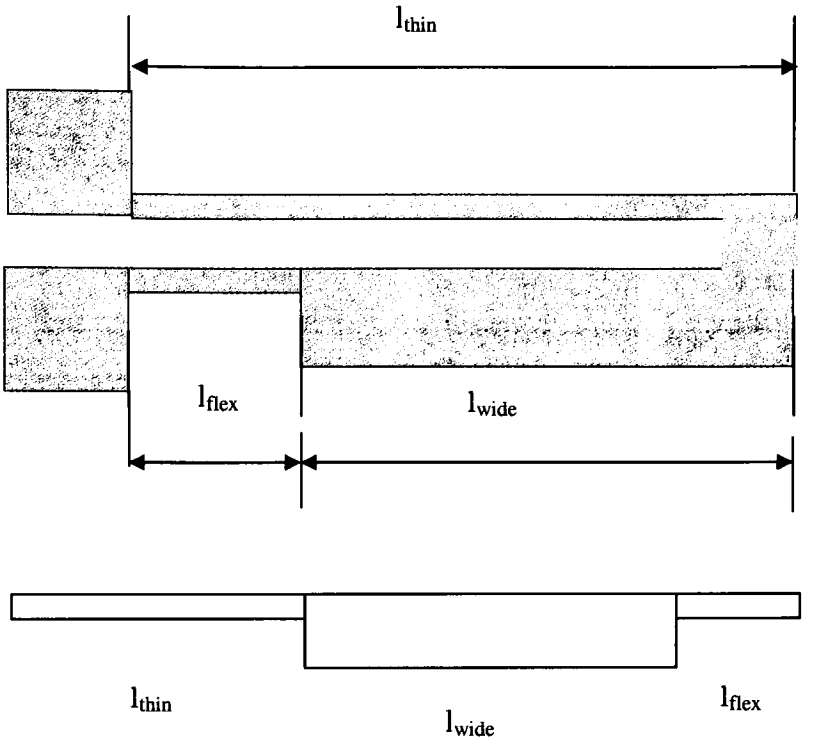

Figure 21: Schematic of thermal actuator (top view) and equivalent analytical model

$$T(x) = \frac{UPT_{\infty} + \dot{q}A_c}{UP} + C_1 \sinh\left(\sqrt{\frac{UP}{k_p A_c}}x\right) + C_2 \cosh\left(\sqrt{\frac{UP}{k_p A_c}}x\right) \tag{4.1}$$

where,

T (x) = Thermal profile along the unfolded thermal actuator

U = Average conductive heat transfer coefficient = 20,000 $W/m^2{}^{\circ}C$

P = Cross-sectional perimeter of a particular component

A_c = Cross-sectional area of a particular component

k_p = Average thermal conductivity of polysilicon = 50 $W/m^{\circ}C$

T_{∞} = Ambient temperature

$\dot{q}$ = Volumetric heating rate = V^2/RL

V = Applied voltage

R = electrical resistivity

L = Length of a particular component

Using the effective thin arm temperature dT the deflection is computed by equation (4.2)

$$\delta y = \frac{1}{2}\frac{(a^4 - a^2 + 2a)Ar\alpha\Delta TL^2}{5a^4I + a^4r^2A - 2a^3I + 5aI + r^2aA + I + a^5I - 2a^2I} \tag{4.2}$$

where

A = Cross-sectional area of flexure arm and hot arm (assumed same)

I = Moment of Inertia of flexure arm and hot arm (assumed same)

r = Gap between cold arm and hot arm

α = Coefficient of thermal expansion

ΔT = Change in temperature

a = Ratio of lengths of flexure arm and hot arm.

4.5 MESH REFINEMENT

Initially, a mesh refinement study was conducted on a particular thermal actuator using the constant finite element model. The thermal actuator was analyzed for three different mesh densities to compare thermal and deflection characteristics. Table 2 gives the nomenclature of the three mesh densities.

Mesh density number	Number of nodes	Number of elements
1	983	399
2	1778	728
3	4660	1986

Table 2: Mesh density specification

Figures 22 shows the results from the mesh refinement analysis. Both the deflection and thermal profiles show slight decrease as the element size decreases. This implies that the mesh refinement does not significantly affect the results. Hence, an element size that reduces

computation and convergence time is used for analysis of further finite element models in this thesis.

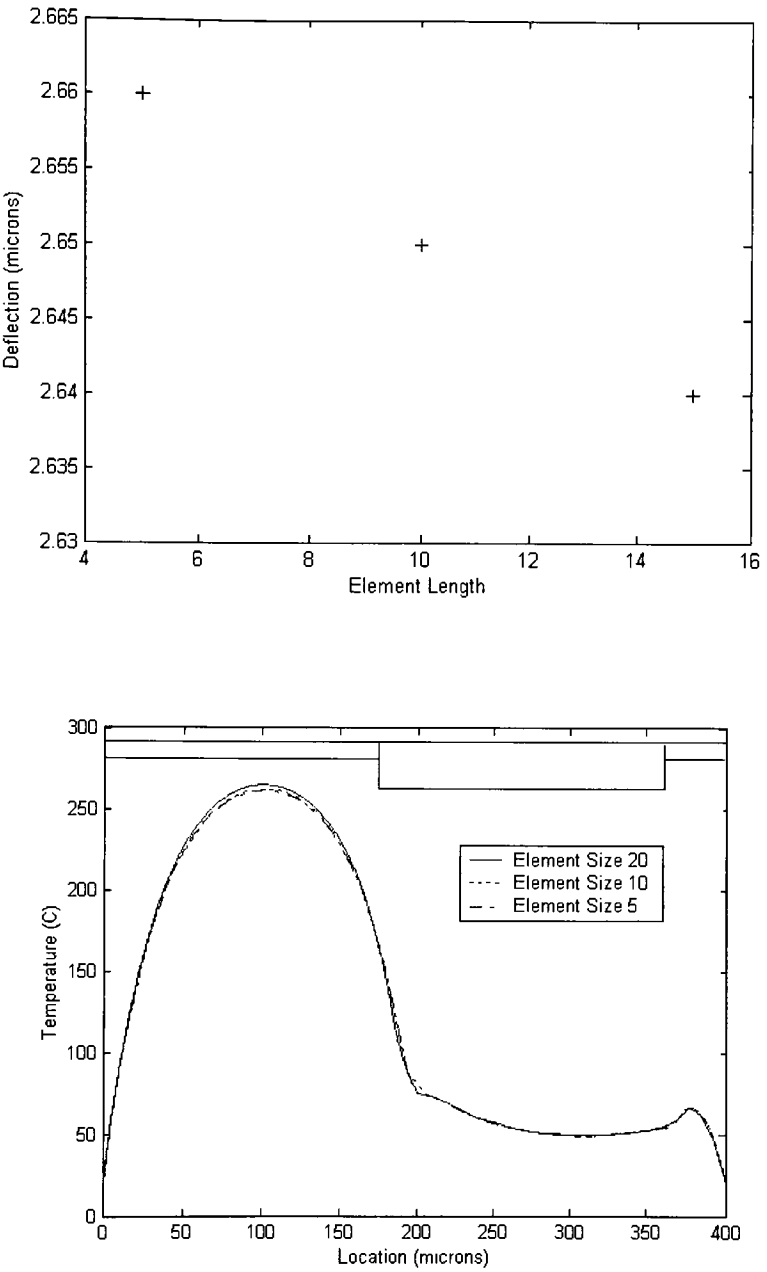

Figure 22: Comparison of deflection (top) and thermal profiles (bottom) for different mesh densities using the Constant FE model. l_t = 200, l_f = 30, w_t = w_f = 2, w_c = 14, g = 2, t = 2,V= 3V

4.6 CONDUCTIVE HEAT LOSS COMPARISON

The deflection of the actuator depends on the thermal profiles. An inconsistent thermal profile might predict incorrect or approximate deflections. As discussed in the Chapter 2 the major heat loss to the substrate is through the base of the actuator. The conductive heat transfer coefficient approximates that heat loss. It is difficult to estimate accurately the heat loss from the vertical sidewalls. So, a shape factor is included to approximate this heat loss. To test whether the shape factor gives an estimation of the heat loss two analyses were conducted.

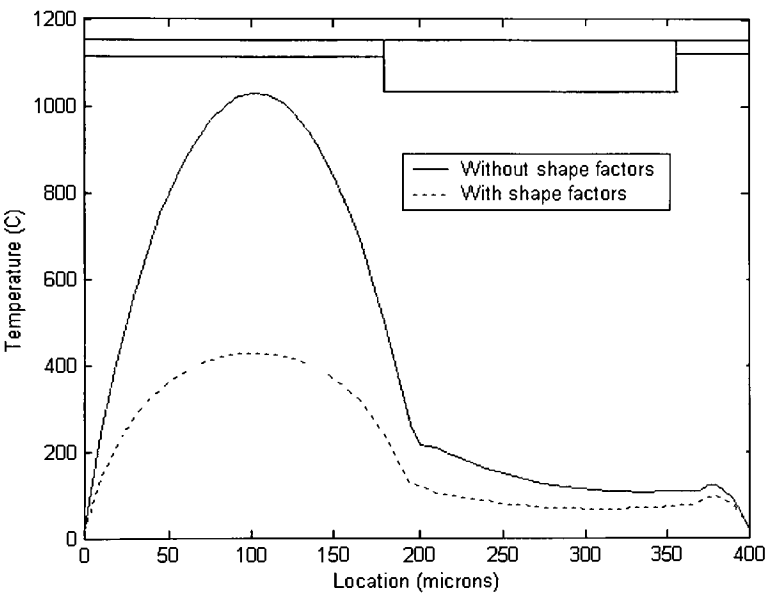

Figure 23: Comparison of the constant (average) finite element model to estimate heat loss by inclusion of shape factors. l_t = 200, l_f = 30, w_t = w_f = 2, w_w = 15, g = 4, t = 2, e=8, V= 5V

The first analysis considers only conduction from the bottom of the substrate while the second analysis takes into account the shape factor. These analyses were compared with a comprehensive analysis, which involves meshing of the air surrounding the actuator [30]. Figure 20 shows a comparison of the thermal profiles of the unfolded thermal actuator from both the analyses. The comprehensive analysis shows a similar thermal profile but for an absence of complete available data the maximum temperature reached in the thermal actuator (at the thin arm) is used as a basis for comparison of the models. The analysis,

which just considers conduction from the base, shows a steady state maximum temperature of 1031°C in comparison with 467°C observed from the comprehensive analysis [30]. Such a high temperature indicates that the heat loss from the sidewalls affects the analysis considerably. The analysis, which accounts the shape factor, shows a maximum steady state temperature of 424°C, which is comparable with the comprehensive analysis. This suggests that the shape factor is reasonable to account for the heat loss from the vertical sidewalls in the finite element model.

4.7 THERMAL PROFILES

The steady state thermal profiles from the finite element model including shape factor effects are compared with the analytical model [30]. The profiles cannot be compared with experimental data because of the difficulty in direct measurement of temperatures. For example, the temperature profiles measured by Hickey [30] for a thermal actuator of particular geometry show a maximum steady-state temperature of 80°C, while the analytical model predicts approximately 600 °C. This has been attributed to errors introduced by the thermocouple used for the measurement of thermal profiles.

4.7.1 Constant model

Figure 24 compares the thermal profiles for the finite element model, which assumes constant material properties to the analytical model. The finite element model with constant room temperature material properties shows a higher maximum temperature (698°C) in comparison to that predicted by the analytical model (537°C). The constant material properties assumption may lead to errors in the thermal profile.

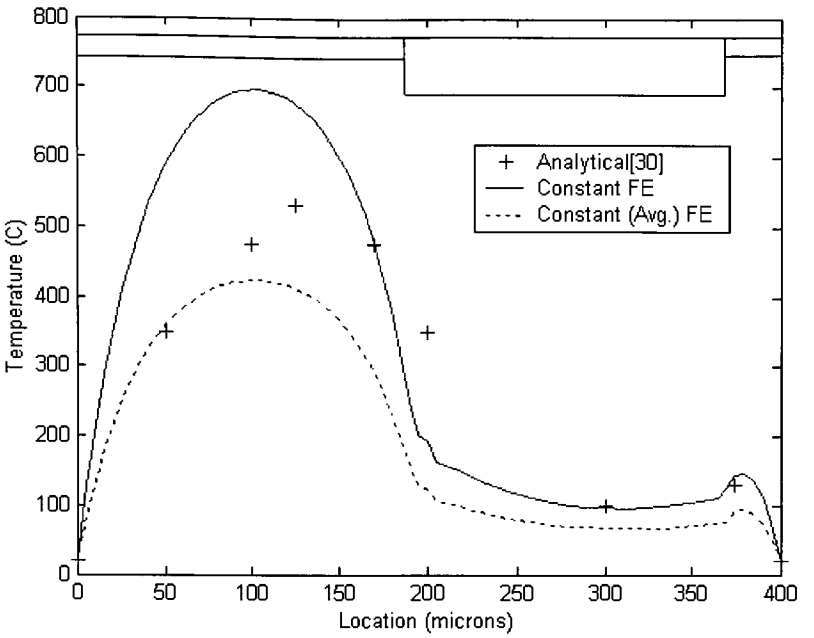

Figure 24: Comparison of finite element models employing constant material properties with analytical data. $l_t = 200$, $l_f = 30$, $w_t = w_f = 2$, $w_w = 15$, $g = 4$, $t = 2$, $V = 5V$

The finite element model, which assumes average material properties to account for the temperature dependencies, shows a large reduction in temperature in comparison with the analytical model that considers the same parameters. This indicates that the average value of thermal conductivity of air in the finite element model generates a greater heat loss than the analytical model. This larger reduction in temperature may also be attributed to the approximation of the heat loss from the vertical sidewalls.

4.7.2 Variation of Electrical Resistivity, Coefficient of Thermal expansion and Modulus of Elasticity

The finite element model, which takes into account the dependence of electrical resistivity with temperature, shows a maximum temperature of 557°C in comparison with 537 °C predicted by the analytical model (Figure 25). As expected, with the increase of electrical resistivity the maximum temperature in the actuator reduces due to a decrease in current.

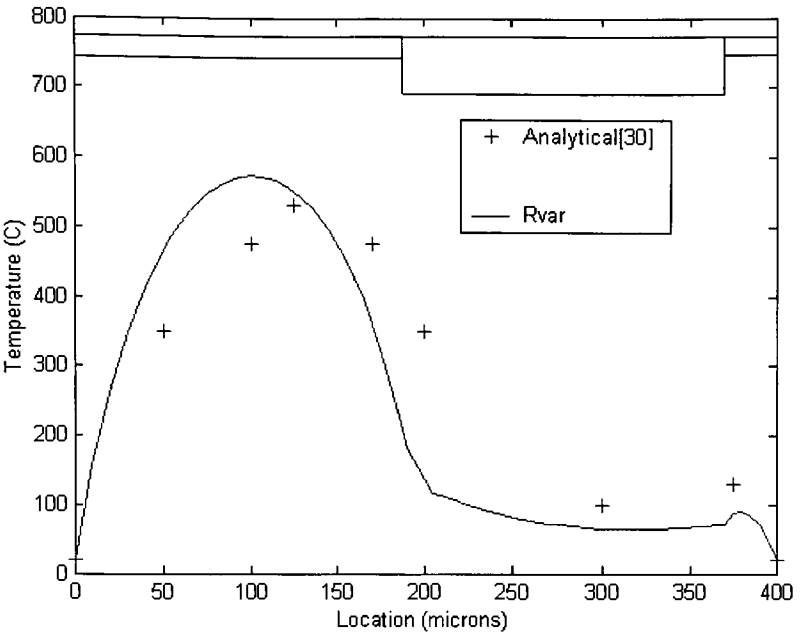

Figure 25: Comparison of finite element models employing variation of electrical resistivity, coefficient of thermal expansion and modulus of elasticity with analytical data. l_t = 200, l_f = 30, $w_t = w_f = 2$, w_c = 15, g = 4, t = 2, V= 5 V.

4.7.3 Variation in thermal conductivity of polysilicon and air

Figure 26 shows the temperature profiles obtained with the k_{pvar} finite element model, which combines the temperature variation of thermal conductivity and electrical resistivity of polysilicon, is quite similar to the curve of Figure 25 that assumes a constant value of thermal conductivity. At low temperatures, the thermal conductivity is higher than the constant value so the k_{pvar} model shows slightly lower temperatures. However at high temperatures, the thermal conductivity approaches the assumed constant value so that computed temperatures are nearly the same.

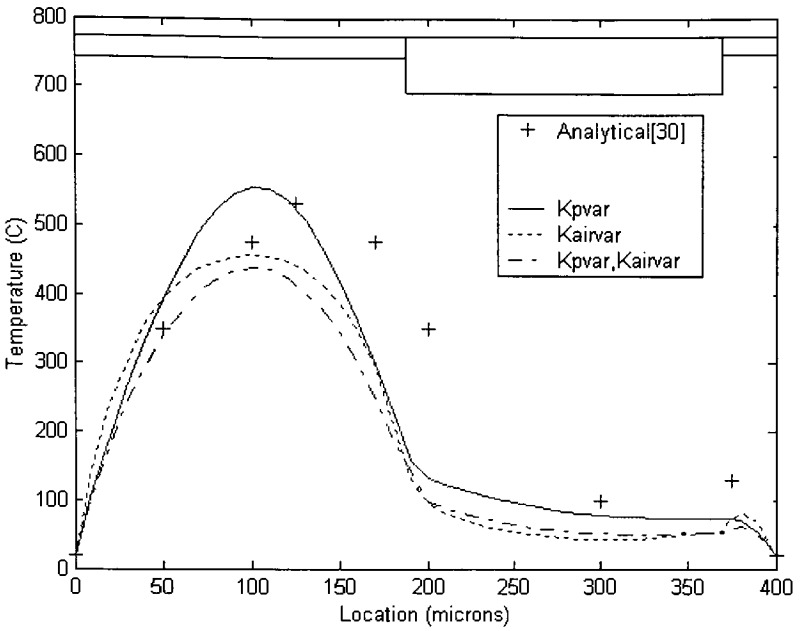

Figure 26: Comparison of finite element models employing variation of thermal conductivity with analytical data. $l_t = 200$, $l_f = 30$, $w_t = w_f = 2$, $w_c = 15$, $g = 4$, $t = 2$, $V = 5$ V.

The thermal conductivity of air strongly affects the analysis. As the conductivity of air increases, the conductive heat loss, which is the major mode of heat transfer, from the actuator increases. This cools the actuator significantly. The finite element model that assumes the temperature dependency of thermal conductivity of air (k_{airvar}) is close to the model that takes into account variations of all the material properties (k_{pvar}, k_{airvar}). This sgows that the thermal conductivity of air strongly dominates the variation of thermal conductivity of polysilicon and is the main factor that affects the thermal profiles.

4.8 DEFLECTION COMPARISONS

As it is extremely difficult to obtain reliably measured thermal profiles from the fabricated device, steady-state deflection profiles from the above models are compared to experimental deflection data. The best validation for steady state serves as a modeling criterion and is employed for comparison with 2D approximations, current comparisons, vacuum environment and dynamic simulations. Experimental data is shown by error bars, which represents one standard deviation from the average value measured.

4.8.1 *Constant model*

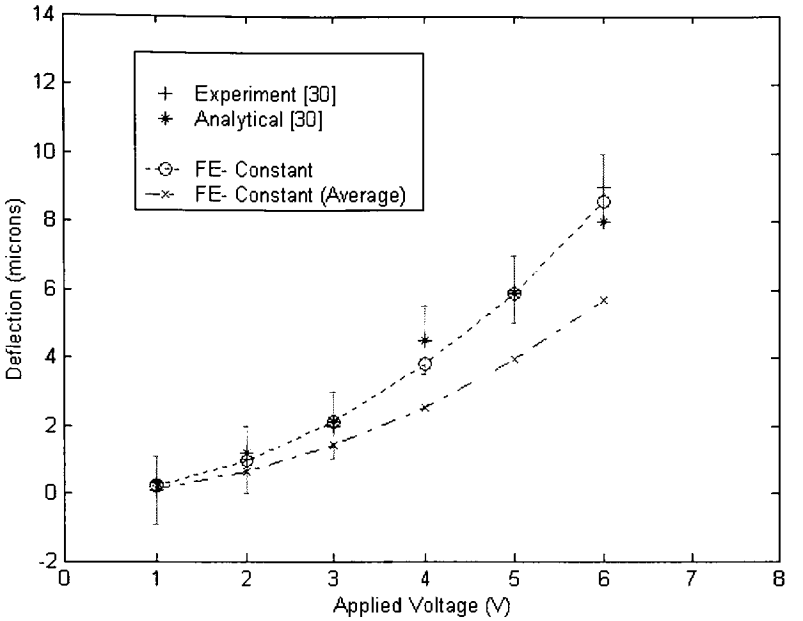

Figure 27: Comparison of constant finite element model with analytical and experimental data. $l_t = 200$, $l_f = 27$, $w_t = w_f = 2$, $w_c = 15$, $g = 4$, $t = 2$

Figure 27 compares the steady-state actuator deflections for the constant finite element model to the experimental and analytical data. The finite element model that assumes constant room temperature material properties, agrees well with the fabricated results. The constant finite element model that assumes average material properties as the analytical model deviates substantially from both data above 3V. This confirms that assumption of an average value of thermal conductivity of air in the finite element model approximates a greater heat loss to the substrate. This additional heat loss lowers the temperature difference in the two arms, which in turn reduces deflection. For example, the model with constant room temperature material properties shows an average temperature of 396°C for the thin arm and 245 °C for the wide arm, which gives ΔT as 151 °C. The constant finite element model with average material properties shows an average temperature of 244 °C for the thin arm and wide arm as 154 °C, which gives ΔT as 90°C.The difference in the average temperatures of the thin and wide arm, ΔT is an important performance parameter as it controls the tip deflection. The constant model is used as a basis for comparison to other

models, which introduce the variation of thermophysical properties in the model. This comparison is made with ΔT.

4.8.2 *Variation of Electrical Resistivity, Thermal coefficient of expansion and Modulus of Elasticity*

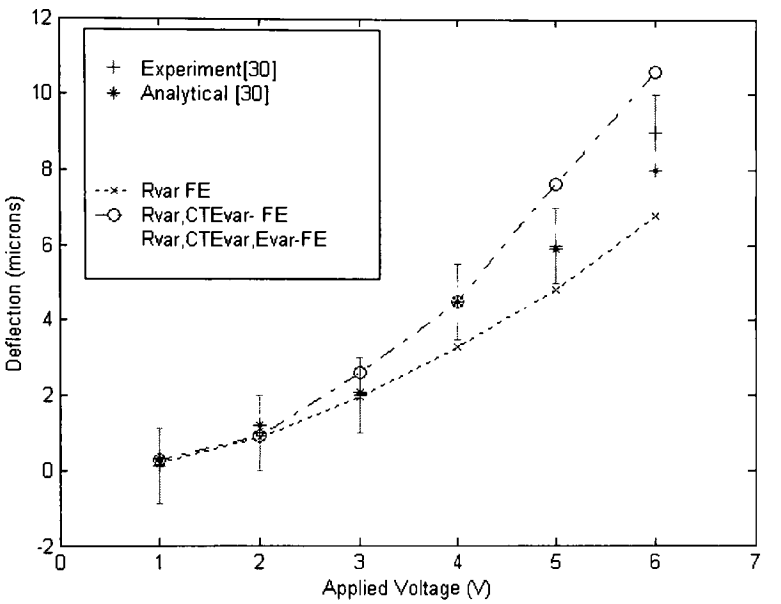

Figure 28: Comparison of finite element model with analytical and experimental data for variation in Electrical Resistivity (Rvar), Coefficient of Thermal Expansion (CTEvar) and Modulus of Elasticity (Evar). $l_t = 200$, $l_f = 27$, $w_t = w_f = 2$, $w_w = 15$, $g = 4$, $t = 2$.

Figure 28 compares the fabricated and experimental data with an introduction of the variations in electrical and structural material properties in the finite element model. The finite element model, which includes the linear dependence of electrical resistivity with temperatures (R_{var}), shows significant difference in the deflection profiles from the model that assumes a constant electrical resistivity. At low voltages this difference is not apparent. At voltages above 3 V the predicted finite element model deflections show large variations.

With an introduction of the variation of coefficient of thermal expansion (R_{var} ,CTE_{var}) the finite element analysis shows a better agreement to fabricated data than the R_{var} model, suggesting that the coefficient of thermal expansion is strongly dependent on temperature.

For voltages above 4 V this model predicts higher deflections than measured. The finite element model that includes a temperature dependent modulus of elasticity ($R_{var\ r}$,CTE_{var},E_{var}) shows same deflection as the CTE_{var} model. This indicates that the deflection of the actuator is independent of the modulus of elasticity variation of the material.

4.8.3 Variation of thermal conductivity of polysilicon and air

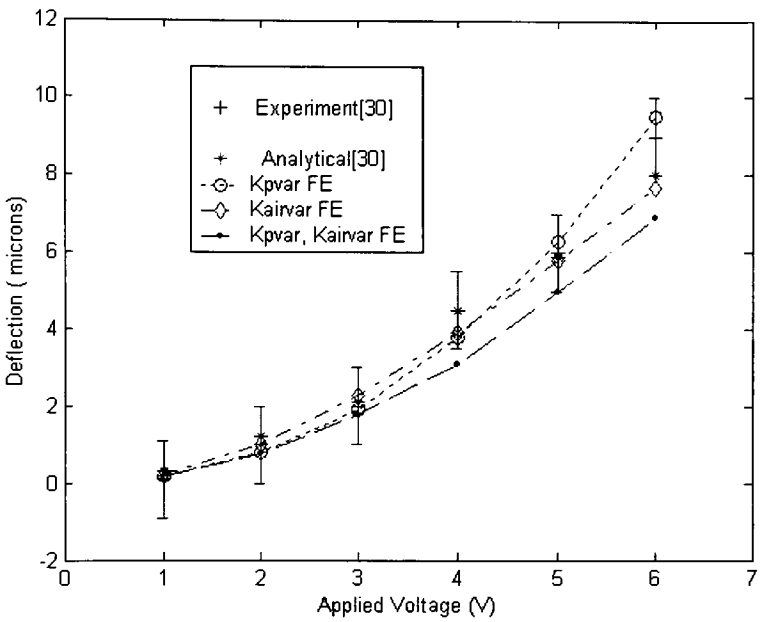

Figure 29: Comparison of finite element model with variation in thermal conductivity of air and polysilicon. l_t = 200, l_f = 27, $w_t = w_f$ = 2, w_c = 15, g = 4, t = 2.

The finite element model (k_{pvar}) that includes the temperature dependency of thermal conductivity of polysilicon using Manginell's equation [31] shows closest agreement with the fabricated and analytical data (Figure 29). At low voltages and hence low temperatures there is no significant difference in the models, which assume a constant value and the temperature dependency. At higher voltages the temperature dependent k_p model predicts closer deflections.

To observe the effect of variation of thermal conductivity of air on actuator deflection two additional finite element models were tested. The first model assumes a constant value of thermal conductivity of polysilicon taking into account the variation of thermal conductivity

of air (k_{airvar}) while the second model assumes the temperature dependency of all the parameters (k_{pvar},k_{airvar}). At low voltages, the k_{airvar} model shows close results to experiment, but at higher voltages it predicts lower deflections. At higher temperatures as the thermal conductivity of air increases more heat is transferred to the substrate from the thin arm than the wide arm limiting deflection. The k_{pvar},k_{airvar} model shows lower deflections than the k_{airvar} model. This indicates that inclusion of the variation of thermal conductivity of air shows significantly different results but a constant value might approximate the deflection of the actuator in its entire range of operation.

4.8.4 Further Validation

From the above comparisons it is clear that it is difficult to predict the model that accurately approximates the actuator deflection. The experimentally measured data is also subject to many errors, especially due to stiction. Hence, the models are compared with the experimental data of five more actuators of different geometry. From the previous results it can be concluded that the variation in electrical resistivity and coefficient of thermal expansion makes a significant difference and must be examined for accurate model predictions. The variation in the thermal conductivity of polysilicon and air must also be investigated in further models. Figures 30 and 31 give a comparison of the previous finite element model with the measured and analytical data to determine the importance of these parameters.

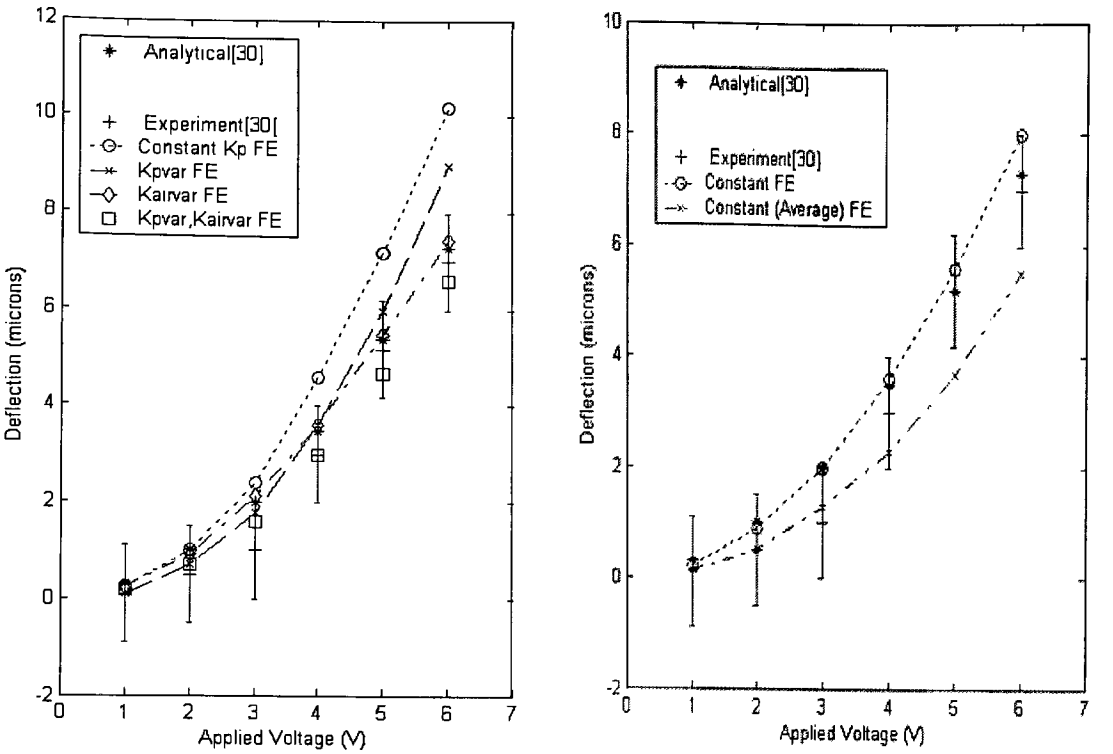

Figure 30: Comparison of finite element models with experimental and analytical data l_t = 200, l_f = 34, $w_t = w_f = 2$, w_w = 15, g = 4, t = 2.

From Figure 30 it can be observed that the finite element model with constant room temperature material properties correlates with the experimental data closely. From the models which employ the temperature dependencies the k_{airvar} and k_{pvar},k_{airvar} models also fall within the error range. This is contradictory to the previous comparison in which only the k_{pvar} model agreed with the experimental results. This indicates that those models which give approximately the same temperature difference as that of the constant model will fall within the error range.

Figure 31 tends to agree with the first actuator comparison. The k_{pvar} model agrees well with the experimental data. The k_{airvar} and the k_{pvar},k_{airvar} models show divergence at high voltages. From Figures 30 and 31 it can be seen that the R_{var},CTE_{var},E_{var} model and the constant model which takes into account the average material properties consistently do not agree with the experiment.

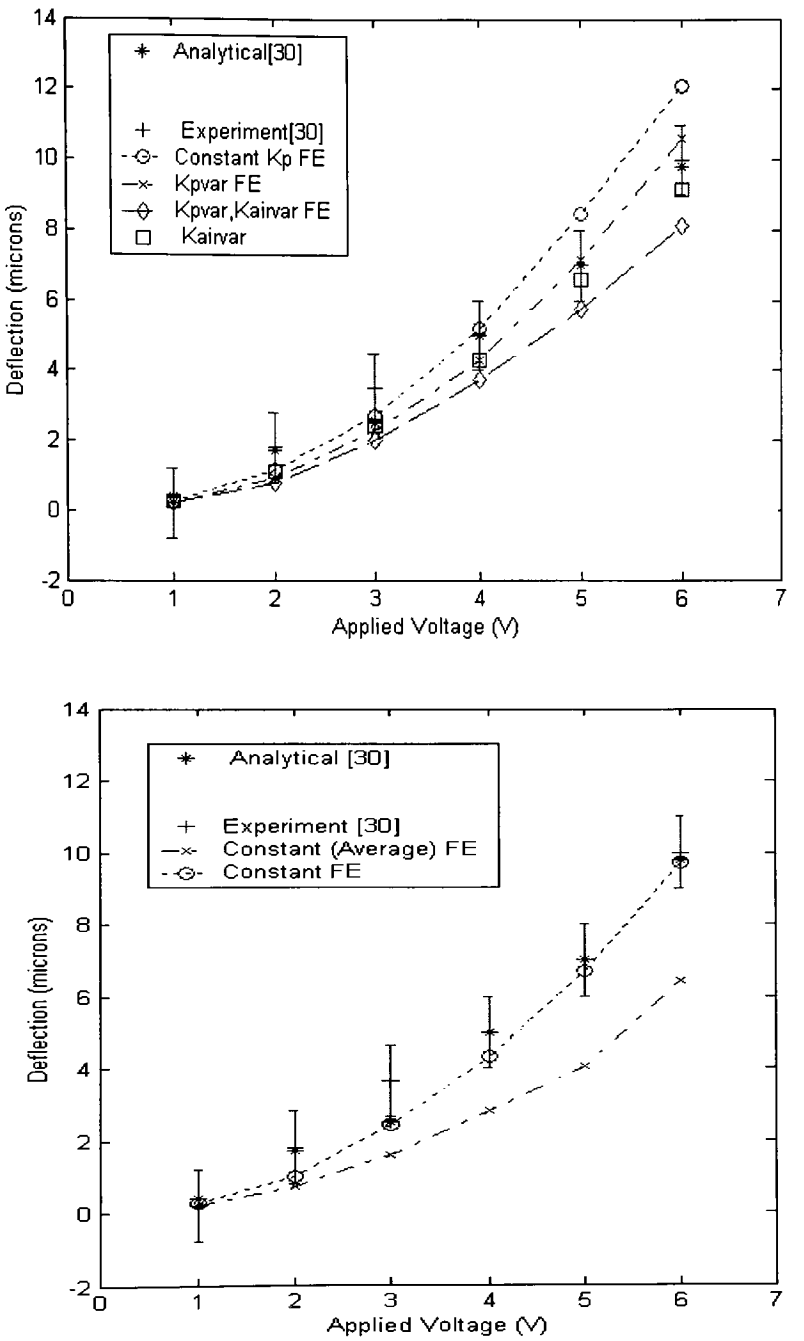

Figure 31: Comparison of finite element models employing temperature dependencies with experimental and analytical data. $l_t = 250$, $l_f = 34$, $w_t = w_f = 2$, $w_w = 15$, $g = 4$, $t = 2$.

Actuator Parameters	Experiment	Constant FE	Constant (Average) FE	R_{var}, CTE_{var}, E_{var}	k_{pvar}	k_{airvar}	k_{pvar},k_{airvar}
l_t=200,l_f= 40,w_t =w_f = 2,w_w=15, g=2, t=2,V=6.5V	12.8 [11]	11.7	7.7	15	13.7	10.2	9.1
l_t=200,l_f= 35,w_t =w_f = 2,w_w=14, g=2, t=2, V =6.7V	11[5]	12.7	9	16	14.5	11.1	10.2
l_t=230,l_f= 50,w_t =w_f = 2.5,w_w=16, g=2.5, t=2,V=4.3V	8 [9]	5	3	6	5.3	4.6	3.4

Table 3: Comparison of actuator tip deflection from finite element models for specific experimental data.

Table 3 shows the comparison of the models for specific measured data. The constant models give a good comparison of the measured data for two actuators. The constant (average) finite element model predicts smaller deflections. The models that employ the temperature dependencies vary in agreement. It is difficult to estimate the model that consistently agrees with experiment. The constant finite element model can be employed for reasonable predictions from observation of the previous trends. The average model can be eliminated completely. From the models that take into account the material property variations it is difficult to point one model that can be employed for accurate predictions due to the observed variations in agreement with the experimental data. This variation is

attributed to the assumption of shape factors, which may be causing errors in the thermal profiles leading to model inconsistencies.

The constant model is thus used for further simulations. Though this model predicts fairly consistent results close to experiment considering the melting point of polysilicon, from the thermal analysis perspective the model will always predict higher temperatures, which may or may not be reached in actual experiment.

4.9 2D APPROXIMATIONS

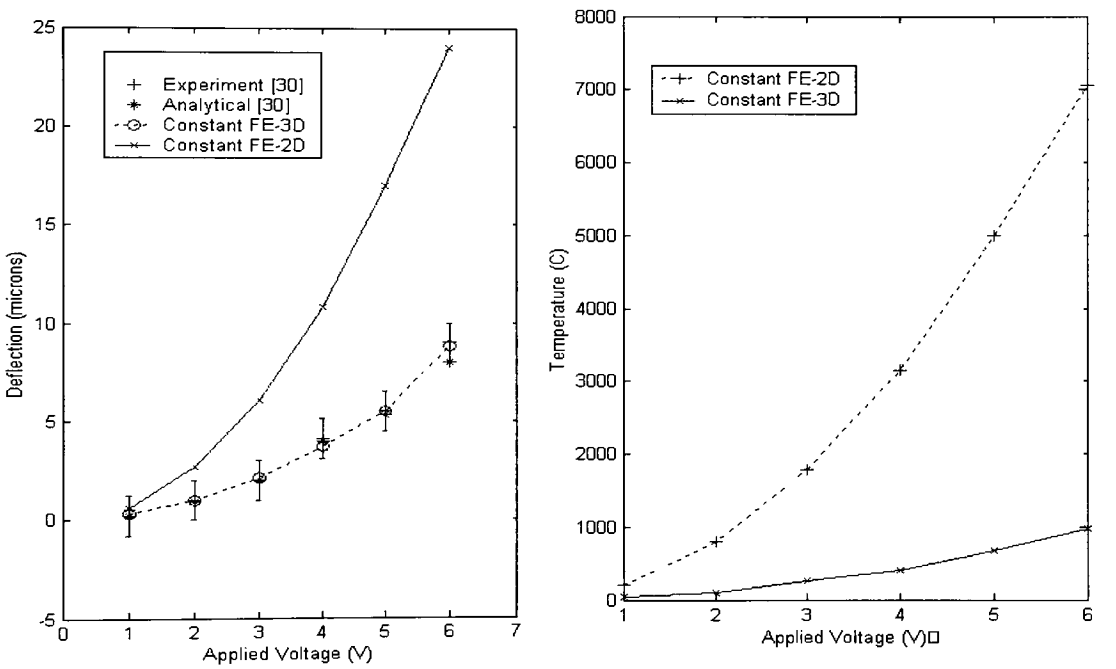

Figure 32: Comparison of 2D and 3D finite element models. $l_t = 200$, $l_f = 27$, $w_t = w_f = 2$, $w_c = 15$, $g = 4$, $t = 2$.

Figure 32 compares the deflection and thermal profile for the 2D and 3D constant models. From the deflection profiles it is clear that the 2D approximation cannot characterize the actuator deflections. The 2D actuator shows significant higher deflections. As the 2D analysis cannot model conductive heat loss to the substrate the maximum temperatures seen in the actuator are extremely high as compared to the 3D model. The 2D model indicates melting for voltages slightly above 3V. The percentage error in the thermal profile increases with the

applied voltages. This signifies the inaccuracies that might result from ignoring conductive heat loss to the substrate.

4.10 VACUUM COMPARISONS

The major limitations of MEMS thermal actuators are the amount of power and energy consumed to achieve a steady- state deflection. The application of these actuators in vacuum is examined as a possibility for power and energy savings. The vacuum environment provides insulation by removing the medium of heat transfer (air). The heat flow to the substrate by conduction is removed and the actuator requires smaller input voltages to reach the same maximum temperatures as that in air. This leaves just conduction through the anchors to the substrate and radiation as the only paths for heat flow.

Figure 33 compares the thermal profile of the actuator in vacuum for the finite element model which assumes constant thermal conductivity of polysilicon (R_{var},CTE_{var},E_{var}), the model that takes into account the variation on thermal conductivity (k_{pvar}) and the model with constant material properties. From the figure it can be observed that the thermal profile in vacuum is considerably different from that in air (Figure 25). Since there is no heat conduction in vacuum, which is the primary source of heat loss in air, the actuator reaches high temperatures for small voltages. For example, when the same actuator was modeled in air it required approximately 5-6 V to reach the same steady state temperatures. The thermal profile of the wide arm in vacuum shows high temperatures, which gradually slope down towards the flexure arm while in air the temperature profile of the wide arm decreases rapidly. This is because in air the wide arm conducts more heat as it has a larger area than the cold arm and flexure arm. In vacuum, since there is no heat loss, the actuator shows higher temperatures for each component.

The constant model consistently shows higher temperatures than the other two. The R_{var}, CTE_{var}, E_{var} model that includes the temperature dependencies of electrical resistivity shows significantly lower temperatures than the constant model.

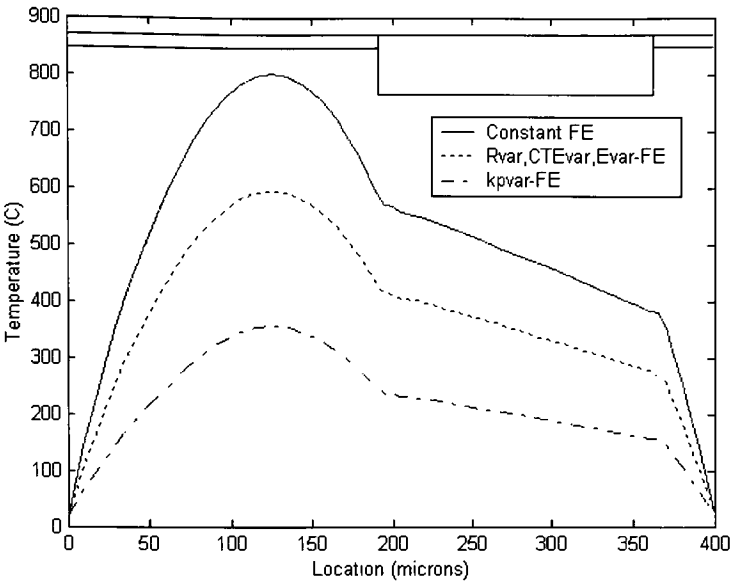

Figure 33: Comparison of thermal profiles in vacuum. l_t = 200, l_f = 30, w_t = w_f = 2, w_c = 14, g = 2, t = 2,V= 2V

This thermal profile is also affected when the variation of thermal conductivity is introduced. A point to be noted is that the variation of thermal conductivity in air does not change the thermal profile to such a large degree as in vacuum. This again confirms that the thermal conductivity of air is strongly dominant over the thermal conductivity of polysilicon. In vacuum, since the air layer is absent, the variation of thermal conductivity causes a significant difference in the thermal profile.

Figure 34 compares the deflection profiles in vacuum. Experimental results taken from Butler et al. [17] where the thermal actuator was operated under an environmental pressure of 20mTorr show a good agreement when the temperature dependency of polysilicon is included in the model. This is agreement with Lott's [28] observations. The model that assumes constant material properties deviates completely from the experiment above 2V. The thermal profiles in this case (not shown) also indicate melting temperatures, which is inconsistent with experimental data. The R_{var},CTE_{var},E_{var} model predicts lower deflections than those measured. These results indicate that in vacuum where there is an absence of the air layer the thermal conductivity of polysilicon plays an important role in predicting actuator

deflection and the full temperature dependency must be included for accurate model predictions.

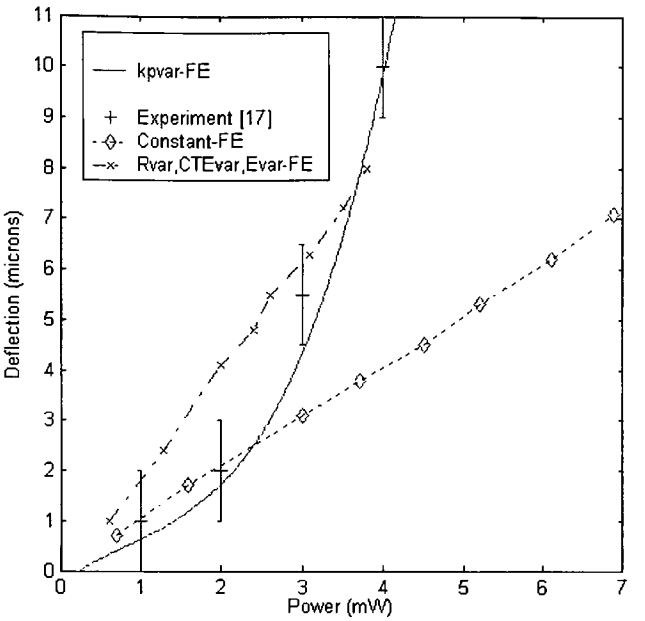

Figure 34: Comparison of deflection profiles in vacuum. l_t = 200, l_f = 30, w_t = w_f = 2, w_c = 14, g = 2, t = 2, Pressure = 20mT

In comparison with the actuator in air, the actuator in vacuum gives greater deflections for the same power consumption. This is because the actuator in vacuum reaches higher temperatures than that in air for the same power input leading to a greater temperature difference. This deflection though is limited up to 8-10 μm. Above these deflections the temperature in the actuator are sufficient to cause melting. In air the large surface area of the wide arm allows more conductive heat loss than the thin arm increasing the deflection. Since this path for heat loss is removed in vacuum the deflections are limited to 8-10 microns to achieve power savings.

4.11 CURRENT COMPARISONS

Figure 35 shows the current comparisons for the results predicted by the finite element model to that recorded experimentally in both air and vacuum environments. From the profiles it can be observed that the current shown by the finite element model is always less than the experimental. This trend remains consistent with increase in the applied voltage.

This was originally attributed to the inaccuracies in the finite element model arising possibly out of the assumptions in the analysis but simulations in ABAQUS also show similar trends [40]. This suggests that some other factor like the contact resistance at the anchors might be affecting power and current consumption.

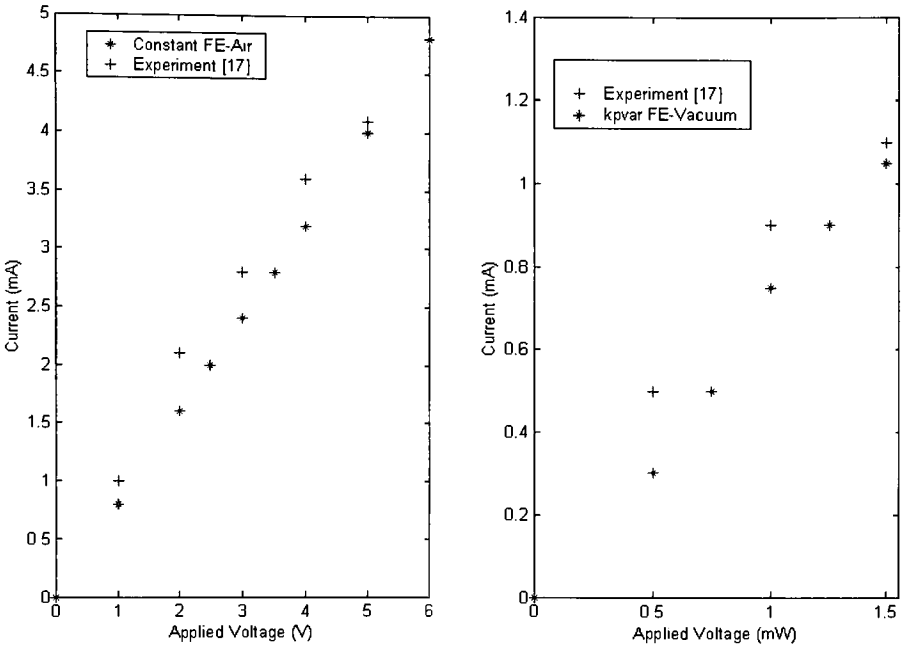

Figure 35: Comparison of current characteristics of the Kpvar model for air and vacuum. l_t = 230, l_f = 50, $w_t = w_f$ = 2.5, w_c = 14, g = 2.5, t = 2

4.12 DYNAMIC RESPONSE

The constant finite element model approximates experimental data closely and this model is used for dynamic simulations in air. The transient characteristics give insight into the energy consumption and power requirements of the actuator to maintain a steady state displacement profile. When this is known the thermal actuator can be selected for microsystems that have limited power or energy to supply.

Figure 36 shows the transient thermal and deflection response of the actuator for a step input of 3V. The actuator typically cools down completely to room temperature over a large time step. For the deflection profile, the finite element model shows a convergence problem

at extremely small time increments. At sufficiently large time increments a completely stabilized solution cannot be obtained. A simple modal analysis characterizes resonant frequency of these actuators as 38 kHz. A comparison of the results from the finite element model to the experimental and analytical data is given in Table 3:

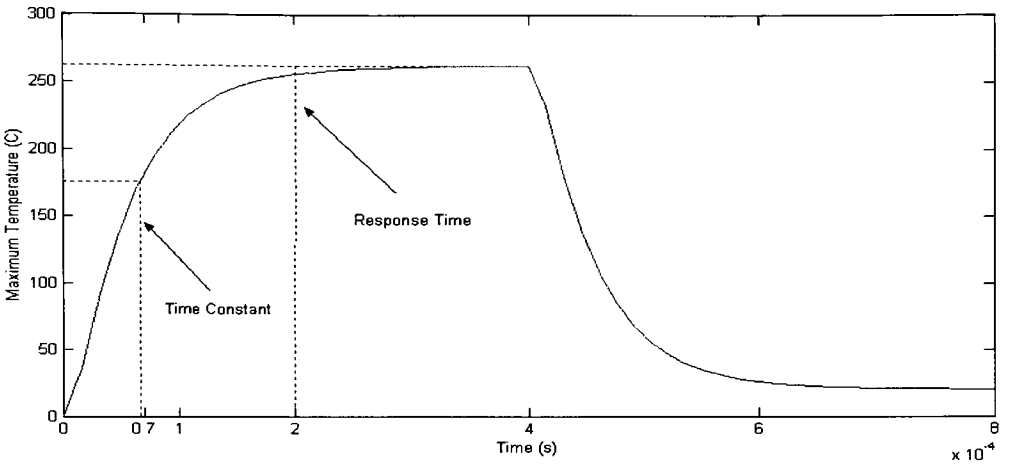

Figure 36 (a): Dynamic thermal response of the actuator in air. l_t = 200, l_f = 30, w_t = w_f = 2, w_c = 15, g = 4, t = 2, V = 3V

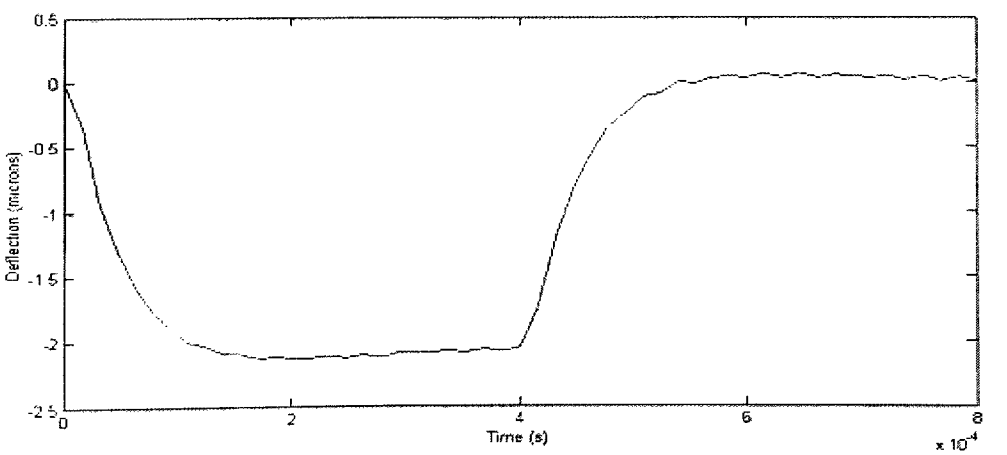

Figure 36 (b): Dynamic deflection response of the actuator in air. l_t = 200, l_f = 30, w_t = w_f = 2, w_c = 15, g = 4, t = 2, V = 3V

Step Input Response	Time constant (μs)	Response Time (μs)
Finite Element-Constant	70	200
Analytical [30]	67	300-400
Measured [30]	115+/- 20	450 +/- 100

Table 4: Comparison of dynamic response of finite element model with analytical and measured data

The thermal time constant of the actuator depends upon the heat capacity of the actuator and the resistance to heat transmission. The devices in air take approximately 0.2 ms to reach steady state temperatures and 0.2 ms to cool down completely. The thermal time constant agrees well with the analytical model, but the response time predicted by the analytical model is higher than the finite element model. In comparison with the experimental results the finite element model and analytical predicts lesser values than those recorded. This may be either due to inaccuracies in the finite element model arising possibly out of the assumptions or the inaccuracies in measuring the experimental data [30], [56].

Figure 37 shows the actuator response in vacuum. The dynamic response of the actuator in vacuum is compared to the response in air (Figure 36 (a)) to reach approximately the same steady state deflections. The transient response of the actuator in vacuum (4 ms) is approximately 20 times slower than that in air (approximately 0.2 ms). This is because the vacuum environment acts as a resistance to the conductive heat loss to the substrate, which is the major mode of heat transfer in air. The vacuum environment increases the thermal resistance, which increases the thermal time constant.

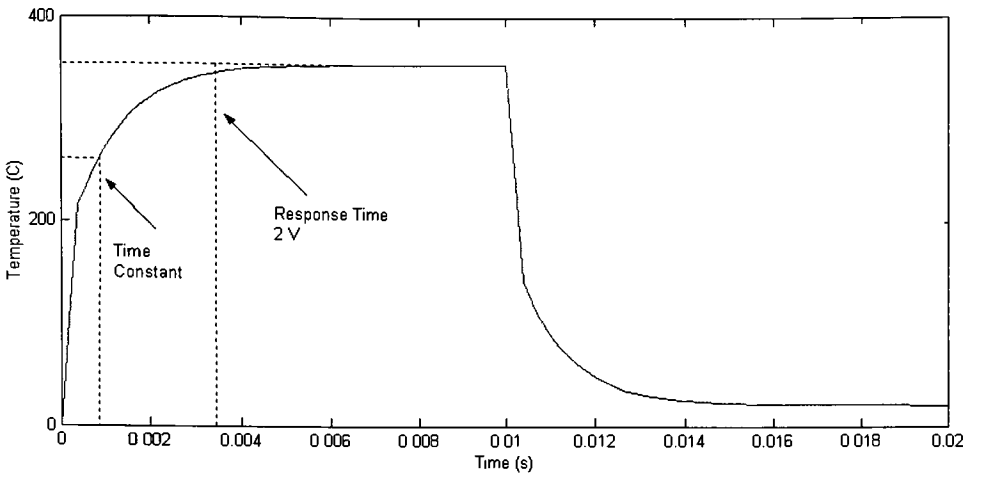

Figure 37: Dynamic thermal response of the actuator in and vacuum. $l_t = 200$, $l_f = 30$, $w_t = w_f = 2$, $w_c = 15$, $g = 4$, $t = 2$.

4.13 POWER AND ENERGY CONSUMPTION

Power consumption and energy requirements are the major drawback of such thermal actuators. This becomes especially important when arrays of such actuators are coupled together. The energy required during transient response can be calculated by integrating the average instantaneous power applied to the actuator for a given step input [28]. The energy required is computed from time the step input is applied to the time the transient is 90% complete. The response time for the actuator in air is approximately 0.2 ms compared to that in vacuum 4 ms. Figure 38 shows the power and energy requirements from the actuator in air and vacuum. These characteristics are compared for the actuator to reach approximately same maximum steady-state deflection.

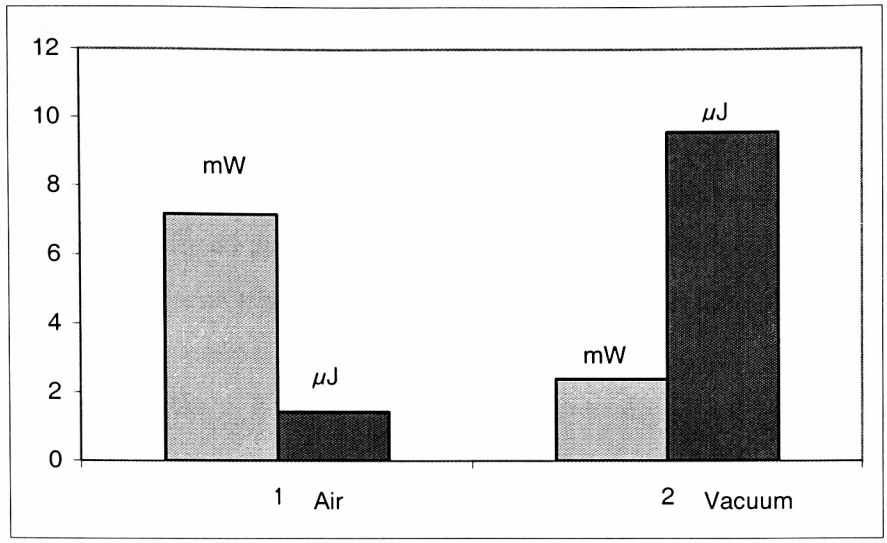

Figure 38:Power and energy consumption comparison of actuator in air and vacuum. l_t = 200, l_f = 30, $w_t = w_f = 2$, $w_c = 15$, g = 4, t = 2, V = 3V

The actuator in vacuum requires a lower steady-state power (2.4 mW) to obtain approximately the same deflections because of the low applied voltages, as compared to the power consumed in air (7.2 mW). The energy required in vacuum (9.6 μJ) is almost 7 times as more than that in air (1.4 μJ). This signifies that the actuator in vacuum can be employed for same deflections as in air up to 8-10 μm with a power savings but at the expense of higher energy consumption.

4.14 PULSE SIMULATIONS

Another application of the transient response of these devices is the ability for a pulse width modulation scheme. A pulse width modulation scheme is useful as a single drive voltage can supply the required displacement. This will simplify the implementation of the thermal actuator in a microsystem. Figure 39 shows the dynamic response of these actuators when driven by a pulsed drive signal in air. By observing the transient response, the width of the drive signal was varied to obtain the required temperature and deflection response. For example, an application of 4 V for 0.1 ms in air brings the actuator to a maximum steady-

state temperature of 310°C. At high frequencies the actuator does not have time to reach steady state and will heat and cool cyclically.

In vacuum, an improved energy response can be achieved by applying a high drive voltage for a short duration. Figure 40 illustrates an example. When the actuator was driven with a 4 V pulse for 0.06 ms the same the same temperature difference could be obtained to achieve approximately the same steady-state deflection as that when driven by a 2 V pulse for 4 ms. A steady application of the 4 V pulse would result in melting of the actuator but for the applied time the maximum temperature of the actuator reaches 402°C. This results in an energy consumption of 1.02 μJ in comparison with 3.02 μJ in air, for approximately similar deflections, which is an energy savings of almost 70%. The actuator deflection in vacuum though will only be limited till 8-10 μm for reasons discussed earlier.

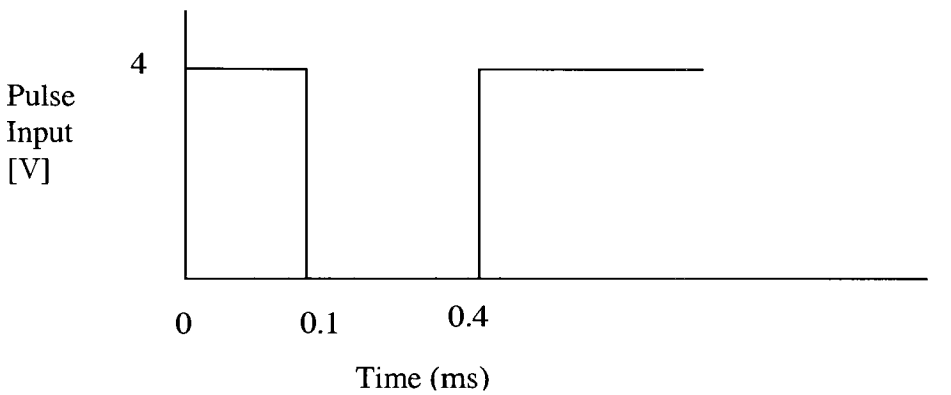

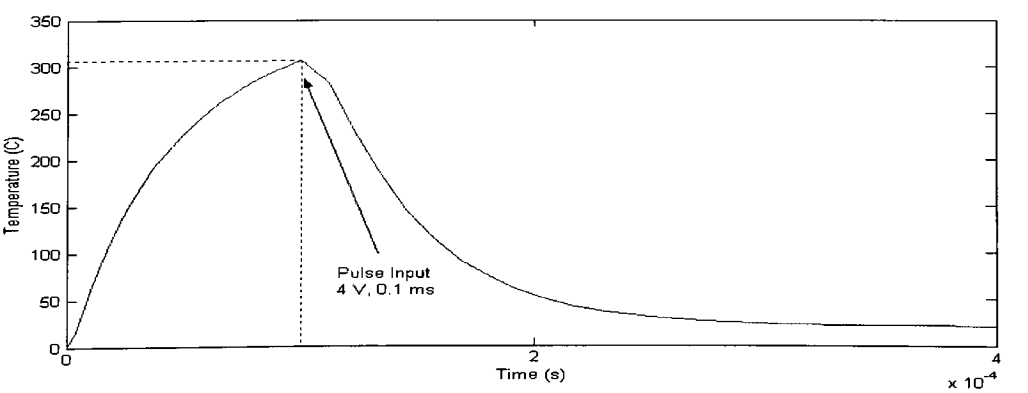

Figure 39:Pulse width modulation in air. $l_t = 200$, $l_f = 30$, $w_t = w_f = 2$, $w_c = 15$, $g = 4$, $t = 2$, $V = 3V$

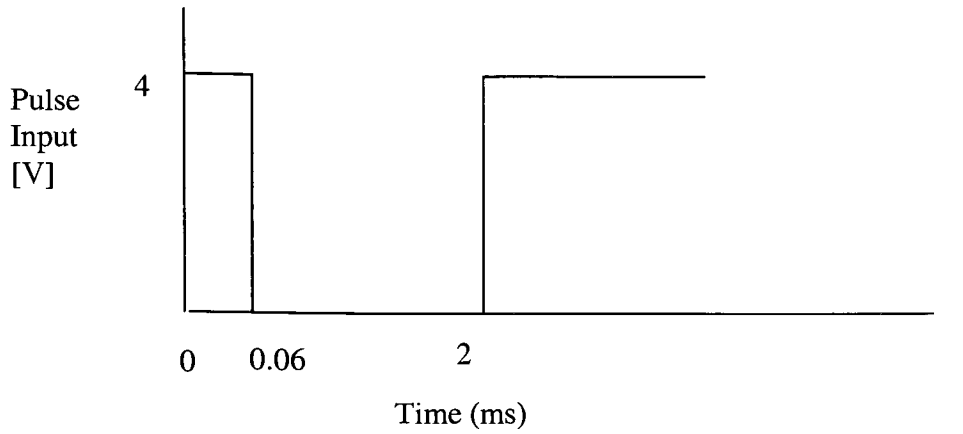

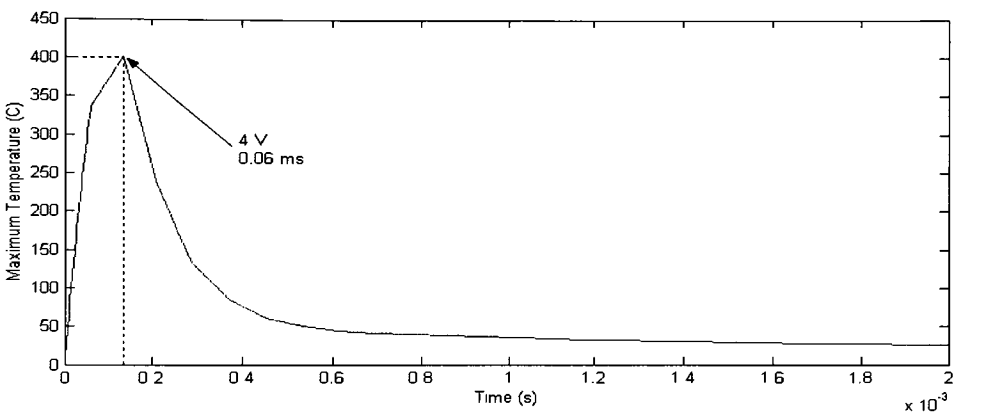

Figure 40:Pulse width modulation in vacuum. $l_t = 200$, $l_f = 30$, $w_t = w_f = 2$, $w_c = 15$, $g = 4$, $t = 2$, $V = 3V$

4.15 FORCE MEASUREMENTS

As explained in Chapter 2, if there are N actuators coupled together the range of force available from the actuator array is given by

$$F = Nk(d - d_0(V)) \tag{4.3}$$

The electro-thermal-elastic simulations will determine d_{max}, which for a single actuator of dimensions $l_t = 200$, $l_f = 40$, $w_t = w_f = 2$, $w_c = 15$, $g = 2$, $t = 2$, $V = 6.8V$ is 12.7 μm as predicted by the constant model. The compliance of these actuators can be found by a

simple ANSYS simulation by applying a unit force to compute the deflection. The compliance of this actuator is characterized as 1.6 μm/μN. This modifies equation (4.3) for a single actuator as

$$F = 0.625d - 7.9375 \tag{4.4}$$

In terms of design it is easiest to fix the required actuation distance. Then the force available from the actuators can be determined. Alternatively you can fix force as the design criteria and determine the maximum actuation distance the actuator can provide while still meeting the force design criteria. Figure 40 shows the force available from the actuators at specified deflections. The absolute value of this expression will give the force available at the required actuation. The maximum force of 7.9 μN predicted by Equation (4.4) compares well with the experimentally measured value (8 μN) [19].

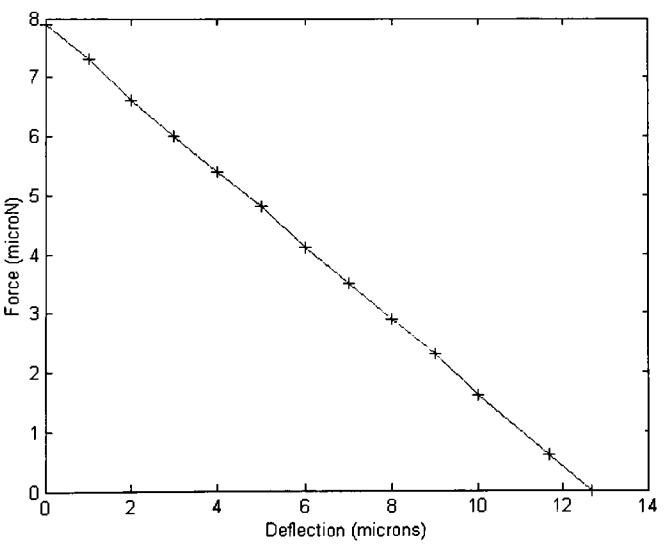

Figure 41: Range of forces available from the actuator. l_t = 200, l_f = 27, w_t = w_f = 2, w_c = 15, g = 4, t = 2, V = 6.8 V

CHAPTER 5

DESIGN OPTIMIZATION

The main disadvantage of thermal actuators is the amount of power consumed to obtain the required deflection and force. Typically arrays of actuators are coupled to increase the amount of delivered force, which again leads to increased drive power and space required. Improving the force and the deflection characteristics of an individual thermal actuator allows for fewer numbers of actuators to be employed in an array, decreasing the space requirements and power consumption. This chapter explains the methodology of design optimization using finite element analysis, which can be implemented to improve the deflection and force characteristics of the thermal actuator at the same or lower power consumption levels. The optimization batch file developed using the ANSYS Parametric Design Language (See Appendix B) can be employed to completely design or study the effect of change of different design variables on the performance of the thermal actuator based on user specified limits. Section 5.1 explains the optimization terminology and the finite element method employed for optimizing the thermal actuator parameters. Section 5.2 recommends design guidelines for optimizing the actuator for deflection and force characteristics. Section 5.3 presents the results of an optimization study conducted on a particular thermal actuator.

5.1 PROBLEM FORMULATION

Design optimization is a technique that seeks to determine a design configuration that meets all the specifications at the minimum expense of certain factors (objective functions) such as the applied power. For any design optimization problem, certain design criteria are involved which constrain the problem. The terminology [53] for the thermal actuator design optimization problem is explained below.

5.1.1 Terminology

Design Variables: Design variables are independent geometric quantities that are varied in order to obtain an optimum design. For the thermal actuator, the design variables are the geometric parameters, which are namely, the thin arm length and width, flexure arm length and width, wide arm length and width and the spacing or gap between the thin and cold arm. The constraints on the design variables are upper and lower limits based on the available package size. In addition, applied voltage may also be specified as a design criterion.

State Variables: State variables are a function of the design variables and typically are used to constrain the design by specifying upper and lower limits. For the thermal actuator the maximum temperature limit is a state variable that will constrain the variation of the geometric parameters.

Objective Function: The objective function is the dependent variable that is to be minimized. It is a function of the design variables and any change in the design variables should change the objective function. For the thermal actuator involved here, the applied power is an objective function.

Design sets: The design set is a set of parameter values that represents the optimization variable values that are obtained at the end of the optimization subroutine. Typically a number of design sets with variations in the optimization variables is available for review after the analysis. A design set is considered to be feasible if it satisfies all the required constraints. If any one of the constraints is not satisfied the design set is considered to be infeasible. The best design set satisfies all the constraints and gives the minimum value of the objective function.

Analysis file: The analysis file is an input file that contains the commands of a complete finite element analysis of the thermal actuator. This file is used by the optimization solver to perform a number of analysis evaluation modification cycles. The file is a generalized file created using the ANSYS Parametric Design Language (APDL) [53] which can be employed for the optimization of the thermal actuator (See Appendix B).

5.1.2 Optimization Techniques

ANSYS offers a large number of optimization tools [53] that can be used to understand the design space of the problem. The actual optimization can be done using two methods-the Subproblem Approximation Method and the First Order Method [53]. The Subproblem Approximation Method uses curve fitting to all the dependent variables (state variables and objective function) to obtain a minimum value of the objective function. The First Order Method uses gradients of the dependent variables with respect to the design variables to obtain an optimal design. This method, though more accurate than the Subproblem Approximation Method, is extremely computationally expensive, especially for such a multi-variable non-linear optimization problem. Hence, the subproblem approximation method is implemented for design optimization of the thermal actuator.

The Subproblem Approximation Method establishes a relationship between the objective function and the design variables by basic curve fitting. The objective function is computed for several sets of different design variables by performing a number of iterations through the optimization file (See Appendix B) and a least squares fit is generated for the data points obtained. The resulting fit is an approximation. Any iteration through the design file generates a data point and the approximation is updated. This is done for both design and state variables. The type of fit can be linear or quadratic. At the end of any iteration a convergence check is performed which determines the change in the objective function variable from the best feasible design and the current design.

Since this method is based on an approximation of the objective function, a number of random designs can be performed by changing the initial geometry of the thermal actuator or specifying a different design criterion to check for an optimized design. This can be done using the Random Design Generation Tool [53]. Using this tool a specified number of design sets can be generated using random values of design variables to develop and review trial designs in order to check the design space of the problem as a precursor to the Subproblem Approximation Method.

5.2 OPTIMIZATION CONSTRAINTS

The procedure to optimize the thermal actuator depends on the application of the actuators. The application of the actuators will depend upon whether or not the actuator will be required to deflect under an external load. Though the optimization constraints are typically dependent on the designer implementing the thermal actuator, the constraints specified below narrow down the design space of the thermal actuator, which helps in a more effective optimization.

5.2.1 Unloaded Thermal Actuator

For an unloaded thermal actuator where no or little force is required the optimization constraints are straightforward:

Design variables:

1. *Length of the actuator:* A longer actuator is capable of a larger deflection but as the length increases the overall electrical resistance increases which requires an increased applied voltage to obtain a sufficiently high current density [5]. Increasing the length of the thin arm also tends to increase the possibility of buckling, sagging of the thin arm into the ground plane and reduces the overall compactness of the device. At large lengths like 300 μm the thin arm bows down touching the substrate and loses heat causing it to shrink up out of contact and reheat cyclically [14]. The typical maximum length of thermal actuators in different applications has been observed to be 250 μm. The design limit on the maximum length of the thin arm is set to 250 μm.

2. *Width of the thin arm:* Decreasing the width of the thin arm reduces the surface area for dissipating heat and increases the current density leading to higher maximum temperatures and deflections. The MUMPs process [46,57] limits the width of the thin arm to 2 μm. The design constraint on the minimum width of the thin arm is set to 2 μm.

3. *Width of the wide arm:* Increasing the width of the wide arm gives a larger surface area for heat dissipation decreasing the current density. This leads to a higher temperature difference between the two arms giving higher actuator deflections. It has been observed that as the ratio of the wide-to-thin arm width is increased, the resulting deflection increases [5]. This deflection increase is dramatic up to wide-to-thin arm ratios of 4:1. Beyond 4:1 and till 7:1 slight increase is obtained with no increase after 7:1. This is because increasing the width of the wide arm lowers current density until the wide arm has no significant expansion in comparison with the thin arm [5]. The design constraint for the maximum wide-to-thin arm width ratio is set as 8:1.

4. *Gap:* Decreasing the thin arm-wide arm spacing increases the overall deflection. The design constraint on the separation, which is limited by the MUMPs process [46], [57] is set to 1.75 μm [15].

5. *Flexure length:* Increasing the flexure length will reduce the force lost in bending the thermal actuator [5]. This increase is limited by the fact that a longer flexure will begin to act as the thin arm resulting in a thermal expansion at the wide arm side. It has been observed that an increase in flexure length has a limited effect on the deflection [5]. The point of no increase in deflection though has not been determined. This limits the design constraint on the maximum flexure length in a range of 50-70 μm.

6. *Thickness:* Increasing the actuator thickness has a limited effect on the overall deflection. The design constraint on the actuator thickness is set to 2 μm.

State Variables: Thermal actuators are limited in their applications because at high temperatures polysilicon can deform plastically leading to actuator failure. At high temperatures the thermal actuator has been observed to emit visible radiation [58]. Above the brittle to ductile transition temperature (660 °C) the thin arm deforms plastically changing the position of the actuator [58]. Beyond 800-1000 °C the material properties of polysilicon will also significantly be affected [28]. This suggests that the

maximum temperature in the thermal actuator should be limited to 800°C to ensure a conservative design.

Objective function: Typically the thermal actuator should be optimized for minimum power consumption. This however is a difficult approach in finite element analysis. An indirect approach can be employed which will provide a greater deflection for the same applied voltage while performing a check to ensure that the maximum temperature is less than 800°C. Since the Subproblem Approximation Method always minimizes the objective function it is convenient to take the negative deflection as an objective function.

5.2.2 Loaded Actuators

Typically actuators are used to support some type of load. One of the important points in an optimization for loaded actuators is that a tradeoff exists between actuator deflection and force. For example, increasing the wide arm length increases deflection but not force and vice versa. Because of this tradeoff a careful selection of the optimization variables must be done.

Design variables:

1. *Length:* Increasing the length of the actuator will decrease the force output. A significant decrease in the length, however, will provide a large force reducing the deflection. It has been observed that actuators with a length of 200 to 250 μm provide good deflection and force [15]. This sets the design constraint on the actuator length from 200 to 250 μm.

2. *Width of thin arm:* Increasing the thin arm width from 1.75 to 2.5 μm increases force output but this levels off and even decreases after a width slightly greater than the actuator thickness [15]. Increasing the thin arm width also increases power consumption. This sets the design constraint on the width of the thin arm from 1.75 to 3.5 μm.

7. *Width of wide arm:* Decreasing the width of the wide arm will reduce the temperature difference reducing the deflection by a significant amount. The design constraint for the wide-to-thin arm width ratio must be set from at least 3:1 to 8:1 to ensure a conservative design.

3. *Gap:* Increasing the separation between the two arms increases the delivered force with a reduced power consumption [15]. The deflection is however reduced. This sets the design constraint on the actuator separation from 1.75 to 4 μm.

4. *Flexure arm length:* The flexure arm length has the most significant effect on the actuator performance. For low force applications longer flexure require more power while for high forces the power varies depending on the actuator length [15]. Optimal thermal actuators have been observed to have a flexure arm length to wide arm length ratio from 1:3 to 1:4. This sets the design constraint on the flexure arm length from 30 to 60 μm.

5. *Thickness:* Increase in the actuator thickness increases the force but at the expense of higher power consumption. The increase in thickness leads to a larger cross-sectional area of the thin arm, which requires more current to provide the required current density [15]. Using the MUMPs process [57], there are three possible thickness of the polysilicon layers: 1.5 μm, 2 μm, 3.5 μm. The design constraint on the actuator thickness is set to 2 μm.

State Variables: The state variable is the same as in the case of unloaded actuators, which sets the maximum temperature to 800°C.

Objective function: For a loaded actuator an increased force leads to a decrease in deflection. The objective function in this case is the absolute value of the maximum deflection. Using the design constraints above the optimization routine will minimize the deflection within a reasonable range to achieve a tradeoff between the force output and deflection.

5.3 OPTIMIZATION STUDY

An optimization study is useful to determine the basic geometric design parameters of the actuator. Chen et al. [59] have conducted a finite element study to investigate the effect of dimension variation on the actuator performance by analyzing different models. As an alternative, the optimization subroutine can be easily employed to study the effect of change of variables on the deflection, force and power requirements of the actuator. As mentioned earlier the optimization study should be conducted to reduce the power consumption of the thermal actuator. This however is a difficult approach in finite element analysis giving infeasible results. Hence, for an unloaded thermal actuator an indirect approach was implemented which maximizes the deflection of thermal actuator for the same applied voltage while keeping the maximum temperatures reached within safe limits. This is a more efficient approach and gives a large number of feasible design sets. By studying the design sets the best thermal actuator that gives a greater steady-state deflection for the same or lesser power consumed can be selected for the required application. For loaded thermal actuators, the optimization is more difficult since the deflection is minimized for the same applied voltage to obtain a larger force. From the feasible design sets, the thermal actuator that a larger force for the same or lesser power consumed with a reasonable steady-state deflection can be selected for the required application.

5.3.1 Unloaded Actuator

Table 5 compares the original and the optimized thermal actuator parameters. The optimization subroutine is conducted using the design guidelines in the previous section. For an unloaded actuator the most significant difference in deflection is obtained from the increase in actuator length, decrease in the thin and wide arm spacing, an increase in the wide arm width and decrease in flexure length. This is consistent with the experimental results. The optimization subroutine determines the optimum flexure length for thermal actuator. It has been observed that as the applied voltage increases the optimum flexure length also increases.

Table 5 shows the optimized actuator parameters for an applied voltage of 5 V. From the feasible design sets available the best thermal actuator that gives the maximum deflection for a lesser power consumption was selected as optimum. The optimized actuator shows a 21% reduction in the power consumed with a 27% increase in the maximum steady-state deflection for the same applied voltage. This percentage reduction in power consumption and increase in maximum deflection is observed to remain consistent for the range of applied voltages. Figure 41 illustrates this point. The optimized thermal actuator shows a reduced maximum temperature for any applied voltage. This is mainly contributed by the change in the gap, the width of the wide arm and flexure arm length.

Parameters	l_t	l_f	w_t	w_w	g	V	Max. Temp.(°C)	Deflection (μm)	I (mA)	Power (mW)
Initial	200	36	2	15	2	5	673	7.2	3.9	19.5
Optimized	250	30	2	16	1.75	5	510	9.2	3.1	15.5

Table 5: Comparison of original and optimized actuator parameters for maximum steady-state deflection.

The optimization comparison was done with the same applied voltage since this is the only input, which can be controlled and hence facilitates a comparison between the different actuator parameters. The optimization subroutine can also be employed to design a complete thermal actuator based on the changes in the design and state variable. For example, specifying the applied voltage as a design variable within any required limits and the maximum temperature as a state variable allows for a complete selection of an optimized thermal actuator for the required maximum steady state deflection based on the design sets.

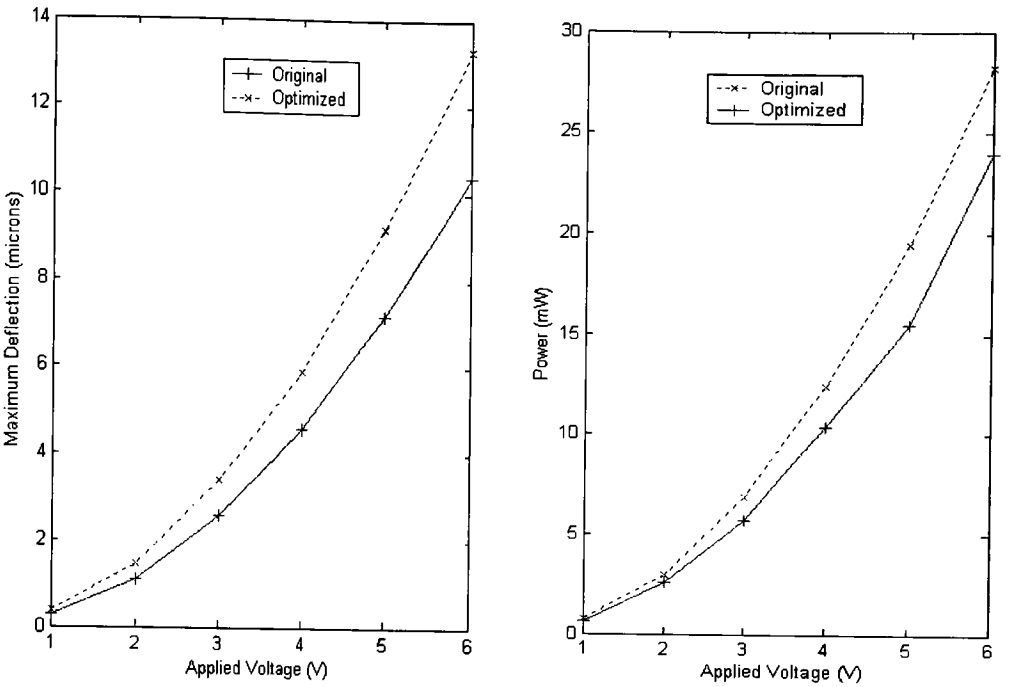

Figure 42: Comparison of original and optimized unloaded actuator performance for range of applied voltages.

5.3.2 Loaded actuators

The optimization of loaded actuators requires significant optimization iterations for a complete design. This is because as the force provided by the thermal actuator increases the available deflection decreases. Since, the optimization subroutine is employed to minimize the deflection in this case, a tradeoff between the available force and deflection must be done. The optimization subroutine can be employed to design the thermal actuator based on a required steady-state deflection in order to optimize the force.

Table 6 compares the original and optimized actuator parameters for loaded actuators. From the feasible design sets, the best thermal actuator that gave a higher force while giving a reasonable value of deflection for the same power consumed was chosen as the optimum. Since the deflection is minimized the significant parameters that affect the force output from the thermal actuator are a decrease in the actuator length, increase in the width of the thin arm, decrease in the width of the wide arm and increase in the thin arm and wide arm

spacing. The flexure arm length in this case is observed to increase with the applied voltage. The typical optimized flexure arm length from the design sets is observed to be between 35-50 μm. The optimized thermal actuator shows an 8% increase in the force output from the original geometry for approximately the same power consumed. Further increase in the force output leads to a significant decrease in the deflection, which dominates over the benefit of obtaining more force. This trend remains consistent over the range of applied voltages (Figure 42). Extensive analysis of the thermal actuator must be done by variation of the design variables to achieve an optimum tradeoff between force and deflection. The increase in force output is consistent as the applied voltage increases. The power consumed by the optimized actuators is slightly higher than the original actuators.

Parameters	l_t	l_f	w_t	w_w	g	V	Max. Temp. (°C)	Deflection (μm)	Force (μN)	I (mA)	Power (mW)
Original	200	36	2	15	2	5	673	7.2	4.7	3.9	19.9
Optimized	235	50	2.8	13	3	5	543	5.2	5.1	4	20

Table 6: Comparison of original and optimized actuator parameters for maximum force output

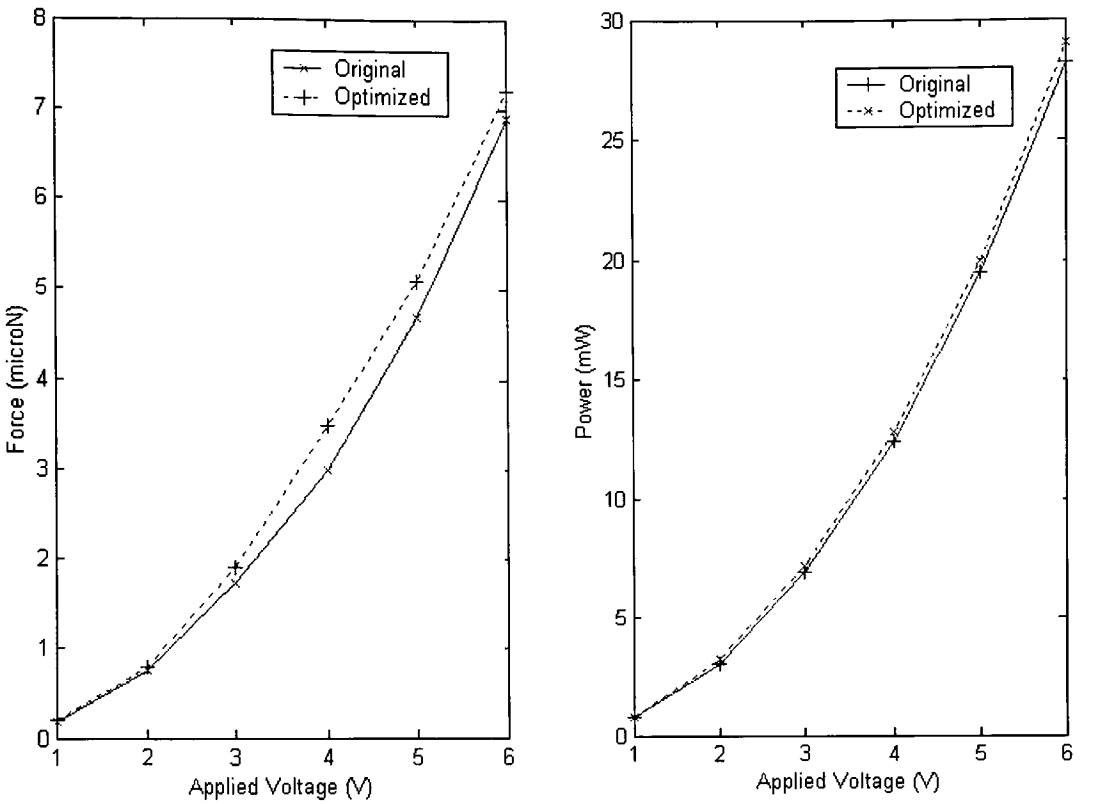

Figure 43: Comparison of original and optimized loaded actuator performance for range of applied voltages

CHAPTER 6

SUMMARY AND CONCLUSIONS

This chapter initially reviews the thesis objectives and contributions described in Chapter 1. Then the results from the different analyses conducted on the actuator are summarized. Finally, recommendations for future work on the models are discussed.

6.1 PROBLEM OBJECTIVES

In MEMS, polysilicon electrothermal microactuators have been established as providing an easily controlled micro-actuation method with desirable characteristics such as large output forces and displacements, ease of fabrication and compatibility with standard microelectronics. The thermal microactuator analyzed in this thesis is a similar microactuator in the above category with the only limitations being large power consumption and potential failure by stiction or buckling.

The problem objective in this thesis is to examine the characteristics of the actuator by investigating the importance of temperature dependent parameters that affect the analysis through a comprehensive finite element analysis. The best modeling approach at steady state is employed for further dynamic analysis to compare the results from analytical solutions and experimental measurements. The problem is also extended to compare the performance of the actuator in a vacuum environment with that in an air environment and for design optimization to minimize power consumption.

6.2 THESIS CONTRIBUTIONS

1. The finite element models of the thermal actuator developed in this thesis determine the significance of material properties of polysilicon that influence the actuator response. The actuator is analyzed for each thermophysical property and its

variations. This approach provides insight into the influence of polysilicon material properties on thermal actuator analysis.

2. The actuator characteristics are investigated entirely within a generic finite element analysis package. This thesis attempts to establish a design methodology that can be applied to analysis of any surface micromachined MEMS actuator using finite element simulations.

3. The thesis extends itself from previous work to study in more detail the transient characteristics of these actuators. A comprehensive analysis, which includes all the relevant thermophysical properties, temperature dependencies and heat losses, is conducted to get an accurate prediction of the transient response. Effects of pulse width modulation, which affect the transient response of the actuators, are analyzed.

4. The device behavior is analyzed in air and vacuum. The steady state power required for a specific deflection and the total energy consumption of the actuator, for both, air and vacuum are compared. This may or may not validate the use of these actuators for low power consumption.

5. Design optimization of the thermal actuator is investigated by using the ANSYS Parametric Design Language (APDL). The optimization subroutine can be implemented to investigate and compare the performance of the thermal actuator or to design a thermal actuator by changing of the design variables to obtain a thermal actuator geometry that gives optimum force and deflection output for minimal power consumption.

6.3 CONCLUSIONS

The finite element model shows significant differences depending upon the thermophysical properties of polysilicon. Since, the material properties of heavily doped polysilicon are highly dependent on temperature the performance of the actuator is typically expected to follow the full temperature dependencies. The assumption of constant room temperature

material properties seems to agree well with the experimental data for most of the actuator simulations. Any model that predicts approximately the same temperature difference agrees with the experimental measurements. A finite element model that consistently agrees with experiment cannot be characterized. The variation in the different comparisons should probably arise from the assumption of shape factors that approximate the heat loss from the vertical sidewalls of the thermal actuator. Typically the shape factors seem to overestimate the heat loss. Another possibility for such variations might also be arising from the material property variations of thin film polysilicon. The current material property variations might not accurately characterize the thermal actuator performance consistently. The comparison of the thermal actuator is limited by validation with only steady-state deflection data.

The thermal actuator behavior in vacuum is highly dependent on material property variations in polysilicon and the full temperature dependencies must be employed to characterize the actuator behavior. The dynamic performance of the thermal actuator predicted by finite element analysis shows a large deviation from the measured results. This variation should be typically due to errors in thermal profile arising out of shape factor assumptions or material property variations. In comparison of the thermal actuator performance in vacuum and air the actuator performance in vacuum shows a limited improvement over that in air.

Design optimization of unloaded thermal actuators shows a good possibility for designing thermal actuators for reduced power consumption. For loaded thermal actuators however a significant amount of analysis is required to obtain an optimum design that provides a tradeoff between deflection, force and power consumption. Finite element analysis though provides an easier method for optimization of these thermal actuators than the previous trial and error approach.

6.4 RECOMMENDATIONS FOR FUTURE WORK

The models analyzed in this thesis have led to observations for future research on the analysis of the thermal actuator.

The most important parameter that affects the analysis is the shape factor that accounts for the heat loss from the vertical sidewalls. There is no definite approximation to estimate the heat loss from the vertical faces. Any errors in the shape factors will lead to an inaccurate thermal profile and deflection predictions. The constant model agrees well for all fabricated actuators but the thermal profile from this model is assumed to be approximate. The models, which take into account the variation of thermal conductivity of polysilicon and air, also come close to the measured results. Though this is in agreement with Lott's [28] results the models though are not consistent over the compared data. This can be either due to errors in experiment or due to the assumption of shape factors.

To resolve this a comprehensive analysis should be conducted on the thermal actuator by using the guidelines and procedures followed in the thesis. This comprehensive analysis will consist of a mesh of air around the thermal actuator and the silicon substrate. As an example, bent beam electro thermal microactuators modeled by Messenger [60] using a comprehensive finite element analysis overestimate the output deflection of these actuators by almost two times with the assumption of constant material properties. The comprehensive analysis will eliminate the use of shape factors in the analysis thus removing any inaccuracies that might arise out of their assumptions. The comprehensive analysis can be conducted by modeling the air and substrate using SOLID87 elements [53] and employing the sequential solution to solve the electro-thermal and thermal-elastic analysis separately to speed computation and convergence time.

At high temperatures above 800-1000°C the electrical resistivity of polysilicon shows a decrease with temperature due to high current and heating causing local melting of boundary layers between polysilicon crystal grains [28]. The use of the linear dependence of electrical resistivity with temperature in the analysis might lead to inaccurate profiles at high voltages. Mankame [25], [26] has implemented an alternative solution to modeling this temperature dependency, by determining the device resistance as a function of voltage and using the device geometry to obtain voltage dependent electrical resistivity. This should be done experimentally for MUMPs polysilicon and implemented for further analysis of the thermal actuators investigated in this thesis.

Though limited in their applications, simulations in vacuum provide a promising alternative for power savings. A high level of vacuum may or may not be needed to achieve these power savings. Hickey [30] has investigated the deflection of the thermal actuator with variation in the vacuum pressure. The thermal actuator should be implemented in vacuum using Hickey's [30] results and the analysis done in this thesis. A method for improvement of the energy response of the actuator in vacuum was investigated by providing short high voltage pulses to the thermal actuator to achieve approximately the same steady state deflections. These results should be tested experimentally. The finite element analysis also does not predict accurate dynamic deflection response. This analysis should be investigated further.

The analytical model developed by Hickey [30] described in the previous chapter agrees with the finite element models, which estimate the experimental data closely. For a particular actuator of geometry l_t = 200, l_w = 170, t_t = 2, t_f = 2,t_w = 15, g = 4, this analytical model predicts a maximum steady state deflection of 11.2 μm. The finite element models predict a significantly lesser deflection (6 μm) than the analytical model. This inconsistency in the prediction of the actuator deflection has also been confirmed by a 2D finite element analysis that uses the same temperature difference and material properties as that employed by the analytical model. The analytical model also tends to predict a greater force output available from the thermal actuator. The analytical model should be investigated for these inconsistencies.

Design optimization of the thermal actuator should be investigated further by using definite temperature variations in the material properties. The trends observed from the constant model may or may not be consistent with the inclusion of polysilicon material property variations. The optimization of loaded thermal actuators should be analyzed extensively. This will require significant optimization runs by narrowing the design space to obtain a thermal actuator design that provides optimum force output and deflection for minimal power consumption.

APPENDIX A

THE MUMPs PROCESS

MEMS fabrication methods such as surface micromachining, bulk micromachining, LIGA (an acronym from the German words for lithography, electroplating, and molding) exist. The MUMPs (Multi User MEMS Process) [46] has been successfully applied previously to micro-optical systems employing arrays of thermal actuators to control the positioning of scanning and rotating micromirrors and rotary stepper motors (see for example Comtois and Bright [1]).

MUMPs is a surface micromaching process that uses three structural layers of polysilicon. In surface micromachining, thin films of material are deposited by methods such as oxidation, sputtering, evaporation or low-pressure chemical vapor deposition (LPCVD). With polysilicon, thin films are deposited with alternating layers of silicon oxide, which acts as the sacrificial layer.

The process starts with a silicon wafer. Phosphorus is used to dope the surface of the wafer. The doping is done in a standard diffusion furnace. Doping prevents charge feed through to the substrate and imparts to the layer a desired electrical resistivity. The doping process can be uniform or done selectively on parts of the device or uniformly. This is an important step in surface micromachining because the behavior of electro-thermo-mechanical devices is strongly dependent on the electrical resistivity.

Then, a thin silicon nitride layer is deposited. The layer, which acts as an electrical isolator, is deposited by LPCVD. A sacrificial layer is deposited using wet oxidation. A layer of photoresist is deposited and patterned. The photoresist is developed and exposed areas are removed chemically. This creates an anchor hole for the silicon dioxide. The photoresist is stripped. Amorphous polysilicon is deposited and annealed to obtain a polycrystalline structure. The photolithography process is repeated for each sacrificial and structural layer. A stack may contain four to five layers. After all layers are deposited a final release etch is performed which removes the sacrificial material leaving the structural layers free to perform

mechanical functions. These steps are illustrated in Figure A1, which explain the fabrication of a simple cantilever beam to explain the surface micromachining process [37].

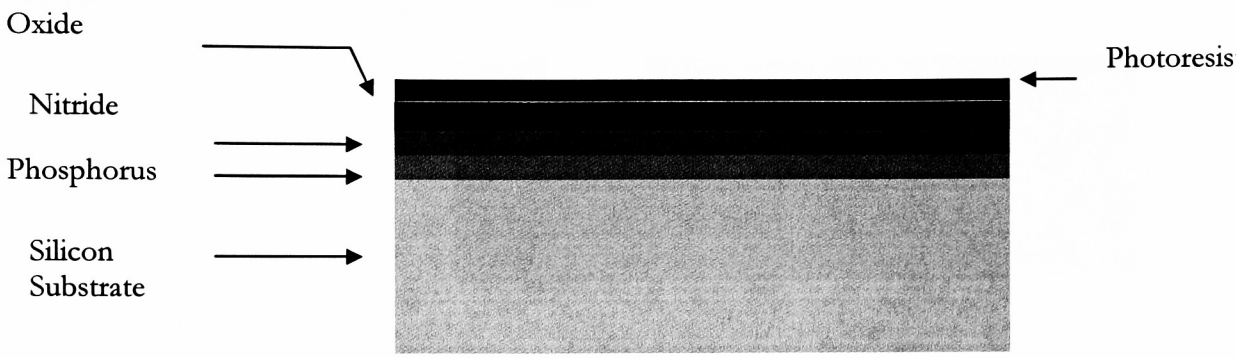

Figure A1 (A)- Deposition of layers

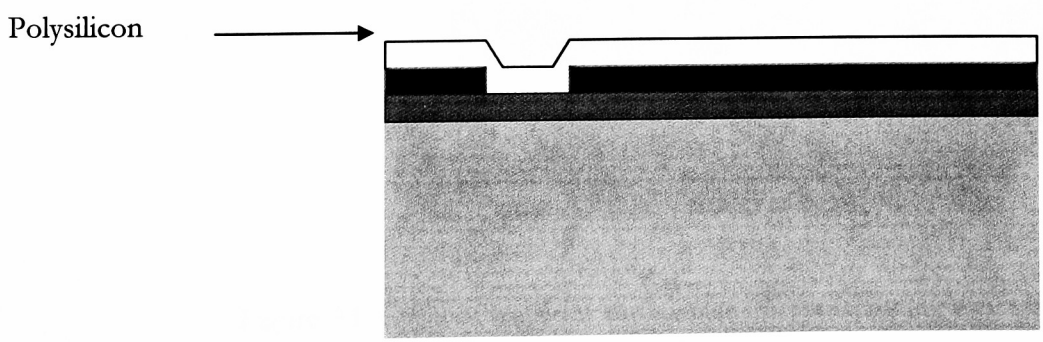

Figure A1 (B)- Deposition of polysilicon

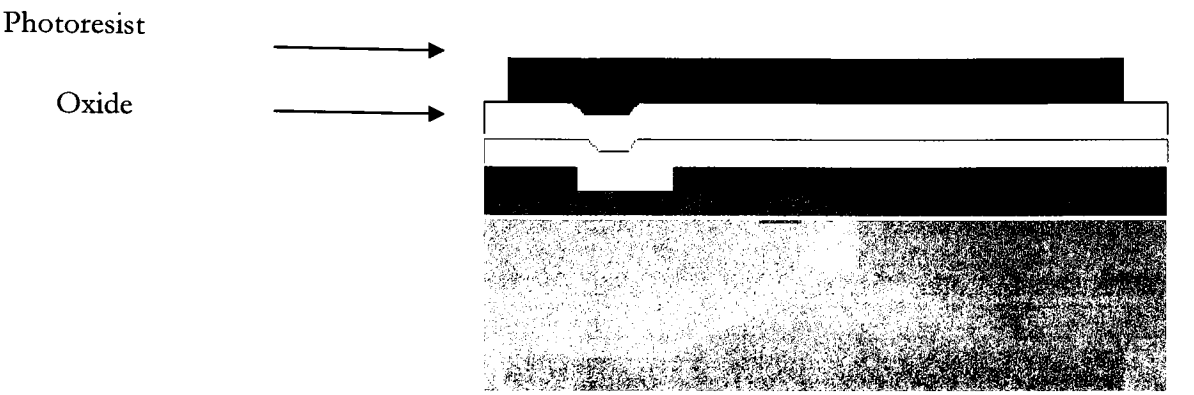

Figure A1(C)- Patterned photoresist ready to etch away underlying polysilicon

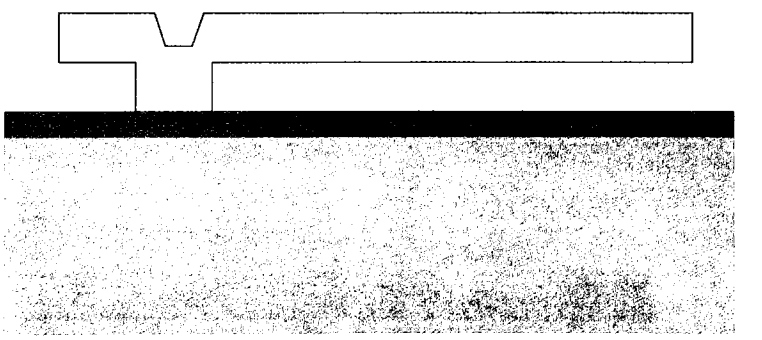

Figure A1 (D)- Cantilever beam

Figure A1: Cycle of steps for the surface micromachining process [37]

The major problem with fabricating suspended beam like structures is the variance of stress in the materials developed during fabrication. This stress causes the structures to curl up or down depending on the type of stress (tensile or compressive). However the LPCVD

process promoted by the DARPA sponsored MUMPs foundry service provided by Microelectronics center of North Carolina (MCNC) produces nearly stress free polysilicon structures [6,12].

Figure A2 gives a cross sectional view of the materials in the MUMPs process. The first polysilicon layer poly0 is 0.5 μm thick and non-releasable. It is commonly used for local wiring and address electrodes. The upper two polysilicon layers poly1 and poly2 are 2.0 μm and 1.5 μm. They can be released to form micromechanical devices. A high temperature anneal follows the deposition of polysilicon to relieve residual stress in these layers. The release is achieved by etching away the two oxide layers (2.0 μm and 0.75 μm) deposited between the polysilicon layers. Gold is deposited on the poly2 layer for bond pads, low resistance wiring and reflective surfaces. All the layers are built above a 0.5 μm thick silicon nitride layer, which insulates them from the heavily n-doped silicon substrate [6,12]

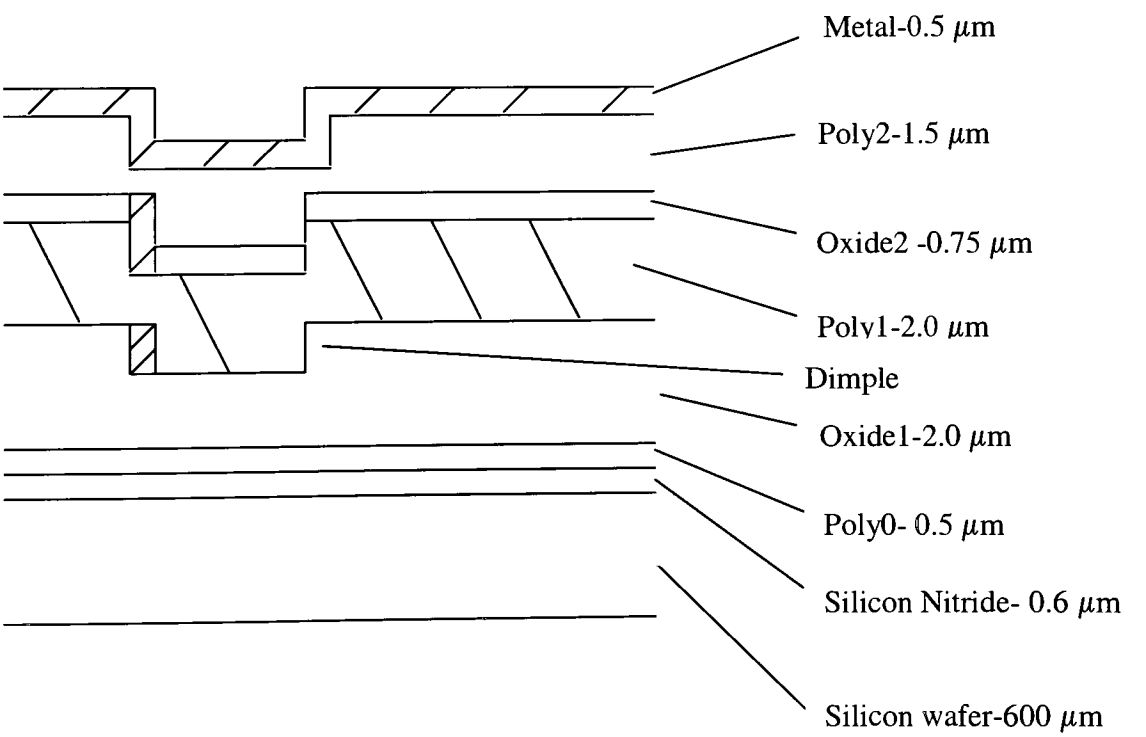

Figure A2: Cross sectional view of materials used in the three layer surface micromachining MUMPs technology [12]

The steps in a typical MUMPs run are explained briefly [28,57]:

1. A 100 mm diameter silicon wafer is heavily doped with phosphorus $POCL_3$ is used as a dopant source.
2. A 0.5 μm thick silicon nitride layer is deposited by LPCVD.
3. A 0.5 μm Polysilicon layer (Poly0) is deposited and patterened lithographically.
4. Poly0 is etched by RIE.
5. A 2.0 μm thick phosphosilicate glass layer (Oxide1) is deposited by LPCVD.
6. Dimple layer is patterened into Oxide1 and etched by RIE.
7. Anchor1 is patterened and etched by RIE. This is a cut through Oxide1 and forms a hole for poly1 to contact the underlying layers to form a support anchor.
8. Poly1 is deposited (2.0 μm), covered with PSG and annealed at 1050^0C.
9. Poly1 is lithographically patterned and etched by RIE.
10. Any remaining PSG is removed.
11. Oxide2 is deposited at 0.75 μm thick and patterned twice. A cut through oxide2 called p1p2 via which opens a hole for the poly1 to contact poly2. Anchor2 is a hole through the oxide for poly2 to form support anchors.
12. Poly2 is deposited (1.5 μm), covered with PSG and annealed.
13. Poly2 is patterned and etched.
14. Any remaining PSG is removed.
15. Gold is deposited (0.5 μm) and patterned using lift-off.
16. A photoresist protective layer is applied.
17. The wafer is diced for shipment.

APPENDIX B

APDL DESIGN OPTIMIZATION BATCH FILE

```
/BATCH
/COM,ANSYS RELEASE 6.1    UP20020321      13:24:44    05/17/2003
/input,menust,tmp,"",,,,,,,,,,,,,,,1
/GRA,POWER
/GST,ON
/PLO,INFO,3
/GRO,CURL,ON
/REPLOT,RESIZE
/PREP7
ET,1,SOLID98                                    ! ELEMENT TYPE
KEYOPT,1,1,0                                    ! DOF SELECTION
KEYOPT,1,3,0
KEYOPT,1,5,0


! MATERIAL PROPERTY DATABASE

MPTEMP,1,20,220,420,620,820                     ! TEMPERATURES
MPDATA,EX,1,169E3,169E3,169E3,                  ! MODULUS OF ELASTICITY
169E3,169E3
MPDATA,PRXY,1,.22,.22,.22,.22,.22               ! POISSON'S RATIO
MPDATA,ALPX,1,2.7E-6,2.7E-6,2.7E-6,             ! COEFFICIENT OF THERMAL
                                                  EXPANSION
2.7E-6,2.7E-6
MPDATA,KXX,1,32E6,32E6,32E6,                    ! THERMAL CONDUCTIVITY
32E6,32E6
MPDATA,EMIS,1,.6,.6,.6,.6,.6                    ! EMISSIVITY
MPDATA,RSVX,2E-11,2E-11,2E-11,2E-11,2E-11       ! ELECTRICAL RESISTIVITY
MPDATA,HF,1,75,120,135,140,160                  ! CONVECTION COEFFICIENT FOR
                                                  THIN ARM, FLEXURE ARM AND
                                                  END CONNECTION
MPDATA,HF,2,47,76,85,88,90                      ! CONVECTION COEFFICIENT
                                                  FOR WIDE ARM


! MODEL PARAMETERS

*SET,lt,200                                     ! LENGTH OF THIN ARM
*SET,lf,0.18*lt                                 ! LENGTH OF FLEXURE ARM
*SET,lw,lt-lf                                   ! LENGTH OF WIDE ARM
*SET,wt,2                                       ! WIDTH OF THIN ARM
*SET,wf,wt                                      ! WIDTH OF FLEXURE ARM
```

```
*SET,ww,15          ! WIDTH OF WIDE ARM
*SET,g,2            ! GAP
*SET,e,8            ! END CONNECTION
*SET,t,2            ! THICKNESS OF POLYSILICON LAYER
*SET,V,3            ! APPLIED VOLTAGE
*SET,ta,2           ! THICKNESS OF AIR GAP
*SET,tn,0.6         ! THICKNESS OF NITRIDE LAYER
*SET,tsi,600        ! THICKNESS OF SILICON SUBSTRATE
*SET,ka,0.026e6     ! THERMAL CONDUCTIVITY OF AIR
*SET,kn,2.25e6      ! THERMAL CONDUCTIVITY OF
                     NITRIDE
*SET,ksi,150e6      ! THERMAL CONDUCTIVITY OF
                     SILICON SUBSTRATE
*SET,Tbulk,20       ! BULK TEMPERATURE OF AIR
*SET,S,5.67e-8      ! STEFAN BOLTZMANN CONSTANT
*SET,esize,10       ! ELEMENT SIZE


! CONDUCTION PARAMETERS


*SET,h,(1/((ta/ka)+(tn/kn)+(tsi/ksi)))   ! CONDUCTIVE HEAT PATH TO
                                          SUBSTRATE

*SET,ht,(((t/wt)*((2ta/t)+1))+1)*h       ! CONDUCTIVE HEAT LOSS FOR
                                          THIN AND FLEXURE ARM
*SET,hw,(((t/ww)*((2ta/t)+1))+1)*h       ! CONDUCTIVE HEAT LOSS FOR
                                          WIDE ARM
*SET,he,(((t/we)*((2ta/t)+1))+1)*h       ! CONDUCTIVE HEAT LOSS FOR
                                          END CONNECTION


! GEOMETRY OF THERMAL ACTUATOR

K,1 ,0,0,,          ! ANCHOR1 KEYPOINTS
K,2 ,40,0,,
K,3 ,40,40,,
K,4 ,0,40,,
K,5 ,40,40-wf,,     ! FLEXURE ARM KEYPOINTS
K,6 ,40+lf,40-wf,,
K,7 ,40+lf,40,,
K,8 ,40+lf,40-ww,,  ! WIDE ARM KEYPOINTS
K,9,40+lt,40-ww,,
K,10 ,40+lt,40,,
K,11 ,40+lt-e,40,,  ! END CONNECTION KEYPOINTS
K,12 ,40+lt-e,40+g,,
```

```
K,13 ,40+lt,40+g,,                    ! THIN ARM KEYPOINTS
K,14 ,40+lt,40+g+wt,,
K,15 ,40,40+g,,
K,16 ,40,40+g+wf,,
K,17 ,40,80+g,,                       ! ANCHOR2 KEYPOINTS
K,18 ,0,80+g,,
K,19 ,0,40+g,,
A,1,2,3,4                             ! ANCHOR1
A,5,6,7,3                             ! FLEXURE ARM
A,7,8,9,10                            ! WIDE ARM
A,10,13,12,11                         ! END CONNECTION
A,13,14,16,15                         ! THIN ARM
A,15,17,18,19                         ! ANCHOR2
VEXT,ALL                              ! VOLUMES
VADD,ALL
ESIZE,esize,0,
VMESH,ALL                             ! MESH


! AREA PARAMETERS

*SET,A1,45                           ! ANCHOR1
*SET,A2,47                           ! ANCHOR2
*SET,At1,43                          ! THIN ARM BOTTOM SURFACE
*SET,At2,46                          ! THIN ARM TOP SURFACE
*SET,Af1,2                           ! FLEXURE ARM BOTTOM SURFACE
*SET,Af2,24                          ! FLEXURE ARM TOP SURFACE
*SET,Aw1,48                          ! WIDE ARM BOTTOM SURFACE
*SET,Aw2,13                          ! WIDE ARM TOP SURFACE
*SET,Ae1,4                           ! END CONNECTION BOTTOM
                                      SURFACE
*SET,Ae2,49                          ! END CONNECTION TOP SURFACE


! BOUNDARY CONDITIONS

DA,A1,UX                             ! ANCHORS CONSTRAINED TO
                                      SUBSTRATE
DA,A2,UX
DA,A1,UY
DA,A2,UY
DA,A1,UZ
DA,A2,UZ
DA,A1,TEMP,20                        ! ESSENTIAL BOUNDARY CONDITIONS
                                      AT ANCHORS

DA,A2,TEMP,20
```

```
DA,A1,VOLT,0                    ! APPLIED VOLTAGE AT ANCHORS
DA,A2,VOLT,V
SFA,At1,,CONV,ht,Tbulk          ! CONDUCTION AT THIN ARM
SFA,Af1,,CONV,hf,Tbulk          ! CONDUCTION AT FLEXURE ARM
SFA,Aw1,,CONV,hw,Tbulk          ! CONDUCTION AT WIDE ARM
SFA,Ae1,,CONV,he,Tbulk          ! CONDUCTION AT END CONNECTION
SFA,At2,,CONV,-1,Tbulk          ! CONVECTION AT THIN ARM
SFA,Af2,,CONV,-1,Tbulk          ! CONVECTION AT FLEXURE ARM
SFA,Aw2,,CONV,-1,Tbulk          ! CONVECTION AT WIDE ARM
SFA,Ae2,,CONV,-2,Tbulk          ! CONVECTION AT END CONNECTION
SFA,At2,,RDSF,-1,1,             ! RADIATION AT THIN ARM
SFA,Af2,,RDSF,-1,1,             ! RADIATION AT FLEXURE ARM
SFA,Aw2,,RDSF,-1,1,             ! RADIATION AT WIDE ARM
SFA,Ae2,,RDSF,-1,1,             ! RADIATION AT END CONNECTION
NEQIT,100                       ! MAXIMUM NUMBER OF EQUILIBRIUM
                                  ITERATIONS


! RADIOSITY SOLVER

/AUX12
STEF,S                          ! STEFAN-BOLTZMANN CONSTANT
TOFFST,0
RADOPT,0.10000000149,0.999999974738E-04,0,
1000,0.10000000149,0.10000000149
SPCTEMP,0,20

! SOLUTION

SOLVE
FINISH


! RESULTS

/POST1
NSORT,U,Y,1,1,,                 ! MAXIMUM DEFLECTION PARAMETER
*GET,D,SORT,,MAX,               ! SCALAR DATA OF MAXIMUM
                                  DEFLECTION
NSORT,TEMP,,1,1,,               ! MAXIMUM TEMPERATURE PARAMETER
*GET,TEMP,SORT,,MAX,            ! SCALAR DATA OF MAXIMUM
                                  TEMPERATURE
ASEL,S,,,A1                     ! SELECT ANY ANCHOR AREA
NSLA,S,1                        ! SELECT ALL NODES
PRRSOL,AMPS                     ! CURRENT CONSUMPTION
SAVE
```

```
! DESIGN OPTIMIZATION

/OPT
OPANL,'file','log',' '                  ! ASSIGN BATCH FILE
OPVAR,LT,DV, ,250, ,                    ! DESIGN VARIABLES
OPVAR,WW,DV, ,8*wt, ,
OPVAR,WT,DV,2,, ,
OPVAR,V,DV, ,10, ,
OPVAR,G,DV,1.75,, ,
OPVAR,TEMP,SV, ,900, ,                  ! STATE VARIABLES
OPVAR,D,OBJ, , , ,                      ! OBJECTIVE VARIABLE
OPTYPE,SUBP                             ! OPTIMIZATION SOLVER
OPSUBP,30,7,
OPEQN,0,0,0,0,0,
OPEXE                                   ! SOLVE
```

REFERENCES

1. Comtois, J.H., Bright, V.M., "Surface micromachined polysilicon thermal actuator arrays and applications," Technical Digest, Solid State Sensor and Actuator workshop, Hilton Head, SC, 1990, pp. 174-177.
2. Sandia National Laboratories, Personal Communication, November 2002.
3. Senturia, S., *Microsystem Design*, 2002, Kluwer Academic Publishers.
4. Guckel, H., Klein, J., Christenson, T., Skrobis, K., Laudon, M., Lovell, E., "Thermo-magnetic metal flexure actuators," Technical digest, Solid State Sensor and Actuator Workshop, 1992, pp 73-75.
5. Comtois, J .H., Bright Victor M., Phipps, M.W., "Thermal microactuators for surface-micromachining processes", *Proc. SPIE*, Vol.2642, 1995, pp. 10-21.
6. Comtois, J.H., Bright, V.M., "Design techniques for surface-micromachining MEMS processes," *Proc. SPIE*, Vol.2639, 1995, pp. 211-222.
7. Reid, J., Bright, V.M., Comtois, J., "Arrays of thermal microactuators coupled to micro-optical components," Actuator technology and Applications, vol. 2865, 1997, pp. 74-82.
8. Comtois, J.H., Bright, V.M., "Applications for surface-micromachined polysilicon thermal actuators and arrays," *Sensors and Actuators A*, vol.58, 1997, pp.19-25.
9. Butler, J.T., Bright, V.M., Reid, R.J., "Scanning and rotating micromirrors using thermal actuators," *Proc.SPIE*, Vol.3131, 1997, pp. 134-144.
10. Moulton, T., Ananthasuresh, G.K., "Micromechanical device with embedded electro-thermal-compliant actuation", *Sensors and Actuators A,* vol. 90, 2001, pp. 38-48.
11. Kolesar, E.S., Allen, P.B., Howard, J.T., Wilken, J.M., Boydston, N, "Thermally-actuated cantilever beam for achieving large in-plane mechanical deflections," *Thin Solid Films*, 1999, vol. 355-356, pp 295-302.
12. Allen, P.B, Boydston, N.C., Howard, J.T., Ko, S.Y., Kolesar, E.S., Jr., "Theoretical and experimental characterization of the in-plane tip force and deflection achieved with asymmetrical polysilicon electro thermal microactuators", Micromachined Devices and Components, *Proc.SPIE*, Vol.4176, 2000, pp.148-158.

13. Lerch, P., Slimane, C.K., Romanowicz, B., Renaud, P., 1996, " Modelization and characterization of asymmetrical thermal micro-actuators," *Journal of Micromechanics and Microengineering*, vol. 6, 1996, pp.134-137.
14. Comtois, J.H., Michalicek, M., Barron, C., "Electro thermal actuators fabricated in four-level planarized surface micromachined polycrystalline silicon," *Sensors and Actuators A*, vol. 70, 1998, pp. 23-31.
15. Reid, J., Bright, V.M., Comtois, J.H., "Force measurements of polysilicon thermal microactuators," Micromachined Devices and Components, vol.2882, 1996, pp. 296-306.
16. Butler, .T., Bright V.M, "Electrothermal and fabrication modeling of polysilicon thermal actuators," ASME DSC-MEMS, vol.66, 1998, pp.571-576.
17. Butler, J.T., Bright, V.M., Cowan, W.D., "SPICE modeling of polysilicon thermal actuators," *Proc.SPIE*, vol.3224, 1997, pp. 284-293.
18. Reid, J.R., Silversmith, D.J., " Joule heating simulation of polysilicon thermal micro-actuators," International Conference on Modeling and Simulation of Microsystems, vol.2, 1999, pp. 613-616.
19. Allen, P.B., Howard, J.T., Kolesar, E.S., Wilken J.M., "Design, finite element analysis and experimental performance evaluation of thermally-actuated beam used to achieve large in-plane mechanical deflections," Solid State Sensor and Actuator Workshop, MEMS Conf., Late News Poster Session, 1998, pp. 5-6.
20. Huang, Q.A., Lee, N.K.S., "Analysis and design of polysilicon thermal flexure actuator," *Journal of Micromechanics and Micrengineering*, vol.9, 1999, pp. 64-70.
21. Huang, Q.A., Lee, N.K., "A simple approach to characterizing the driving force of polysilicon laterally driven thermal microactuators," *Sensors and Actuators*, vol.80, 2000, pp. 267-272.
22. Lin, L., Chiao, M., "Electrothermal responses of lineshape microstructures," *Sensors and Actuators A*, vol.55, 1996, pp.35-41.
23. Mastrangelo, C., His-jen Yeh, J., Muller, R., "Electrical and optical characteristics of vaccum sealed polysilicon microlamps", IEEE Transactions on Electron Devices, vol.39, no.6, 1992, pp. 1363-1374.
24. Pan, C.S., Hsu, W., "An electro-thermally and laterally driven polysilcon microactuator," *Journal of Micromechanics and Microenginnering*, vol. 7, 1997, pp. 7-13.

25. Mankame, N.D., "Modeling of electro-thermal-compliant mechanisms," M.S. Thesis, University of Pennsylvania, Philadelphia, PA, 2000.
26. Mankame, N.D., Ananthasuresh, G.K., "Comprehensive thermal modeling and characterization of an electro-thermal-compliant microactuator," *Journal of Micromechanics and Microengineering*, vol.11, 2001, pp. 1-11.
27. Mankame, N.D., Ananthasuresh, G.K., "Effect of thermal boundary conditions and scale on the behaviour of electro-thermal-compliant micromechanisms," Proc. of Modeling and Simulation of Microsystems, 2000, pp. 609-612.
28. Lott, C.D., "Electrothermomechanical modeling of surface-micromachined linear displacement microactuator," M.S. Thesis, Brigham Young University, Provo, Utah, 2001.
29. Lott, C.D., McLain, T.W., Harb, J.N., Howell, L.L., "Thermal modeling of a surface micromachined linear thermomechanical actuator," Modeling and Simulation of Microsystems, ISBN 0-9708275-0-4, 2001, pp. 370-373.
30. Hickey, R., "Analysis and Optimal Design of Micro-machined Thermal Actuators", M.A.Sc Thesis, Dalhousie University, Nova Scotia, CA, 2001.
31. Manginell, R.P., "Polycrystalline- Silicon microbridge combustible gas sensor," Ph.D Thesis, University of New Mexico, Albuquerque, NM, 1997.
32. McConnell, A.D., Uma, S., Goodson, K.E., "Thermal conductivity of doped polysilicon layers," *Journal of Microelectromechanical Systems*, vol. 10, 2001, pp. 360-369.
33. Okada,Y., Tokumaru, Y., "Precise determination of lattice parameter and thermal expansion coefficient of silicon between 300 and 1500 K," *J. App. Physics*, vol.56., no.2, 1984, pp. 314-320.
34. Lide, D., Kehiaian, H., *CRC Handbook of Thermophysical and Thermomechanical Data*, 1994, CRC Press, Ann Arbor, MI.
35. Sharpe, W. N., Jr., Eby, M. A., and Coles, G., "Effect of Temperature on Mechanical Properties of Polysilicon," *Proc.Transducers'01*, pp 1366-1369, 2001.
36. Kato, K., Ono, T., 1982, "A physical mechanism of current induced resistance decrease in heavily doped polysilicon resistors," IEEE Transaction on Electron Devices, vol.29, no.8, pp. 1156-1160.
37. Cragun, R., "Thermal microactuators for microelectromechanical systems", M.S. Thesis, Brigham Young University Provo, Utah, 1999.

38. Halliday, D., Resnick, R., *Fundamentals of Physics*, 1988, New York.
39. Burns, D.M., Bright, V.M, "Design and performance of a double hot arm polysilicon thermal actuator", *Proc.SPIE*, vol.3224, 1997, pp.296-306.
40. Dong, Y., "Mechanical design and modeling of MEMS thermal actuators for RF applications", M.A.Sc Thesis, University of Waterloo, Waterloo, CA, 2002.
41. Mankame, N.D., Personal Communication, December 2002.
42. Mills, A., *Basic Heat and Mass Transfer*, 1999, Prentice Hall.
43. Touloukian, Y.S., Powell, R.W., Ho, C.Y., and Klemens, P.G., *Thermophysical properties of matter*, IFI/Plenum, 1970.
44. Slack, G.A., "Thermal conductivity of pure and impure silicon, silicon carbide and diamond," *J.App.Physics*, vol. 35, 1964, pp. 3460-3466.
45. Tai, Y.C., Mastrangelo, C.H., Muller, R.S., "Thermal conductivity of heavily doped LPCVD polycrystalline silicon films," *J. App. Physics*, vol.63, no.5, 1988, pp.1442-1447.
46. Cronos Integrated Microsystems, www.memsrus.com, JDS Uniphase.
47. Cronos Integrated Microsystems, JDS Uniphase, Personal Communication, July 2002.
48. Jin, J., Zhou, Z., "Simulation and modeling of a micro pressure sensor array," Modeling and Simulation of Microsystems, ISBN 0-9708275-7-1, 2002, pp. 306-309.
49. Automated design for MUMPs, www.sfu.ca.
50. ANSYS, Version 5.6/7.0, Swanson Analysis Systems, ANSYS Inc., Pittsburgh, PA.
51. Bhashyam, G.R, 2002, "ANSYS Mechanical- A Powerful Nonlinear Simulation Tool", www.ansys.com, ANSYS Inc., Canonsburg, PA.
52. Kohnke, P.C., Swanson, J.A., "Thermo-electric finite elements," International Conference on Numerical Methods in Electrical and Magnetic Field Problems, Session 2, 1976, pp. 85-89.
53. ANSYS Online Help Manual, Version 5.6/7.0.
54. Song, S., Lee, S., Au, V., Moran, K.P., "Constriction/Spreading resistance model for electronic packaging", Proceedings of the 4th ASME/JSME Thermal Engineering Joint Conference, vol. 4, 1995, pp. 199-206. 2.

55. Song, S., Lee, S., Au, V., "Closed form equation for thermal Constriction/Spreading resistances with variable resistance boundary condition," Proceedings of the 1994 IEPS Conference, 1994, pp. 111-121.

56. Hickey, R., Sameoto, D., Hubbard, T., Kujath, M., "Time and Frequency Response of Two-Arm Micromachined Thermal Actuators," *J. Micromech. Microeng.*, vol.13, 2003, pp. 40-46.

57. Koester, D., Mahadevan, R., Hardy, B., Markus, K., "Multi-user MEMs processes (MUMPs) Design Handbook," Cronos Integrated Microsystems, JDS Uniphase, NC, Revision 6.0, 2001.

58. Muller, R.S., Conant, R.A., "Cyclic fatigue testing of surface-micromachined thermal actuators", Paper available online at www-bsac.eecs.berkeley.edu/~rconant/papers/ASME-thermal-paper.pdf.

59. Chen, R.S., Kung, C., Lee, G., "Analysis of the optimal dimension on the electro thermal microactuator", *J.Micromech.Microeng.*, vol.12, pp. 291-296, 2002

60. Personal communication with Rob Messenger, Brigham Young University, Utah, April 2003.